Metalloproteins containing iron and tungsten: biocatalytic links between organic and inorganic redox chemistry

Metalloproteins containing iron and tungsten: biocatalytic links between organic and inorganic redox chemistry

Proefschrift

ter verkrijging van de graad van doctor
aan de Technische Universiteit Delft,
op gezag van de Rector Magnificus prof. dr. ir. J.T. Fokkema,
voorzitter van het College voor Promoties,
in het openbaar te verdedigen op maandag 28 oktober 2002 om 16:00 uur
door

Peter-Leon HAGEDOORN

ingenieur in de landbouw- en milieuwetenschappen
geboren te Amersfoort

Dit proefschrift is goedgekeurd door de promotor:
Prof. dr. W.R. Hagen

Samenstelling promotiecommissie:

Rector Magnificus	voorzitter
Prof. dr. W.R. Hagen	Technische Universiteit Delft, promotor
Prof. dr. S. de Vries	Technische Universiteit Delft
Prof. dr. J.G. Kuenen	Technische Universiteit Delft
Prof. dr. C.D. Garner	University of Nottingham, UK
Prof. dr. ir. A.J.M Stams	Wageningen Universiteit
Prof. dr. C. Veeger	Wageningen Universiteit
Dr S.P.J. Albracht	Universiteit van Amsterdam

The studies presented in this thesis were performed at the Kluyver Department of Biotechnology, Delft University of Technology. This research has been financially supported by the Council for Chemical Sciences of the Netherlands Organization for Scientific Research (CW-NWO) under project number 700-28-102.

Published and distributed by: DUP Science

DUP Science is and imprint of
Delft University Press
P.O. Box 98
2600 MG Delft
The Netherlands
Telephone: +31 15 27 85 678
Telefax: +31 15 27 85 706
E-mail: Info@library.TUDelft.NL

ISBN 90-407-2349-4

Keywords: metalloprotein, redox chemistry, tungsten enzyme

Copyright © 2002 by P.L. Hagedoorn

All rights reserved. No part of the material protected by this copyright notice may be reproduced or utilized in any form or by any means, electronic or mechanical, including photocopying, recording or by any information storage and retrieval system, without written permission from the publisher: Delft University Press.

Printed in the Netherlands

Contents

Chapter 1 1

General introduction

Chapter 2 23

Hyperthermophilic redox chemistry: A re-evaluation

Chapter 3 35

Pyrococcus furiosus glyceraldehyde-3-phosphate oxidoreductase has comparable $W^{VI/V}$ and $W^{V/IV}$ reduction potentials and unusual [4Fe-4S] EPR properties

Chapter 4 51

Steady-state kinetics and tungsten co-ordination of the glycolytic enzyme glyceraldehyde 3-phosphate oxidoreductase from the hyperthermophilic archaeon *Pyrococcus furiosus*

Chapter 5 73

Redox characteristics of the tungsten DMSO reductase of *Rhodobacter capsulatus*

Chapter 6 85

Electroanalytical determination of tungsten and molybdenum in proteins

Chapter 7 101

The effect of substrate, dihydrobiopterin and dopamine on the EPR spectroscopic properties and the midpoint potential of the catalytic iron in recombinant human phenylalanine hydroxylase

Chapter 8 121

Spectroscopic characterization and ligand binding properties of chlorite dismutase from the chlorate respiring bacterial strain GR-1

References 139

Summary 165

Samenvatting 169

Curriculum Vitae 173

List of abbreviations 175

List of publications 177

Nawoord 179

Chapter 1

General introduction

The redox chemistry of iron and tungsten in biology

Important chemical reactions in the main metabolic pathways of living organisms involve reduction and oxidation reactions, i.e. redox reactions. Biological redox chemistry is limited by the oxidation and reduction potentials of the solvent that is always present in biological systems: water. These potentials are +830 mV for the oxidation of water to molecular oxygen and –420 mV for the reduction of protons to molecular hydrogen at 25ºC, pH 7.0, and atmospheric pressure. However in an environment shielded from the solvent inside a protein, an overpotential of a few hundred millivolts above and below these limits is possible. Nature frequently uses transition metal centers or clusters as redox catalysts, because of their ability to take up and donate electrons. This thesis is concerned with a set of proteins that, taken together, offer a wide view into metal based redox biochemistry. Both redox enzymes and electron transfer proteins are considered. As can be seen in table 1 these proteins cover almost the whole biological redox potential range.

Table 1. Redox properties of the metalloproteins studied in this thesis.

Protein	Redox center(s)	E_m vs. NHE (mV)	Chapter(s)
Electron transfer proteins			
Rubredoxin	$Fe(Cys)_4$	+40	2
Ferredoxin	[4Fe-4S]	-350	2
Tungsten enzymes			
Dimethylsulfoxide reductase	W-pterin	-134 and –194	5
Glyceraldehyde-3-phosphate oxidoreductase	W-pterin	-450 and –650	3-4, 6
	[4Fe-4S]	-320	
Iron enzymes			
Phenylalanine hydroxylase	Non heme Fe	+200	7
Chlorite dismutase	Heme iron	+10	8

All but one of these enzymes and proteins contain iron as a redox active center, however in different forms. And two of the enzymes contain a tungsten center, which is a rare element in biochemistry. Note that all the enzymes listed in table 1 catalyze 2 electron (or 4 electron in the case of chlorite dismutase) redox chemistry. In

these enzymes the metal has to be connected to the organic world, in which most redox reactions are 2 electron reactions. Molybdenum and tungsten are excellent metals for 2 electron redox chemistry, but iron is more suitable for 1 electron reactions (as is the case for the electron transfer proteins). Nature has dealt with the limitation of iron by stabilizing higher oxidation states of iron, i.e. compound I and II which are further introduced below. Libraries can be filled with the literature on the biochemistry of iron. Therefore, only a concise introduction will be presented to the different biological forms of iron that are relevant for this thesis. Furthermore, a brief introduction will be given to tungsten enzymes and their family ties with the more common molybdenum enzymes.

Heme iron containing enzymes

Introduction

Probably the most abundant and most studied iron containing proteins are the heme proteins. Several heme cofactors exist, all derivatives of a tetrapyrrole ring system. These cofactors coordinate the metal by the four nitrogens forming a planar coordination environment. Although several heme derivatives have been found in nature, iron-protoporphyrin IX, or heme b, is commonly found in heme enzymes (Figure 1). Often heme iron is used to bind small inorganic compounds (e.g. di-oxygen), to perform oxygen chemistry, or to take up or donate electrons. These basic functionalities afford many different biological functions such as oxygen transport, CO sensing, peroxidations, NO synthesis. Heme proteins have been excellent objects for spectroscopic studies. Allowed π-π^* transitions of the heme moiety result in intense electronic absorption bands, which have been named α and β in the range 450-700 nm and γ (or Soret band) in the range 390-450 nm. The γ band is usually ten times more intense than the α and β bands.

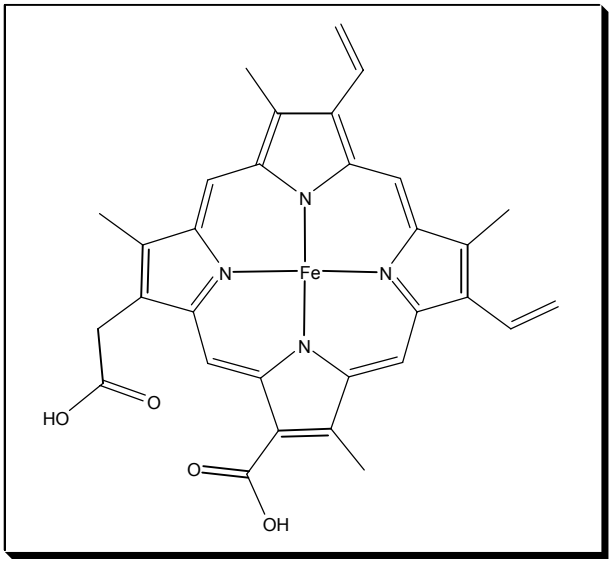

Figure 1. Protoporphyrin IX.

Table 2 gives a summary of Fe(III/II) midpoint potentials of different heme proteins with different proximal ligands of the iron site. Clearly, heme iron is a versatile redox catalyst whose redox potential can be modulated by a proximal amino acid residue which coordinates the iron center. However, as can be seen in table 2, heme proteins with a histidine proximal ligand can have Fe^{III}/Fe^{II} midpoint potentials from –200 to +50 mV. This broad potential range can be explained by taking the hydrogen bonding of other amino acid residues to the proximal histidine (i.e. the electronegativity of the local environment of the proximal histidine) into account [1]. The proximal histidine in peroxidases has a hydrogen bond to a nearby aspartate residue, while in the globins the proximal histidine has a hydrogen bond to a peptide backbone oxygen. As a consequence the proximal histidine in the globins has a less electronegative environment than in peroxidases. Mutational studies on peroxidases have shown a qualitative correlation where the Fe(III/II) midpoint potential decreases as the negative charge on the proximal ligand increases [2, 3]. The Fe^{III}/Fe^{II} couple may not always be relevant for catalysis. Ferric heme is often proposed as the starting oxidation state. For catalases and peroxidases two transient reaction intermediates which are one and two electron oxidized with respect to the ferric state, have been described and named compound II and I, respectively. Compound II has been found to be an oxo-ferryl species and compound I and oxo-ferryl porphyrin π-cation radical. However, since the high valent states of iron are generally transient, the midpoint

potential of the Fe^{IV}/Fe^{III} couple is much more difficult to obtain than that of the Fe^{III}/Fe^{II} couple.

Table 2. Redox properties of protoporphyrin IX containing proteins.

Heme protein	Proximal Ligand	E_m (Fe^{III}/Fe^{II})	E_m (C-II/Fe^{III})	E_m (C-I/Fe^{III})	Ref.
Myoglobin	His	+50			[4]
Myeloperoxidase	His	+21		+1100	[5, 6]
Chlorite dismutase	His	-23 to -21			[7, 8]
Lignin peroxidase	His	-142		+1400	[9]
Cytochrome c peroxidase	His	-194		+740	[10, 11]
Cytochrome P450	Cys	~-200			[12]
Horseradish peroxidase	His	-250	+869	+898	[13, 14]
Catalase	Tyr	<-500			[15]

Chlorite dismutase

To date chlorite dismutase has only been isolated from three bacterial species: strain GR-1, strain CKB, and *Ideonella dechloratans* [7, 16, 17]. However chlorite dismutase activity has been found in whole cell suspensions of several other chlorate respiring bacteria as well [17]. The enzyme catalyzes the reduction of chlorite to chloride, while producing molecular oxygen. A more appropriate name for this enzyme is chloride:oxygen oxidoreductase. The biological function of the enzyme is to detoxify chlorite, which is the product of the respiration on chlorate. Chlorite dismutase has been found to be a homotetramer of 32 kDa subunits containing one iron protoporphyrin IX per subunit. Although it has a common heme cofactor, the spectroscopic features and redox properties of chlorite dismutase are unusual for a heme enzyme (chapter 8).

Mononuclear non-heme iron containing enzymes

Introduction

Mononuclear non-heme iron proteins have been less studied by spectroscopic methods than the heme proteins discussed above. In general these enzymes exhibit no significant electronic absorption in the visible region. Notable exceptions are the enzymes that have one or more cysteine sulfurs in the first coordination sphere of the iron, i.e. desulfoferredoxin and superoxide reductase [18]. An understanding of the redox mechanisms of these non-heme enzymes is emerging, however they are still not fully understood. Phenylalanine hydroxylase, tyrosine hydroxylase and tryptophan hydroxylase are amino acid hydroxylases that are highly similar in amino acid sequence and crystal structure [19]. These enzymes contain a mononuclear non-heme iron site which is coordinated by two N(His), one O(Glu) and two water molecules that can be exchanged with the substrate L-Phe, L-Tyr or L-Trp or inhibitors, such as dopamine.

Phenylalanine hydroxylase

Human liver phenylalanine hydroxylase (PAH) functions in phenylalanine catabolism and it constitutes 0.1-0.3% of the total protein in the liver. If all PAH present in the liver were fully active all L-Phe present in the human body would be hydroxylated within minutes [20]. Therefore it is not surprising that this enzyme is regulated by several effectors. Glucagon and L-Phe are activators and tetrahydrobiopterin, the natural cofactor of this enzyme, is an allosteric inhibitor. The reaction catalyzed by PAH is given in figure 2. Defective mutants of PAH cause hyperphenylalaninemia, or accumulation of L-Phe. Consequently, by action of

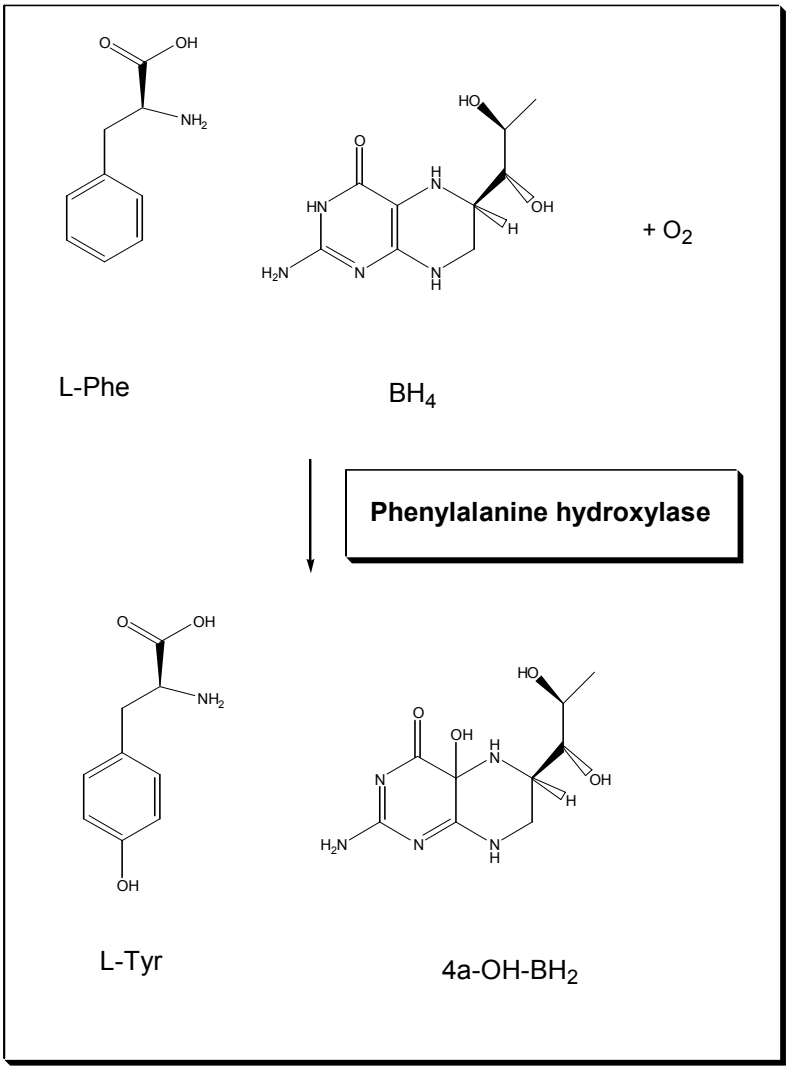

Figure 2. Reaction catalyzed by human phenylalanine hydroxylase (PAH). The midpoint potential of the q-BH_2/BH_4 couple at pH 7 is +174 mV [21].

tyrosine aminotransferase, phenylpyruvate and other neurotoxic metabolites are accumulated. The result is the phenylketonuria (PKU), which manifests itself by severe mental retardation of patients with this disease. Recent crystal structure determinations of PAH with and without cofactor and substrate have provided detailed information on the active site and substrate binding site of the enzyme. However little is known about the redox chemistry and the possible redox role of iron in this enzyme. Ferrous, ferric and even ferryl intermediates have been proposed. In chapter 7 of this thesis the redox potential of the Fe^{III}/Fe^{II} couple and its modulation by substrate, cofactor and an inhibitor is presented.

Iron-sulfur containing proteins

Introduction

Iron-sulfur proteins contain iron centers or clusters coordinated by sulfur ligands. The iron sulfur clusters contain several acid-labile sulfurs, which are not part of an amino acid residue. Several basic structures of iron-sulfur clusters have been characterized, i.e. FeS(Cys)4, [2Fe-2S], [3Fe-4S], and [4Fe-4S] cluster (Figure 3).

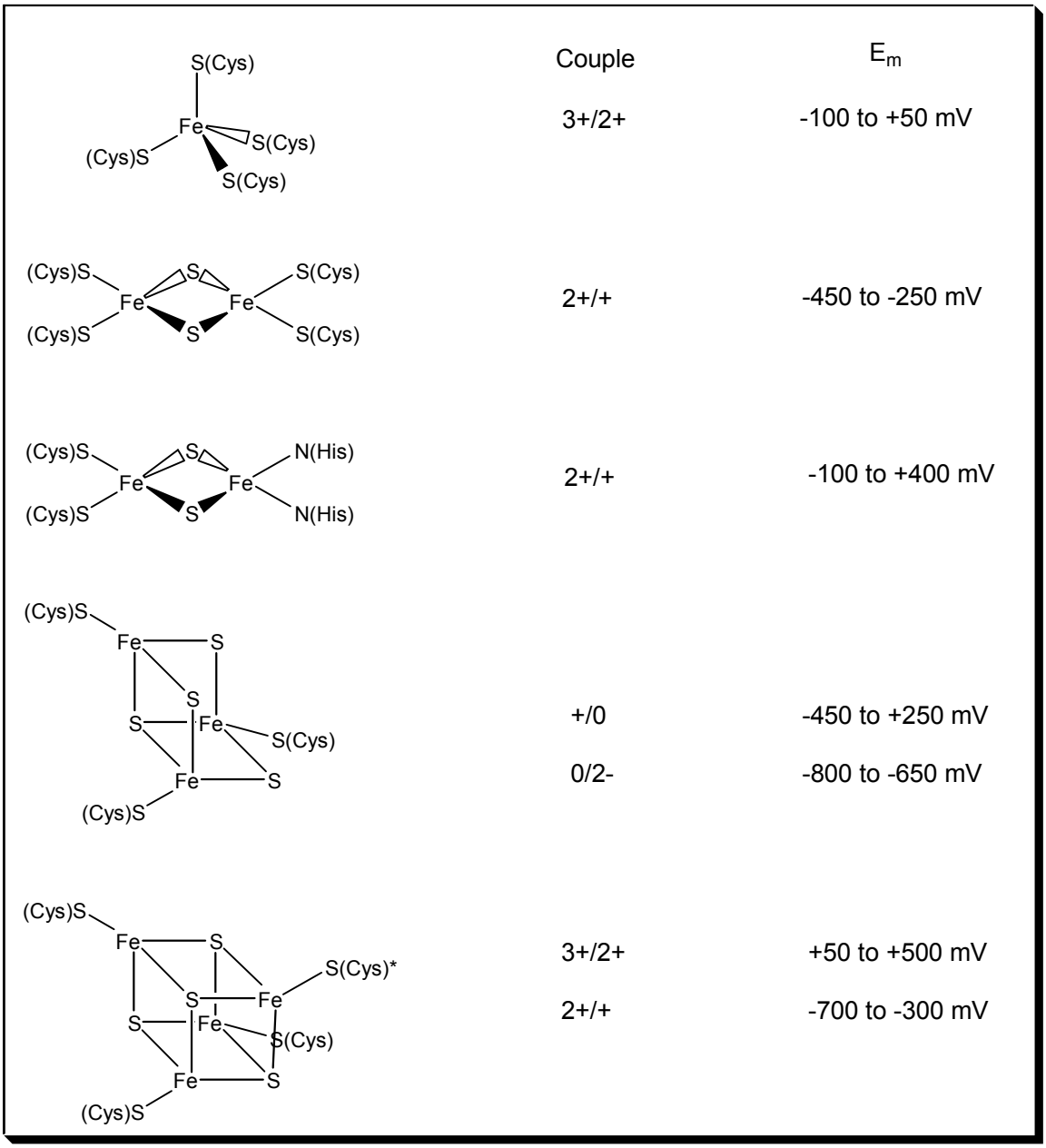

Figure 3. Basic strucures and redox properties of iron-sulfur clusters. *Cys or Asp or His.

Figure 3 shows that iron-sulfur clusters can cover a wide redox potential range. Most iron-sulfur proteins have redox functions. And although catalytic functions of iron-sulfur cluster in enzymes have been discovered, most proteins use iron-sulfur clusters as biological electron wires. This thesis contains studies of three different iron-sulfur containing proteins: rubredoxin, ferredoxin and glyceraldehyde-3-phosphate oxidoreductase. The latter also contains a tungsten center and will be introduced in a separate section describing tungsten enzymes, below. The spectroscopic features and redox properties of the iron-sulfur clusters in these proteins will be described (see chapters 2-4). All three iron-sulfur proteins have been isolated from the hyperthermophilic archaeon *Pyrococcus furiosus*. *P. furiosus* is a fast growing heterotrophic prokaryote growing optimally at 100°C [22] .

Rubredoxin

Rubredoxins are small (~ 6 kDa) proteins that contain a tetrahedral iron sulfur center. The mononuclear iron center is coordinated by four cysteine sulfurs. The first crystal structure of this protein was determined in 1970[23]. In 1991 rubredoxin was first isolated from *P. furiosus* [24]. And more recently the crystal structure of this hyperthermophilic protein has been determined [25]. *P. furiosus* uses rubredoxin as an electron carrier as part of its oxygen defense mechanism [18]. Only rencently such oxygen defense mechanisms have been discovered for several “stricly anaerobic” bacteria and archaea. The proposed mechanism is depicted in figure. 4. Rubredoxin shuttles as an electron carrier between the flavoenzyme NAD(P)H:Rubredoxin oxidoreductase [26] and the non-heme mononuclear iron enzyme superoxide reductase [18, 27, 28].

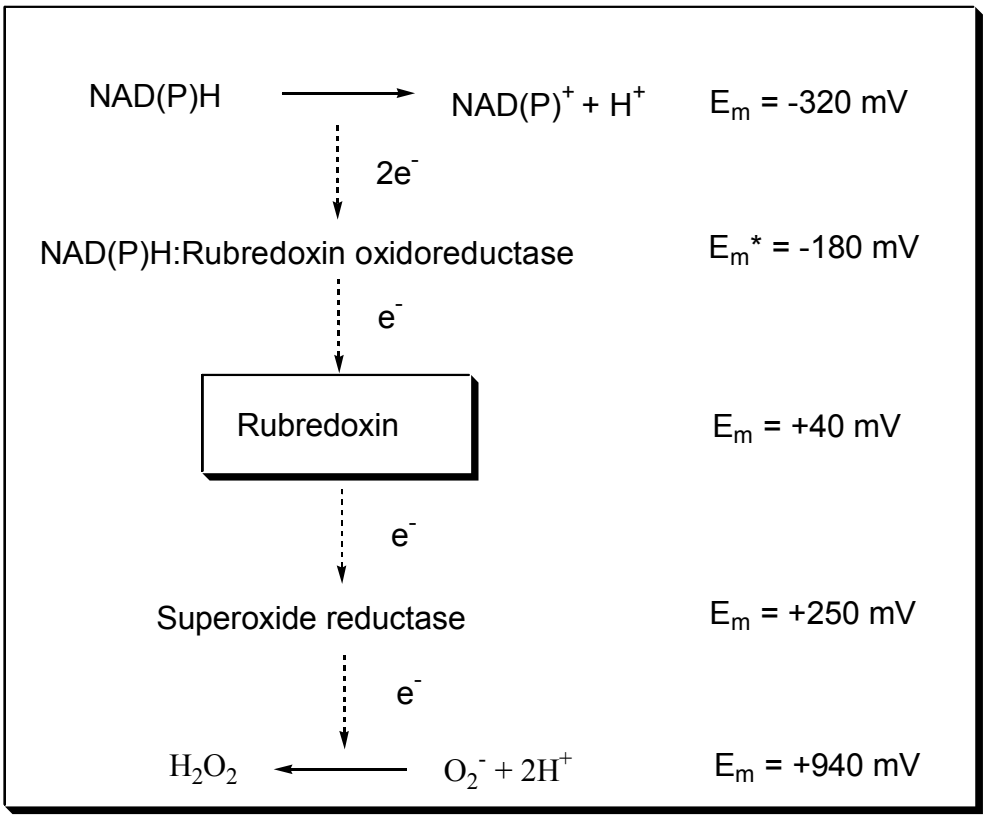

Figure 4. Proposed oxygen defense mechanism of *Pyrococcus furiosus*.
*value for the free FAD/$FADH_2$ couple. The midpoint potential of the FAD in NAD(P)H:Rubredoxin oxidoreductase has not been reported.

Ferredoxin

Ferredoxins are small electron transfer proteins that can be divided in several types based on the number of iron atoms they contain: 2Fe, 3Fe, 4Fe, 7Fe and 8Fe ferredoxins. The plant type 2Fe ferredoxin contains a [2Fe-2S] cluster and in plants and cyanobacteria it is involved in photosynthesis. Enzyme subunits similar to the 2Fe ferredoxin have been found among eukaryotes, bacteria and archaea.
The 3Fe ferredoxin contains a [3Fe-4S] cluster, the 4Fe ferredoxin a [4Fe-4S] clusters, the 7Fe ferredoxin contains [3Fe-4S][4Fe-4S] and the 8Fe ferredoxin two [4Fe-4S] clusters. *Pyrococcus furiosus* contains an unusual 4Fe ferredoxin, which has one cubane [4Fe-4S] cluster of which one iron is coordinated by an O(Asp) instead of a S(Cys). Only in the 8Fe ferredoxins from *Desulfovibrio vulgaris*, *Desulfovibrio africanus*, *Thermoplasma acidophilum* and *Sulfolobus acidocaldarius* and the [4Fe-4S] ferredoxin of *Pyrococcus abyssi* and *Thermococcus profundus* a similar

replacement of one coordinating cysteine by and aspartate has been found [29, 30]. The iron which is coordinated by this Asp can be easily displaced by oxidation with potassium ferricyanide, and a [3Fe-4S] cluster is formed. Reconstitution of this [3Fe-4S] can be performed by adding excess ferrous iron under reducing conditions. However reconstitution with other monovalent (Tl^{+}, Cu^{+}) or divalent (Zn^{2+}, Co^{2+}, Ni^{2+}, Mn^{2+}, Cd^{2+}, Cr^{2+}) cations forming [M3Fe-4S] clusters has been described as well. The spin states and redox properties of heterometal derivatives of ferredoxin are given in table 3. As can be seen in table 3 heterometal ferredoxin has redox potentials spanning a wide potential range from –470 to + 190 mV.

Table 3. Spin states and (room temperature) redox potentials of [M3Fe-4S] clusters of *Pyrococcus furiosus* ferredoxin.

Cluster	Spin state(s) oxidized	Spin state(s) reduced	E_m (mV)	References
$[Cu3Fe\text{-}4S]^{2+/+}$	1/2	2	+190	[31]
$[Ni3Fe\text{-}4S]^{2+/+}$	NR	3/2	+90	[32]
$[Mn3Fe\text{-}4S]^{2+/+}$	NR	0	>-100	[33]
$[Tl3Fe\text{-}4S]^{2+/+}$	1/2	2	+152*	[34, 35]
$[3Fe\text{-}4S]^{+/0/2-}$	1/2	2	-160	[36]
		NR**	-714*	[35]
$[Co3Fe\text{-}4S]^{2+/+}$	1/2	1	-163	[33]
$[Zn3Fe\text{-}4S]^{2+/+}$	2	5/2	-240	[33]
$[4Fe\text{-}4S]^{2+/+}$	0	3/2, 1/2	-345	[36]
$[Cr3Fe\text{-}4S]^{2+/+}$	0	3/2	-440	[31]
$[Cd3Fe\text{-}4S]^{2+/+}$	2	5/2	-470	[31]

*measured at 0°C **an integer ground state spin is expected since the $[3Fe\text{-}4S]^{2-}$ cluster contains only ferrous irons. NR = not reported.

Ferredoxin plays a central role in the metabolism of *Pyrococcus furiosus* since it is a partner (electron acceptor) of the glycolytic enzymes glyceraldehyde-3-phosphate oxidoreductase (GAPOR) and pyruvate oxidoreductase (POR), of the possibly amino acid catabolizing enzymes aldehyde oxidoreductase (AOR) and formaldehyde oxidoreductase (FOR), of indolepyruvate oxidoreductase (IOR)[37], 2-ketoglutarate oxidoreductase (KGOR)[38], 2-ketoisovalerate oxidoreductase (VOR)

[39], and (electron donor) of pyridine dinucleotide metabolic enzyme ferredoxin:NAD(P)$^+$ oxidoreductase (FNOR or sulfide dehydrogenase) and the membrane bound hydrogenase III (Figure 4). Due to its extreme sensitivity towards oxygen KGOR has never been isolated from *Pyrococcus furiosus*, however its activity has been found in cell extracts.

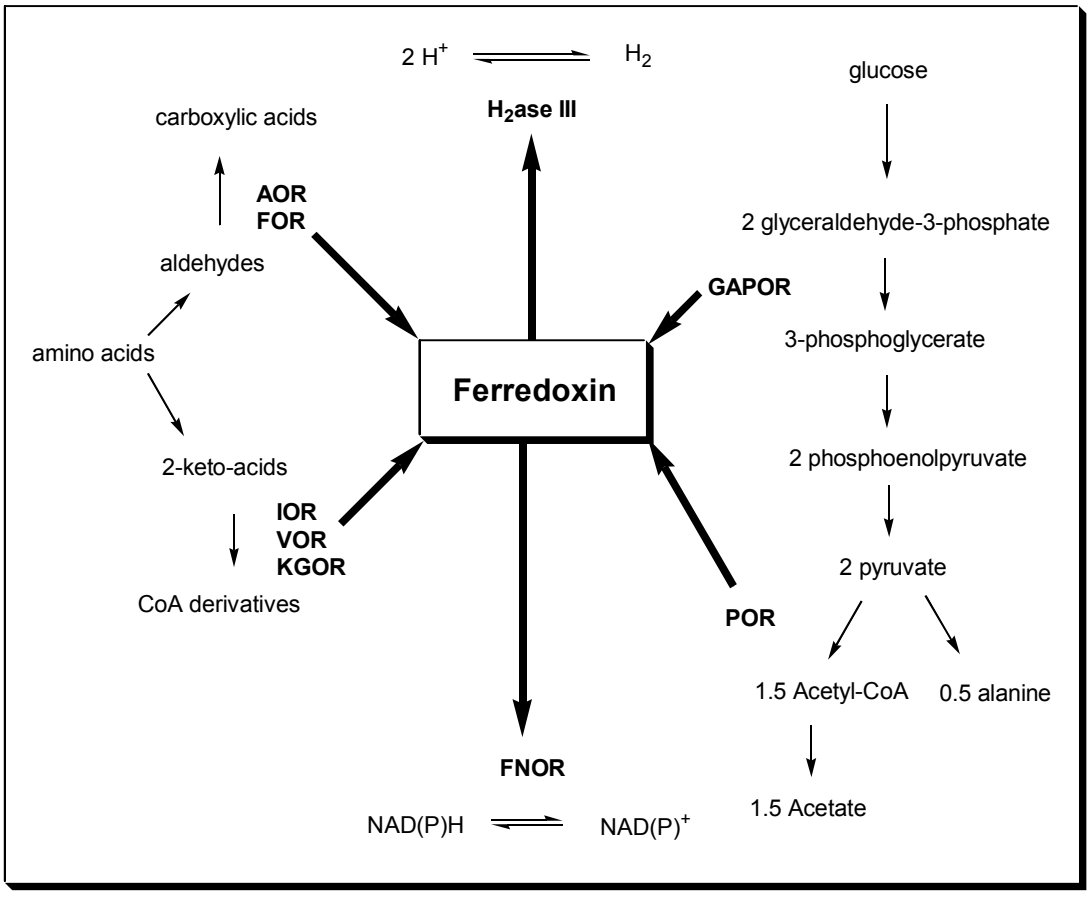

Figure 5. The different roles of ferredoxin in *Pyrococcus furiosus*: amino acid metabolism, pyridine dinucleotide reduction, hydrogen metabolism, glycolysis.

Tungsten containing enzymes

General properties

The research in the biochemistry of tungsten was pioneered with the discovery of tungsten accumulation in *Clostridium thermoaceticum* (recently renamed *Moorella thermoacetica* [40]) formate dehydrogenase by Andreesen and Ljungdahl (1973) [41]. Since then well over 40 research articles and 5 review articles on tungsten containing enzymes have appeared. Table 4 gives an overview of some properties of the tungsten containing enzymes that have been isolated to date. From structural and genomic analysis of tungsten and molybdenum enzymes it has become clear that the biochemistries of these metals are entangled (Figure 6). Together mononuclear molybdenum and tungsten enzymes constitute four enzyme families, named after the most thorough studied enzyme of that family: sulfite oxidase family, xanthine oxidase family, DMSO reductase family, and AOR family [42, 43]. The sulfite oxidase and xanthine oxidase families contain only molybdenum enzymes. The DMSO reductase family contains mostly molybdenum, but also a number of tungsten enzymes (table 4). The AOR family contains tungsten enzymes and only one molybdenum enzyme.

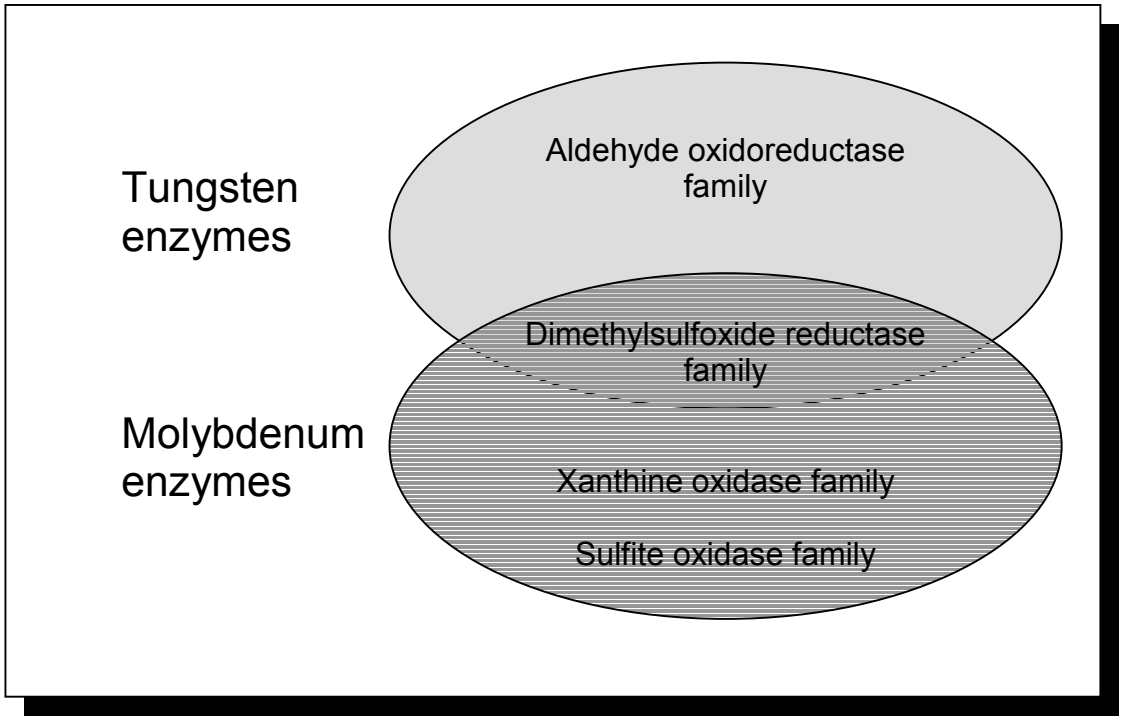

Figure 6. Familiarity of mononuclear molybdenum and tungsten enzymes based on sequence and structure.

All mononuclear molybdenum and tungsten enzymes contain a pterin-derived cofactor, which coordinates the metal. Interestingly, all enzymes from the DMSO reductase and AOR families contain a bis-pterin cofactor, while a monopterin cofactor is found in the molybdenum enzymes from the sulfite oxidase and xanthine oxidase families. From table 4 some general properties of the tungsten enzyme families can be deduced. Enzymes from the AOR family contain a bis-pterin cofactor without additional nucleotides, while in enzymes from the DMSO reductase family an additional guanine diphosphate residue is bound to each pterin ring of the bis-pterin cofactor. The enzymes from the AOR family all appear to contain one or more [4Fe-4S] cluster(s) for intramolecular electron transfer. The natural redox partner of the AOR family enzymes is a ferredoxin. Some DMSO reductase family enzymes contain no additional iron sulfur clusters, but many have [4Fe-4S] and [2Fe-2S] clusters. For many of the DMSO reductase family enzymes the natural redox partner is unknown. In a number of enzymes from the DMSO reductase family selenium has been found, while this element is not found in any of the AOR family enzymes.

Table 4. Properties of the tungsten containing enzymes that have been isolated to date.

Enzyme	Organisms	Sub-units	Subunit mass (kDa)	Redox partner	Metals	Cofactors	Fe-S clusters	O_2 sensitive	References
			Aldehyde oxidoreductase family						
Aldehyde oxidoreductase	*Pyrococcus furiosus*	α_2	75	Ferredoxin	2W, 9Fe	2 PTE	2[4Fe-4S]	Yes	[44-47]
	Thermococcus sp. strain ES-1	α_2	67	Ferredoxin	2W, 9Fe	2 PTE	2[4Fe-4S]	Yes	[48]
	Pyrococcus sp. strain. ES-4	α_2	67	Ferredoxin	2 W, 9Fe	PTE	2[4Fe-4S]	Yes	[46, 49, 50]
	Moorella thermoacetica[2]	$\alpha_3\beta_3\gamma$	64, 14, 43	NADPH, (Viologen)	3.4 W, 82 Fe, 54 S	2.5 PTE, 1.7 FAD	Yes[1]	Yes	[51, 52]
	Clostridium formicoaceticum	α_2	67	(Viologen)	1.4 W, 11 Fe, 16 S	1.6 PTE	[4Fe-4S]	Yes	[53] [54]
Formaldehyde oxidoreductase	*Pyrococcus furiosus*	α_4	77	Ferredoxin	4W, 12Fe, Ca	4 PTE	4[4Fe-4S]	Yes	[55, 56]
	Thermococcus litoralis	α_4	70	Ferredoxin	4W, 12Fe	4 PTE	4[4Fe-4S]	Yes	[57, 58]
Glyceraldehyde-3-phosphate oxidoreductase	*Pyrococcus furiosus*	α_1	80	Ferredoxin	1W, 4Fe, 4S, 2Zn	1 PTE	1[4Fe-4S]	Yes	[59-61]
WOR4	*Pyrococcus furiosus*	α_n	76	NR	W, Fe, S	NR	NR	Yes	[62]
Aldehyde dehydrogenase	*Desulfovibrio gigas*	α_2	62	(Benzyl viologen)	0.7 W, 5Fe, 4S	PTE	[4Fe-4S]	Yes	[63]
HVOR*	*Proteus vulgaris*	α_n	80	(Viologen)	0.9 Mo, 4Fe, 4S	1 PTE	Yes[1]	Yes	[64]

DMSO reductase family									
Formate dehydrogenase	*Moorella thermoacetica*	$\alpha_2\beta_2$	96, 76	$NADP^+$	2 W, 36 Fe, 50 S, 2 Se	PTE	1[4Fe-4S], 1[2Fe-2S]	Yes	[65-67]
	Clostridium cylindrosporum	NR	NR	(Viologen)	W	NR	NR	NR	[68]
	Clostridium acidiurici	NR	NR	(Viologen)	W	NR	NR	Yes	[68]
	Clostridium formicoaceticum	NR	88	(Viologen)	W	NR	NR	Yes	[69]
	Eubacterium acidaminophilum	$\alpha\beta$	98, 62	HymB[3]	W, Se	MGD-PTE	2[2Fe-2S], 8[4Fe-4S]	Yes	[70]
	Syntrophobacter fumaroxidans	$(\alpha\beta\gamma)_2$	89, 56, 19	(Viologen)	0.6 W, 43 Fe, 1 Se	NR	4[2Fe-2S], 12[4Fe-4S]	Yes	[71]
		$\alpha\beta$	92, 33	(Viologen)	0.8W, 17 Fe, 1 Se	NR	2 [4Fe-4S]	Yes	[71]
	Desulfovibrio gigas	$\alpha\beta$	92, 29	(Viologen)	1W, 16Fe, 16 S, 1 Se	MGD-PTE	4[4Fe-4S]	Yes	[72, 73]
Formylmethanofuran dehydrogenase	*Methanobacterium wolfei*	$\alpha\beta\gamma$	64, 51, 35	(Viologen)	0.4 W, 5 Fe	MGD-PTE	NR	Yes	[74, 75]
	Methanobacterium thermoautotrophicum	$\alpha\beta\gamma\delta$	65, 53, 31, 15	(Viologen)	0.4 W, 8 Fe, 8S	MGD-PTE	NR	Yes	[76]
	Methanopyrus kandleri	α	49	(Viologen)	W, Se	NR	NR	NR	[77]
Acetylene hydratase	*Pelobacter acetylenicus*	α	83	-	0.5 W, 5 Fe, 4 S	MGD-PTE	[4Fe-4S]	No	[78, 79]
Dimethylsulfoxide reductase**	*Rhodobacter capsulatus*	α	85	Cytochrome c	1 W	MGD-PTE	-	No	[80, 81]
Trimethylamine-N-oxide reductase**	*Escherichia coli*	α_2	90	Cytochrome c	2.4 W	MGD-PTE	-	No	[82]

* molydenum enzyme with significant sequence homology with the aldehyde oxidoreductase family; **tungsten substituted molybdenum enzymes; 1 only detected by UV-vis absorbance; 2 previously named *Clostridium thermoaceticum* [40]; 3 HymB is a subunit of a hydrogenase which together with formate dehydrogenase forms the formate hydrogen lyase complex in *Eubacterium acidaminophilum* [70]; NR, not reported; PTE, bis-pterin cofactor; MGD-PTE, guanine dinucleotide bis-pterin cofactor; WOR, tungsten containing (aldehyde) oxidoreductase ; HVOR, (2R)-hydroxycarboxylate-viologen-oxidoreductase.

Figure 7 depicts the different reactions catalyzed by tungsten enzymes. All natural tungsten enzymes catalyze oxygen atom transfer at a C-site of a substrate. However oxygen atom transfer at S- and N-sites has been found for the tungsten substituted molybdenum enzymes DMSO reductase and TMAO reductase respectively (Figure 7). Furthermore, all natural tungsten enzymes catalyze low potential redox reactions. Acetylene hydratase is a notable single exception since it catalyzes a hydratation and not a redox reaction. The two catalytically active tungsten substituted molybdenum enzymes DMSO reductase and TMAO reductase catalyze reactions with much higher reduction potentials. So apparently the tungsten center can catalyze redox reactions in a broad potential range, however, high potential reactions will be catalyzed in a unidirectional way (only reduction of the substrate).

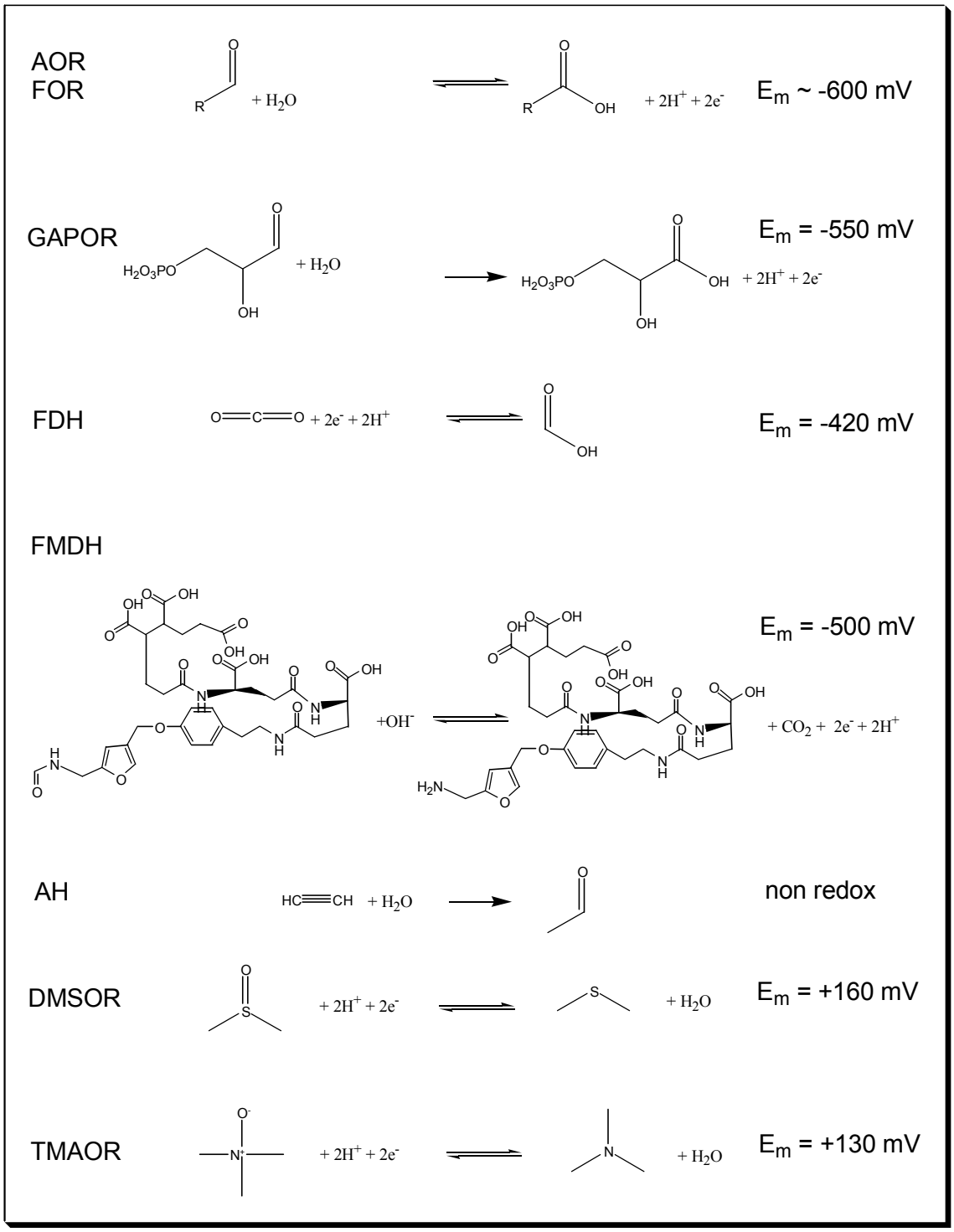

Figure 7. Reactions catalyzed by tungsten containing enzymes.

Glyceraldehyde-3-phosphate oxidoreductase

Glyceraldehyde-3-phosphate oxidoreductase (GAPOR) is a glycolytic enzyme replacing glyceraldehyde-3-phosphate dehydrogenase (GAPDH) and phosphoglycerate kinase (PGK) in the modified Embden-Meyerhof glycolytic pathway of *Pyrococcus furiosus* (Figure 5). Instead of producing ATP and NAD(P)H, only reduced ferredoxin is formed with the oxidation of glyceraldehyde-3-phosphate. Apparently this step has unkown benefits over the traditional pathway, since GAPDH and PGK are present in *Pyrococcus furiosus*, albeit in much lower quantities than GAPOR. Based on the available archaeal genome databases GAPOR genes are also present in *Pyrococcus abyssi, Pyrococcus horikoshii, Methanococcus jannaschii* and *Pyrobaculum aerophilum*. The EPR spectroscopic and redox properties of the tungsten center and the [4Fe-4S] cluster of *Pyrococcus furiosus* GAPOR are presented in chapters 3-4.

Dimethylsulfoxide reductase

Dimethylsulfoxide reductase (DMSO reductase) is a mononuclear molybdenum enzyme isolated from purple acid bacteria that can reduce DMSO to DMS. This reaction is an important part of the global sulfur cycle and even influences the formation of clouds in the sky. It is possible to substitute the mononuclear molybdenum with tungsten by growing the bacterium on tungsten-supplied medium, at least in the case of *Rhodobacter capsulatus*[80]. Interestingly, the enzyme retains DMSO reductase activity and the crystal structure of this enzyme shows that the mononuclear tungsten site is nearly identical to the molybdenum site. This tungsten substituted enzyme provides a good subject to compare the EPR spectroscopic and redox properties of tungsten and molybdenum in the same enzyme (chapter 5).

Outline of the thesis

Chapter 2 describes the re-evaluation of previous reports of unusual redox chemistry of hyperthermophilic redox proteins. We have falsified these reports and have found that the temperature dependent redox potentials and enzymatic activities can be interpreted with straightforward thermodynamics.

Chapter 3 describes a study of the redox properties of the tungsten containing glyceraldehyde-3-phosphate oxidoreductase from *Pyrococcus furiosus*. EPR spectra and redox potentials of the tungsten center and [4Fe-4S] cluster have been determined. An electron transfer chain has been reconstituted in vitro from the substrate first to the tungsten center to the [4Fe-4S] cluster and finally to the ferredoxin.

Chapter 4 describes a further characterization of the tungsten containing glyceraldehyde-3-phosphate oxidoreductase from *Pyrococcus furiosus*. Tungsten L(III)-edge EXAFS spectra at different oxidation states of the tungsten center are presented. Furthermore the steady-state-kinetics of this enzyme is worked out in more detail.

Chapter 5 describes the redox properties of the tungsten DMSO reductase from *Rhodobacter capsulatus*. The redox potential of the tungsten center in DMSO reductase has been found to be *ca.* 325 mV lower than for the equivalent molybdenum center. Relevance is discussed of the redox potentials to the differences in catalytic activity between the tungsten and molybdenum enzymes.

Chapter 6 describes an electroanalytical determination of trace concentration of tungsten from protein samples. An application to search for tungsten and molybdenum containing proteins during a protein purification is presented.

Chapter 7 describes the redox properties of the non-heme iron containing recombinant human phenylalanine hydroxylase. The midpoint potential of the iron center has been found to be close to the midpoint potential of the biopterin cofactor. Changes of the midpoint potential of the non-heme iron center upon binding of substrate, cofactor-analog and inhibitor are found and their mechanistic relevance is discussed.

Chapter 8 describes the spectroscopic properties of the heme iron containing enzyme chlorite reductase from bacterial strain GR-1. Several ligands have been found to bind the ferric and ferrous enzyme and their effect on the optical and EPR spectroscopic properties is presented. Nitrite, a substrate analog for chlorite

dismutase, has been found to bind to the ferric enzyme. The spectroscopic and redox properties of chlorite dismutase have been found to be similar to the globins rather than to the heme enzymes.

Chapter 2

Hyperthermophilic redox chemistry: A re-evaluation

Peter -L. Hagedoorn, Martijn C.P.F. Driessen, Marieke van den Bosch, Ilse Landa, Wilfred R. Hagen

Published in: FEBS Lett. 440, pp. 311-314, 1998.

The redox chemistry of *Pyrococcus furiosus* rubredoxin and ferredoxin has been studied as a function of temperature in direct voltammetry and in EPR monitored bulk titrations. The E_m of both proteins, measured with direct voltammetry, have a normal (linear) temperature dependence and show no pH dependence. EPR monitoring is not a reliable method to determine the temperature dependence of the E_m: upon rapid freezing the proteins take their conformation corresponding to the freezing point of the solution.

Introduction

Hyperthermophiles grow optimally at temperatures above 80°C. Their biochemistry is expected to have characteristics that may differ fundamentally from that of mesophiles. Several claims have been made on unusual redox chemistry in *Pyrococcus furiosus*. The temperature dependent E_m of ferredoxin has been reported to be biphasic and extrapolates to approximately -600 mV at 100°C, as measured by EPR monitored redox titrations [83]. However a recent report of direct electrochemistry on heterologously expressed wild type ferredoxin shows a normal linear temperature dependence of the E_m [84]. The E_m of rubredoxin has been reported to be pH dependent [29], although no significant pH dependence is expected based on the structure of the cluster and its environment. Furthermore the E_m of rubredoxin has a non-linear temperature dependence [29]. The observations described above have several implications which have been discussed in the literature [85]. The non-linear and biphasic temperature dependence of the E_m of rubredoxin and ferredoxin respectively, measured by redox titrations, have been interpreted in terms of a protein dielectric constant that changes non-linearly with temperature [86]. Furthermore molecular dynamics simulations have been used to determine temperature dependent changes in the physical properties of the protein [87].

The differences in the observations of direct electrochemistry and EPR monitored redox titrations on ferredoxin raise the question with which method and under which conditions redox potentials can best be obtained. Furthermore the strange redox behaviour reported for rubredoxin has only been measured in redox titrations. We have studied the temperature and pH dependence of the E_m of ferredoxin and rubredoxin with cyclic voltammetry, and we have compared these with the results obtained with EPR monitored redox titrations.

Materials and methods

Cultivation and protein purification

Pyrococcus furiosus (DSM 3638) was cultivated as previously described [88]. Cells were broken by osmotic shock, diluting with 5 volumes 50 mM Tris pH 8.0 (anaerobic) containing 2 mM sodium dithionite, 5 mM $MgCl_2$, 0.1 mg/l DNase I, 0.1

mg/l RNase. A cell-free extract was obtained as the supernatant after 1 hour centrifugation at 26,000g.

Rubredoxin was purified as described previously [24].

Ferredoxin was not purified as described previously [36], but with a new method. Ammonium sulfate was added to cell-free extract to 60% saturation. After centrifugation (15 min, 3200 g, 4°C) the supernatant was collected and diluted to 40% ammonium sulfate saturation. The supernatant was passed through a Phenyl-Sepharose column (Pharmacia), equilibrated with 40% ammonium sulfate in 50 mM Tris pH 8.0 (anaerobic), yielding pure ferredoxin. As isolated ferredoxin was reconstituted by incubation with 10-fold excess of $FeSO_4$ and 2 mM sodium dithionite under anaerobic conditions. Excess iron was removed on a Biogel P-6DG desalting column (Bio-Rad).

Horse heart cytochrome c was from Boehringer Mannheim.

Electrochemistry and EPR monitored titrations

Cyclic voltammograms were recorded with a BAS CV27 potentiostat (Bioanalytical systems) connected to a Kipp&Zonen x-y-t recorder. The electrochemical experiments were performed with a three-electrode microcell using the method described previously [89]. The working electrode was a nitric acid activated glassy carbon disc (Le Carbon Loraine). As the counter electrode a micro platinum electrode was used. And the potential was measured with reference to a Ag/AgCl reference electrode (Radiometer). All reported potentials have been recalculated with respect to the normal hydrogen electrode (NHE). During the experiments the electrochemical cell was immersed in a thermostated waterbath. A typical experiment was performed on a 20 µl droplet 0.15 mM rubredoxin with 0.10 mM $SmCl_3$ (promoter) or 0.14 mM ferredoxin with 6.7 mM neomycin (promoter) in 35 mM buffer. The buffers used were either Mes (pH 5.6), Bis-Tris (pH 6.5), Mops (pH 7.2), Taps (pH 8.4), Ches (pH 9.2), Caps (pH 10.4). To prevent evaporation 15 µl nujol oil (Perkin Elmer) was added on top of the droplet. At high pH values (above pH 8) 24 mM $MgSO_4$ was used instead of $SmCl_3$.

Both rubredoxin and ferredoxin were redox-titrated at 20°C and 80°C in presence of a mixture of 13 dye mediators as described previously [90]. A typical titration was done on 18.5 µM rubredoxin in 25 mM BisTris pH 6.5 or 0.88 mM

ferredoxin in 25 mM Ches pH 9.3 with equimolar amounts of mediators. Nujol mineral oil (Perkin Elmer) was added to prevent evaporation at 80°C. The potential was measured at a platinum wire versus a Ag/AgCl reference electrode (Radiometer). Substoichiometric amounts of sodium dithionite were added for a stepwise reduction of the protein. Samples were injected in pre-heated Ar, flushed EPR tubes and subsequently rapidly frozen in liquid N_2/isopentane. The freezing time is 0.5s [91].

Results

New purification method for ferredoxin

The new purification yields 260 mg of pure ferredoxin from 400g of cells (wet weight). The protein proved to be pure according to analytical gelfiltration, electronic absorption spectroscopy and EPR. The yield is similar to the five-step purification method described previously [36]. However the two-step purification significantly reduces time and effort needed to obtain the pure protein.

Cyclic voltammetry of rubredoxin

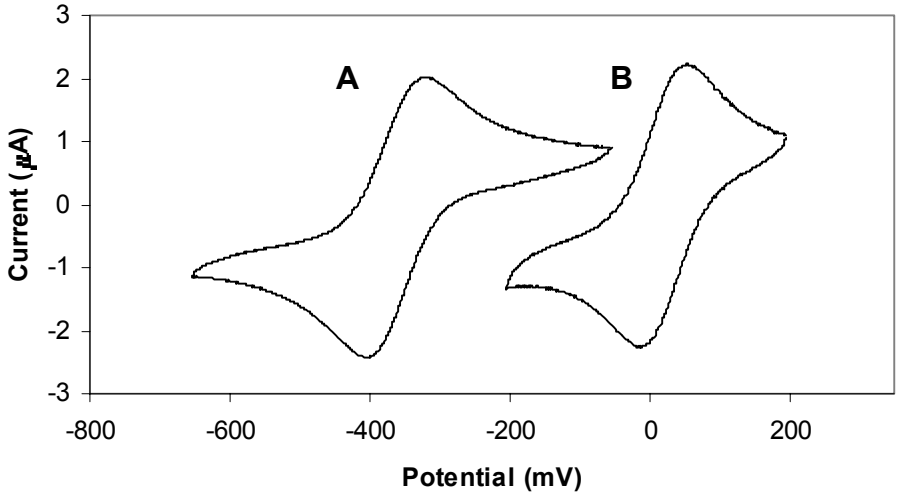

Figure 1. Cyclic voltammograms of *Pyrococcus furiosus* ferredoxin (A) and rubredoxin (B) at ambient temperature. Trace A, voltammogram of 0.14 mM ferredoxin in 25 mM Mops pH 7.2 with 6.7 mM neomycin. Experimental conditions: scan rate of 10 mV/s, temperature 24.9 °C. Trace B, voltammogram of 0.32 mM rubredoxin in 25 mM Bis-Tris pH 6.5 with 0.1 mM $SmCl_3$. Experimental conditions: scan rate of 10 mV/s, temperature 24.5 °C.

Reproducible voltammograms of rubredoxin were obtained in the temperature range from 20 to 90°C. At a scan rate of 10 mV/s the peak seperation was 51 mV where 57 mV is expected for a diffusion-controlled response. The slightly lower value

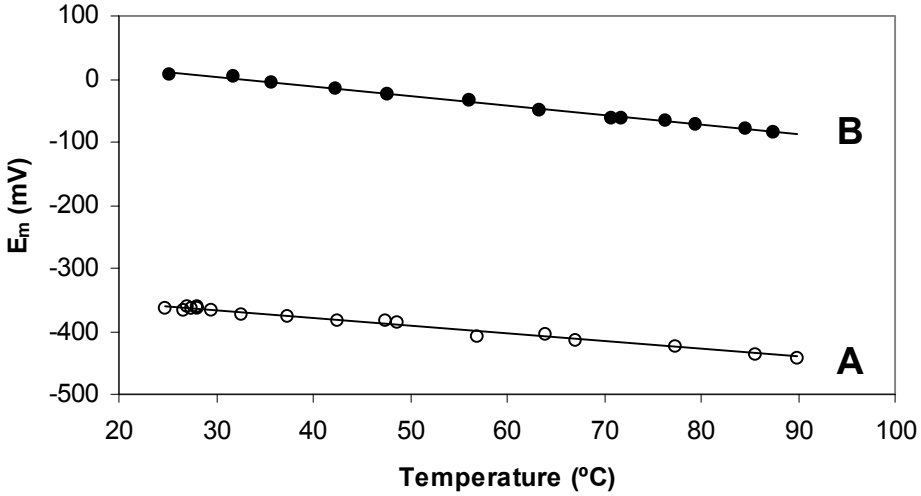

Figure 2. Temperature dependence of the midpoint potential as determined by cyclic voltammetry of *Pyrococcus furiosus* ferredoxin (A) and rubredoxin (B). Trace A, 0.14 mM ferredoxin (○) in 25 mM Mops pH 7.2 with 6.7 mM neomycin, scan rate 10 mV/s. Trace B, 0.15 mM rubredoxin (●) in 25 mM Bis-Tris pH 6.5 with 0.1 mM $SmCl_3$, scan rate 10 mV/s.

may indicate that a minor fraction of the rubredoxin adsorbs onto the electrode. However anodic and cathodic peak currents were similar, and the peak current increased linearly with the square root of the scan rate. Both observations indicate a (quasi) reversible system. A voltammogram of rubredoxin at ambient temperature is given in figure 1. The temperature dependence of the $E_{m,6.5}$ of rubredoxin is linear, contrary to previous observations [86], as can be seen in figure 2. A temperature dependence of -1.53 mV/°C is found for the $E_{m,6.5}$. Thermodynamic parameters calculated from this temperature dependence are given in table 1. Furthermore the E_m is not dependent on the pH in the range 5.6 to 10.4. This contradicts the observation of a non-linear temperature and pH dependence of the E_m reported previously [29].

Table 1. Thermodynamic parameters of *Pyrococcus furiosus* ferredoxin and rubredoxin as determined by cyclic voltammetry.

protein	$\Delta G^{\circ'}$ (kJ·mol^{-1})	$\Delta S^{\circ'}$ (J·mol^{-1}·K^{-1})	$\Delta H^{\circ'}$ (kJ·mol^{-1})
rubredoxin	0.8	-213	-62.6
ferredoxin	34.9	-184	-19.9

Cyclic voltammetry of ferredoxin

Well defined, reversible and reproducible voltammograms of the ferredoxin were recorded in the temperature range from 20 to 90°C. A voltammogram of ferredoxin at ambient temperature is given in figure 1. At a scan rate of 2 mV/s the peak seperation was 59 mV as expected for a fully reversible electron exchange at 25 °C. However a scan rate of 10 mV/s was used to make measurements at higher temperatures feasible. The peak seperation of the voltammograms used to determine the E_m (T) were between 60 and 80 mV. The temperature dependence of the E_m of

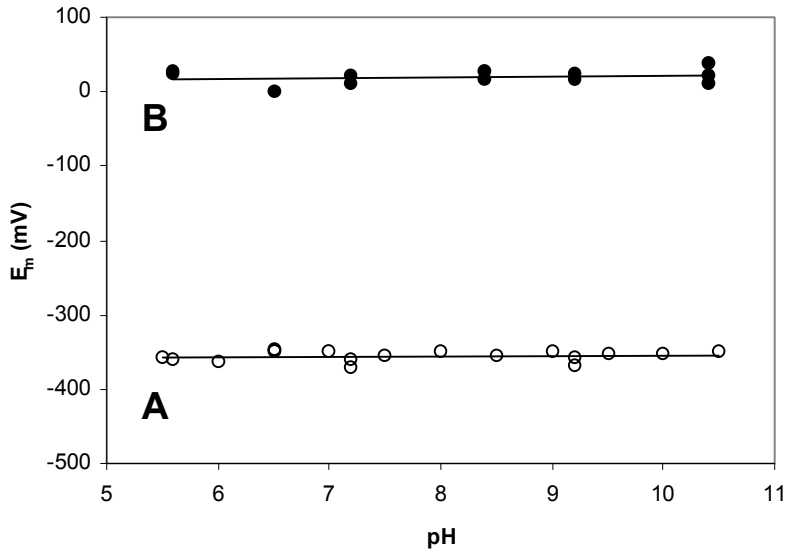

Figure 3. pH dependence of the midpoint potential as determined by cyclic voltammetry of *Pyrococcus furiosus* ferredoxin (A) and rubredoxin (B). Trace A, 0.14 mM ferredoxin (○) in 25 mM buffer with 6.7 mM neomycin, scan rate 10 mV/s. Trace B, 0.15 mM rubredoxin (●) in 25 mM buffer with 0.1 mM $SmCl_3$, scan rate 10 mV/s. The buffers used were Mes (pH 5.6), Bis-Tris (pH 6.5), Mops (pH 7.2), Taps (pH 8.4), Ches (pH 9.2), Caps (pH 10.4).

ferredoxin is linear, as can be seen in figure 2., and not biphasic as reported previously [83]. A temperature dependence of -1.23 mV/°C is found for the $E_{m,7.2}$. Thermodynamic parameters calculated from this temperature dependence are given in table 1. The E_m of the ferredoxin is independent on the pH in the range 5.6 to 9.2.

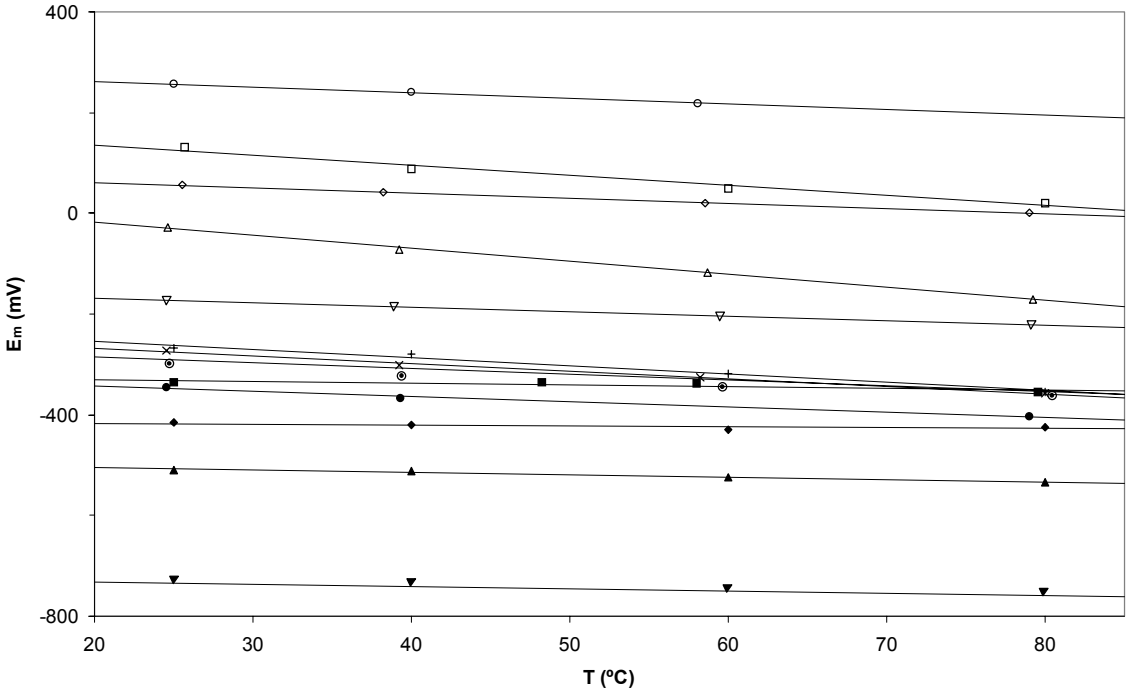

Figure 4. Apparent midpoint potentials* of redox mediators as a function of temperature. Mediators: *N,N,N',N'* tetramethyl *p*-phenylene diamine (○), 2,6-dichlorophenol indophenol (□), methylene blue (◊), indigo carmine (Δ), resorufine (∇), benzyl viologen 1 (+), anthraquinone-2-sulfonate (×), 2-hydroxy-1,4-naphtoquinone (⊙), 3,7-diamino-2,8-dimethyl-5-phenylphenazinium chloride (■), phenosafranin (●), methyl viologen 1 (◆), benzyl viologen 2 (▲), methyl viologen 2 (▼). * Of indigo carmine only the anodic peak potential.

EPR monitored redox titrations

As a standard laboratory routine we use in redox titrations a set of 13 mediators [90]. Two of these, phenazine ethosulfate and neutral red, are known to be unstable at higher temperatures. The 11 remaining dyes have been studied in cyclic voltammetry to determine reduction potential as a function of temperature. All experminents were done in 50 mM EPPS, pH 8.4 at 22 °C, in view of the minimal temperature dependence of this buffer (-0.011 pH-units per degree [92]). For indigo carmine no cathodic wave was identifyable; the asymmetric shape of the voltammogram was virtually independent of temperature (not shown). The ten

remaining dyes afforded reasonably well defined cyclic voltammograms in the temperature range 25-80°C. The cathodic-to-anodic peak separation was usually greater than the the theoretical values 29 or 59 mV for two- or one-electron transfer, respectively, indicating quasi reversibility i.e. relatively slow heterogeneous electron transfer. The apparent reduction potential was determined as the average of the potentials of cathodic and anodic peak current.

The results are presented in figure 4. All dyes have apparent E_m's that are a linear function of temperature. Thus, unlike findings with, e.g., the redox protein cytochrome c [93] the dyes do not exhibit significant structural changes in the tested temperature range. Although the curves differ in slope, the magnitude of these slopes is relatively small. As a result the subsequent E_m's at 80 °C are still reasonably spaced, therefore, this set of dyes is a good redox buffering system over the whole temperature range. The only restriction is on the oxidative side of the potential scale were *N,N,N',N'* tetramethyl *p*-phenylene diamine exhibits a voltammogram at 80 °C that rapidly decreases in amplitude during continuous cycling.

The results of the EPR monitored redox titrations of *Pyrococcus furiosus* rubredoxin and ferredoxin at ambient and high temperatures are given in Table 2. The EPR tubes were either directly frozen in liquid nitrogen (dead time, $\tau \approx 5$ s) or in cold isopentane ($\tau = 0.5$ s). The midpoint potentials obtained are virtually independent of the freezing time or the temperature at which the titrations were performed.

Table 2. Reduction potentials determined in EPR-monitored bulk titrations of *Pyrococcus furiosus* ferredoxin and rubredoxin.

protein	potential	conditions
rubredoxin	+ 80 mV	20°C to liquid N_2
	+ 76 mV	80°C to liquid N_2
	+ 79 mV	80°C to isopentane
ferredoxin	- 363 mV	20°C to liquid N_2
	- 359 mV	90°C to isopentane

Discussion

The redox chemistry of P. furiosus rubredoxin is regular

Proteins of hyperthermophilic origin clearly differ from mesophilic and psychrophilic counterparts in their intrinsic thermostability. The molecular nature of this added stability is beginning to emerge (cf [94]), however, this matter has not been addressed in our present research. We seek to answer the question whether hot redox biochemistry has molecular characteristics sufficiently unusual for a meaningful distinction, in terms of structure-function relationships, from regular redox biochemistry. Several claims in the literature regarding hyperthermophilic redox proteins with quite unexpected properties [29, 83, 95], followed-up by several claims of explanation by theoretical modelling [86, 87], have incited us to initiate a systematic research effort into this matter.

The mononuclear, high-spin Fe(III/II) site in rubredoxins is tetrahedrally coordinated by four cysteinate ligands. The reduction potential of this center is expected to be essentially independent of pH, because protonation of the thiolate(s) would lead to demetallation, and Cys has no protonatable side groups. Consistent with this prediction we have previously found, in a direct electrochemical study, the redox potential of *Megasphaera elsdenii* rubredoxin to be virtually independent of pH in the pH range 5.5-9.5 [96]. In contrast to this observation Adams reported the E_m of *P. furiosus* rubredoxin to be significantly dependent on the pH, with $\Delta E \approx -25$ mV/pH at 20 °C, on the basis of EPR-monitored redox titrations. In addition, the E_m was reported [29] to be non-linearly (approximately quadratically, cf [86]) dependent on the temperature, while, to our knowledge, every $E_m(T)$ plot reported thus far for any redox protein is linear in the temperature. Direct voltammetry, however only at room temperature, on a synthetic rubredoxin identical to the *P. furiosus* rubredoxin has been reported giving the same E_m value as EPR monitored redox titration on the native protein [97].

Smith and collaborators have proposed to explain this non-linearity on the basis of a protein dielectric constant that varies non-linearly with temperature [86]. Also, Swartz and Ichiye have carried out molecular dynamics simulations to evaluate temperature dependent differences in structure, solvation and energies of *P. furiosus* rubredoxin. These authors claim that a temperature-dependent calculated average

electrostatic potential at the Fe site, $\Delta\varphi$, correlates very well with the experimentally determined temperature-dependent E_m [87]. In the present work previously reported experimental $E_m(T)$ results have been found to be erroneous, therefore, the validity of the theoretical studies on rubredoxin [86, 87] based on these results, has also been falsified.

The $E_m(T)$ of small proteins can not be monitored with EPR

From optically-monitored titration studies the E_m of horse heart cytochrome *c* is known to be linearly dependent on the temperature with a break point around 45 °C [93]. We have confirmed this in direct cyclic voltammetric experiments (not shown). We have also found the redox potential of rubredoxin and ferredoxin from *P. furiosus* to be linearly dependent on the temperature over the whole range measured when determined in cyclic voltammetry. When the E_m's of these two proteins is determined in bulk, mediated titrations at room temperature and at high temperature, with subsequent monitoring in low-temperature EPR spectroscopy, we find apparent E_m values that are independent of the temperature and that correspond approximately to the voltammetrically determined E_m's when extrapolated to a temperature of 0 °C or less. The result is independent of the time of freezing the EPR samples, as freezing the filled, thermally equilibrated EPR tubes in liquid nitrogen (dead time, $\tau \approx 5$ s) or in cold isopentane ($\tau = 0.5$ s) gives identical results.

To explain the above results we propose that the small electron-transferring proteins, such as the ones studied by us, have sufficient flexiblity, both in the oxidized and in the reduced state, to allow for rapid (i.e. within 0.5 s) structural adjustment upon temperature change such that the frozen state always approximately corresponds to the equilibrated state near the freezing point of the aqueous solution. A major implication of this proposal is that EPR-monitored redox titrations of small proteins can only determine E_m's near 0 °C.

Our experimental EPR-titration results on rubredoxin and ferredoxin are different from those previously reported by Adams [29]; we are unable to reproduce those results.

P. furiosus ferredoxin redox chemistry is regular

The coordination of clusters in most iron-sulfur proteins is by Cys only, therefore, also here no significant dependence of E_m on the pH is expected. Indeed, only very minor dependencies were found in a study of seven different [4Fe-4S] containing proteins [98]. However, the [4Fe-4S] cluster in *P. furiosus* ferredoxin has one aspartate as a presumably monodentate ligand [99] and a significant pH dependence of the E_m is possible. However, our voltammetric study shows the E_m to be virtually independent of pH. A similar conclusion was recently reached for the *P. furiosus* ferredoxin when expressed in *Escherichia coli* [84].

In contrast to the early EPR study [29, 83] our work also indicates the E_m to have a regular linear dependence on temperature without break points up to 90 °C, and similar results have now been reported for the heterologously expressed wild type ferredoxin [84]. It should be noted, however, that in the latter study the voltammetrically-derived E_m values were reported as plain numbers without presentation of primary data or discussion of uncertainties. This is remarkable because in two earlier studies from the same laboratory rather sluggish responses of ferredoxin were reported as evidenced by considerably broadened differential pulse voltammograms even for very low potential scan rates [85, 100]. However, as reported in the present work, well defined and reversible voltammograms can be obtained even at high temperatures.

Smith et al. have also attempted to theoretically explain the break point in the initially reported $E_m(T)$ curve of ferredoxin [86]. Now that these early data have been found to be incorrect, both for the native protein and for the heterologously expressed wild type ferredoxin, the theoretical analysis has also become irrelevant.

Acknowledgements

This work was supported by the Gebiedsraad Chemische Wetenschappen with financial aid from the Nederlandse Organisatie voor Wetenschappelijk Onderzoek (NWO).

Chapter 3

Pyrococcus furiosus glyceraldehyde-3-phosphate oxidoreductase has comparable $W^{VI/V}$ and $W^{V/IV}$ reduction potentials and unusual [4Fe-4S] EPR properties

Peter -L. Hagedoorn, J. Robert Freije, Wilfred R. Hagen

Published in: FEBS Lett. 462, pp. 66-70, 1999.

Pyrococcus furiosus **glyceraldehyde-3-phosphate oxidoreductase has been characterized using EPR monitored redox titrations. Two different W signals have been found. W_1^{5+} is an intermediate species in the catalytic cycle, with the midpoint potentials: $E_m(W^{VI/V})$=-507 mV and $E_m(W^{V/IV})$=-491 mV. W_2^{5+} represents an inactivated species with $E_m(W^{VI/V})$=-329 mV. The cubane cluster exhibits both S=3/2 and S=1/2 signals with the same midpoint potential: $E_m([4Fe\text{-}4S]^{2+/1+})$=-335 mV. The S=1/2 EPR signal is unusual with all g-values below 2.0. The titration results combined with catalytic voltammetry data are consistent with electron transfer from glyceraldehyde-3-phosphate first to the tungsten center, then to the cubane cluster and finally to the ferredoxin.**

Introduction

Pyrococcus furiosus is a hyperthermophilic archaeon growing optimally at 100 °C. It has three tungsten containing oxo-transferases: aldehyde oxidoreductase (AOR), formaldehyde oxidoreductase (FOR) and glyceraldehyde-3-phosphate oxidoreductase (GAPOR). All three enzymes presumably have ferredoxin as a natural electron carrier. Recently the crystal structures of both AOR and FOR have been published [45, 55] showing the tungsten coordinated by a bis-pterin cofactor and with a [4Fe-4S] cluster close by. AOR has been shown to exhibit several different W^{V} EPR signals at different potentials [46]. Only one signal, the "low potential signal", has been attributed to a catalytically competent species undergoing two subsequent one electron reductions from W^{VI} to W^{IV}. *P.furiosus* GAPOR is to date the only enzyme of the three with a known biological function [59]. It is highly specific for the substrate glyceraldehyde-3-phosphate. Contrarily, FOR and AOR have a broader in vitro specificity for short-chain and longer chain aldehydes [44, 56]. The sequence homology with AOR (15 % identity) [60] and FOR (23 % identity) [56] is relatively low compared to the homology between AOR and FOR (40% identity) [56]. GAPOR has not been characterized in detail spectroscopically. Only a W^{V} EPR signal with g-values near 1.96, 1.89 and 1.83 has been reported for reduced enzyme [60, 101]. We have characterized GAPOR using EPR monitored redox titrations. The results have been compared with what is known about the other two tungsten containing oxo-transferases from *P.furiosus*.

Materials and methods

Cultivation and protein purification

Pyrococcus furiosus (DSM 3638) was cultivated as previously described [88]. Cells were broken by osmotic shock, diluting with 5 volumes 30 mM Tris/HCl, pH 8.0 (anaerobic) containing 1 mM DTT, 1mM cystein, 5 mM $MgCl_2$, 0.1 mg/L DNase I, 0.1 mg/L RNase. Cystein was used as a mild reductant instead of dithionite, which is an inhibitor for GAPOR [59]. A cell-free extract was obtained as the supernatant after 1 hour centrifugation at 26,000 g. GAPOR was purified anaerobically as described previously [60]. GAPOR activity was measured as described [60]. SDS-

polyacrylamide gel gelectrophoresis was performed on Phast System (Pharmacia) holding a PhastGel SDS 8-25%. The purified GAPOR had a specific activity of 30 U/mg at 50°C which compares well with the 25 U/mg previously described with the same purification procedure [60]. The purified protein was shown to be pure by SDS-PAGE (not shown).

EPR spectroscopy and EPR monitored redox titrations

GAPOR was investigated with a dye mediated reductive titration as described previously [90] at 50°C in 30 mM Tris/HCl, pH 8.0, using 47 µM GAPOR. Sodium dithionite was used as reductant to reach low potentials. However sodium dithionite is an inhibitor of GAPOR activity. Therefore another titration without mediators was performed using the substrate/product couple glyceraldehyde-3-phosphate/3-phophoglycerate (GAP/3PG) to poise the potentials. Potentials were calculated using the literature value for the GAP/3PG couple, which is -614 mV vs. NHE at 50°C and pH 8.0 [102]. GAPOR was incubated with different ratios of GAP/3PG for 10 minutes at 50°C. This temperature was chosen to obtain a rapid equilibrium, but at the same time to prevent thermal degradation of GAP. The GAPOR concentration ranged from 65-80 µM. The GAP and 3PG concentrations ranged from 0.1-480 mM. Light reduced GAPOR was prepared by irradiating 35 µM GAPOR, 25 µM deazaflavin, 2 mM EDTA in 30 mM Tris/HCl, pH 8.0 with light from a 150 W tungsten lamp for 60 minutes at ambient temperature. Samples were rapidly frozen in cold isopentane. EPR spectra were recorded on a Bruker ER-200D spectrometer with peripheral equipment and data handling as has been described previously [103]. W^V EPR signals were simulated as previously described [47].

In vitro reconstitution of electron transfer chain

Voltammograms of *P.furiosus* ferredoxin were recorded as previously described [104]. The 20 µl droplet contained 0.15 mM Fd in 25 mM Mops pH 7.25 plus 6.7 mM neomycin as promoter. GAPOR was added to a final concentration of 3 µM and GAP was added to a final concentration of 8 mM. Catalytic waves were recorded with a scan rate of 10 mV/s. The pseudo-first order rate constant was calculated from the ratio of catalytic and diffusion controlled current using a numerical method adapted from Nicholson and Shain [105].

Results

EPR spectroscopy

Based on the amino acid sequence and the structures of AOR and FOR, one [4Fe-4S] cluster and one tungsten center are expected for GAPOR. The $[4Fe\text{-}4S]^{2+}$ can undergo a one electron reduction at low potentials to $[4Fe\text{-}4S]^{1+}$, which is paramagnetic. The $[4Fe\text{-}4S]^{1+}$ is expected to show S = 3/2 or S = 1/2, or both EPR signals. The tungsten center is expected to undergo two subsequent one electron reductions from W^{VI} to W^{IV}. The intermediate W^{V} is paramagnetic and shows a typical S = 1/2 signal with all g-values usually below 2.0, which is still observable at

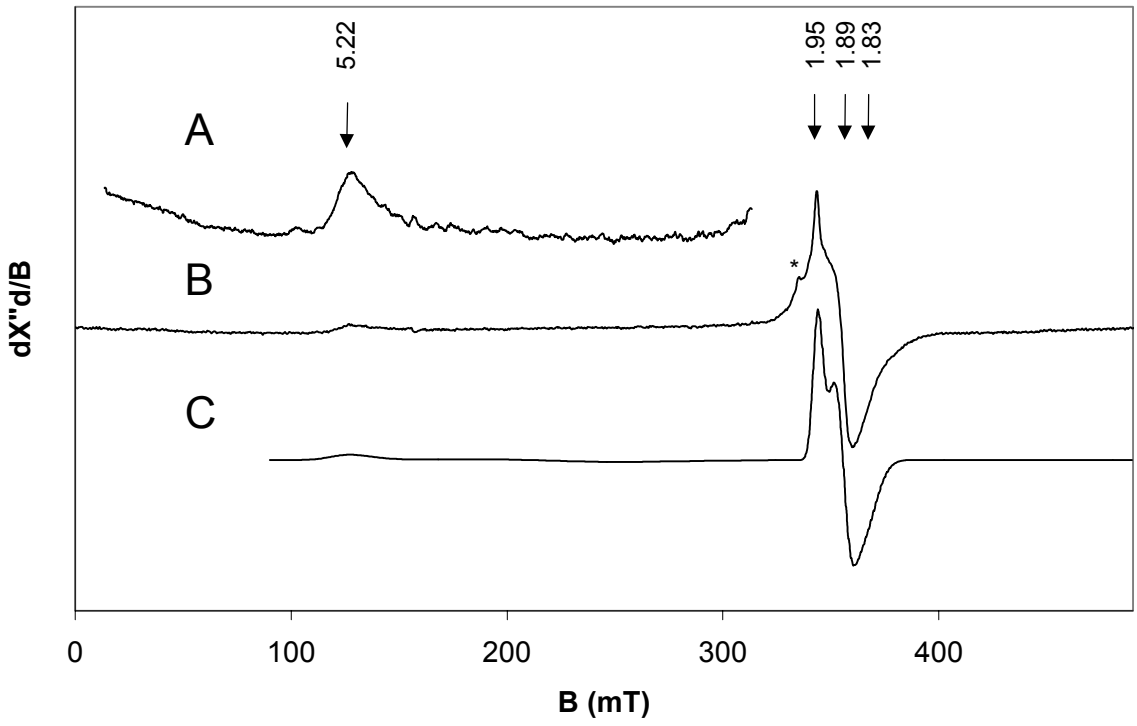

Figure 1. $[4Fe\text{-}4S]^{1+}$ EPR signals of *Pyrococcus furiosus* GAPOR poised at -664 mV in the GAP/3PG titration. Trace A, S=3/2 signal. EPR conditions: microwave frequency, 9.41 GHz; modulation frequency, 100 kHz; modulation amplitude, 1.0 mT; microwave power, 200 mW; temperature, 7.5 K. Trace B., $[4Fe\text{-}4S]^{+}$ S=3/2 and S=1/2 signal. EPR conditions: same as for trace A except: gain, 10 times lower and temperature, 11.8 K. Trace C. Simulation of S = 1/2 and S = 3/2 signals. Simulation parameters S = 1/2: $g_{x,y,z}$ = 1.830, 1.885, 1.952; line $width_{x,y,z}$ = 0.032, 0.019, 0.013 (in g-value units). Simulation parameters S = 3/2: : $g_{x,y,z}$ = 1.398, 1.920, 5.218; line $width_{x,y,z}$ = 0.450, 0.450, 0.450. The minor feature indicated with an asterisk is not part of $[4Fe\text{-}4S]^{1+}$ EPR signals because it has different power saturation behaviour and the intensity is independent of potential.

temperatures as high as 100 K. The redox titrations of GAPOR produced S = 3/2 and S = 1/2 signals that can be attributed to the $[4Fe\text{-}4S]^{+}$ cluster (Figure 1. and Figure 2.). The same signals were observed in deazaflavin/light reduced GAPOR (not shown). The S = 1/2 signal has $g_{z,y,x}$ = 1.95, 1.89, 1.83. Integration of the S = 1/2 signal yielded 0.43 spins/molecule. The signal could not be exactly simulated assuming only g-strain broadening (Figure 2.). The experimental spectrum has broad wings at high and low field that are not reproduced in the simulation. Apparently the $[4Fe\text{-}4S]^{1+}$ interacts with another paramagnet close by. Of the S = 3/2 signal only a low field feature at g = 5.22 is observed. No additional signals, with higher g-values, were observed at temperatures from 4.5 to 9.0 K, where the S = 3/2 signal is best measured, that could account for the g_z of the higher doublet. Apparently the effective g_z-values are almost equal for the two doublets. Under the standard spin Hamiltonian $H = D[S_z^2 - S(S+1)] + E(S_x^2 - S_y^2) + \beta B \cdot g \cdot S$ this can be explained either with a $D >> h\upsilon$ (= 0.31 cm^{-1}) , g ≈ 1.92 and E/D ≈ 1/3 or with a $D/h\upsilon \approx 1.30$ (i.e. D ≈ 0.41 cm^{-1}), g ≈ 2.00 and E/D ≈ 1/3. The S = 3/2 signal can approximately be simulated assuming E/D = 1/3 and g = 1.92. The ratio (S = 1/2):(S = 3/2) is estimated to be 1:2 using the simulations for both spectra. If the S = 3/2 signals represents the sum of both doublets the total quantitation of the $[4Fe\text{-}4S]^{1+}$ signals is 0.86 spins/mol. If only the ground state doublet of the S = 3/2 species is observed the total quantitation would be 1.3 spins/mol.

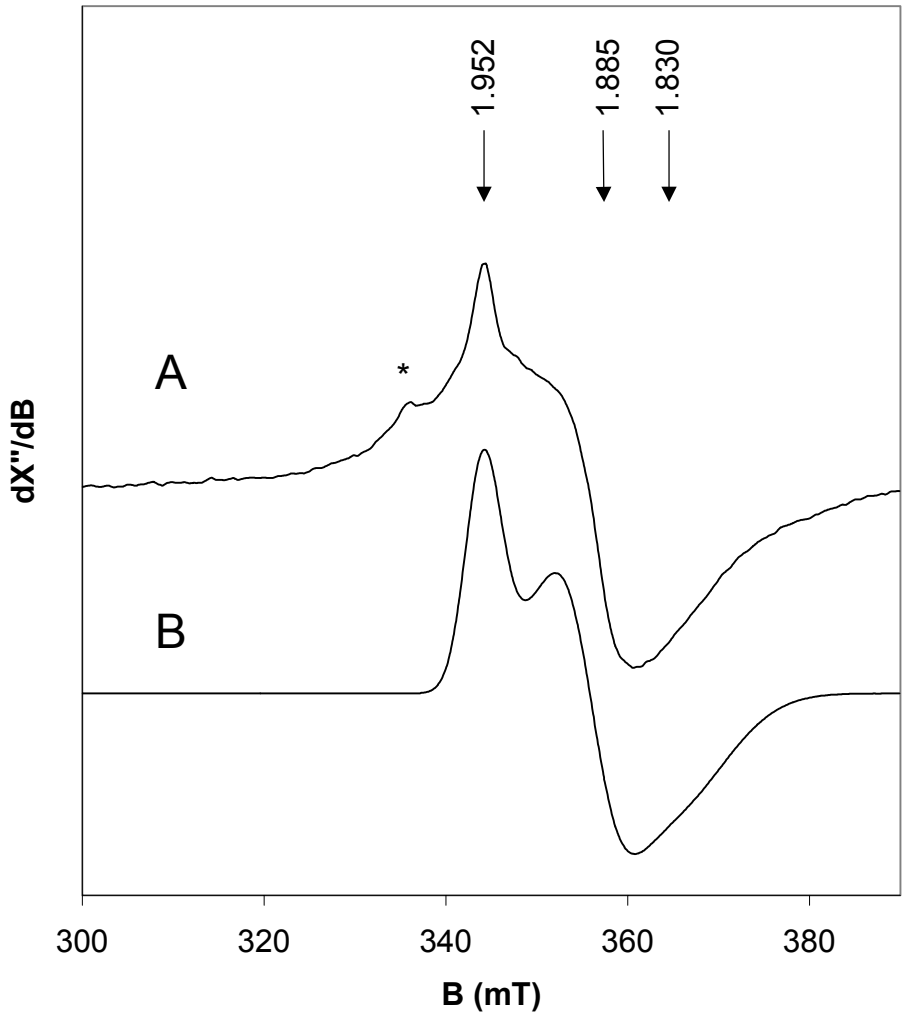

Figure 2. $[4Fe\text{-}4S]^{1+}$ S = 1/2 EPR signal of GAPOR poised at -664 mV in the GAP/3PG titration. Trace A. Experimental spectrum. EPR conditions: microwave frequency, 9.41 GHz; modulation frequency, 100 kHz; modulation amplitude, 1.0 mT; microwave power, 200 mW; temperature, 11.8 K. Trace B. Simulation of A. Simulation parameters given in legend to figure 2. The signal (*) is not part of $[4Fe\text{-}4S]^{1+}$ EPR signal (cf legend to figure 2.).

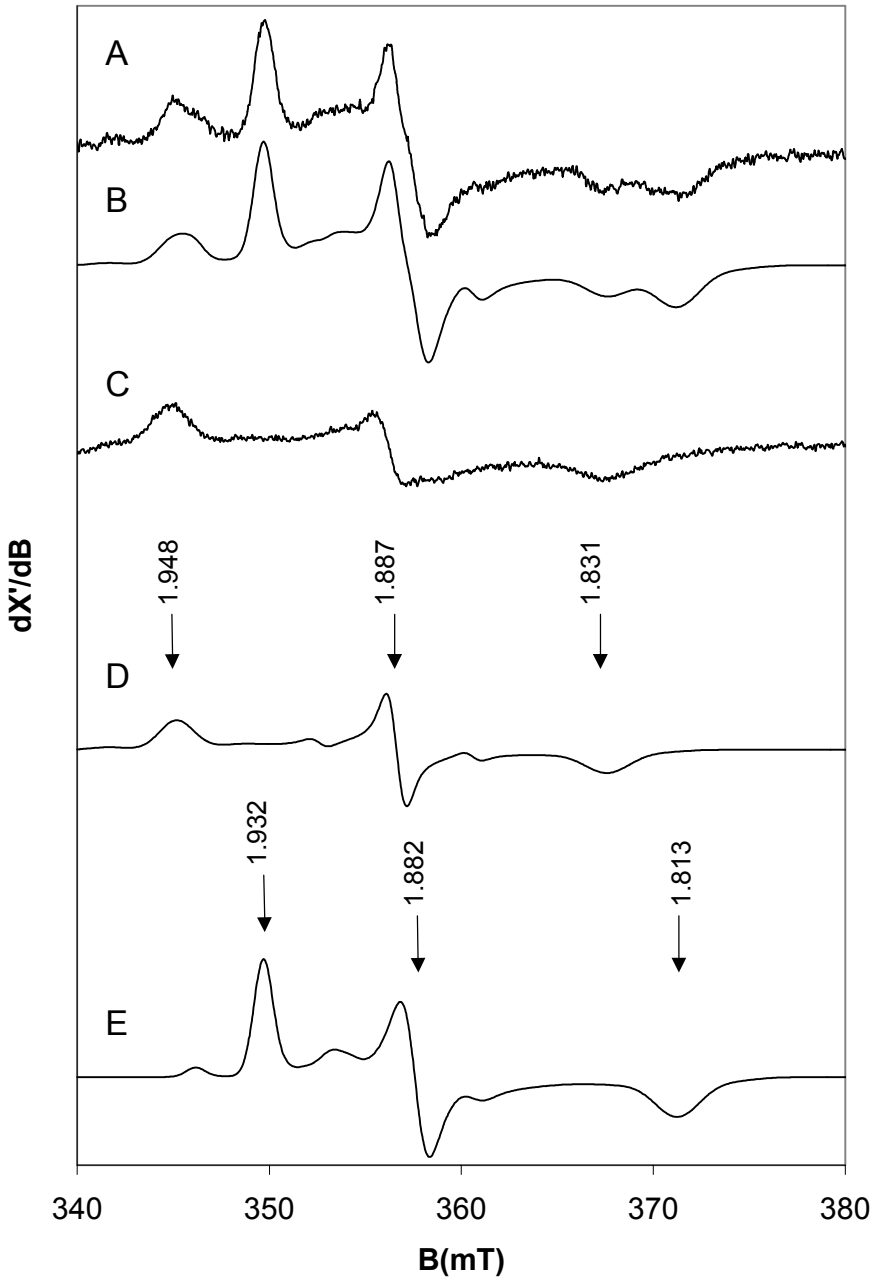

Figure 3. EPR spectra of *Pyrococcus furiosus* GAPOR W^V. Trace A, experimental spectrum with potential poised at -510 mV in the GAP/3PG titration. Trace B, sum of simulation D and simulation E. Trace C, experimental spectrum with potential poised at -674 mV. Trace D, simulation of C. Trace E, simulation of A - D. EPR conditions: microwave frequency, 9.42 GHz; modulation frequency, 100 kHz; modulation amplitude, 0.5 mT; microwave power, 3.2 mW; temperature, 34 K.

A W^V EPR signal is detected at potentials lower than -300 mV (Figure 3) which resembles the W^V signals that have been reported for GAPOR previously [60, 101]. Integration of this W^V signal yield 0.12 spins/molecule. However also another W^V signal is found with different g-values and a quantity up to 0.30 spins/molecule. This signal has not been reported previously. The latter signal will be designated as $W_1{}^V$, and the other, with the lower quantity, as $W_2{}^V$. The designations used in the literature for FOR and AOR (i.e. low, mid and high potential W^V) are not functional for GAPOR, since both W^V signals are found are low potentials. The simulation parameters for both tungsten EPR signals are given in table 1. The saturation behavior at 19 K of the tungsten signals and the S = 1/2 signal of the [4Fe-4S] cluster can be seen in a power plot Figure 4.

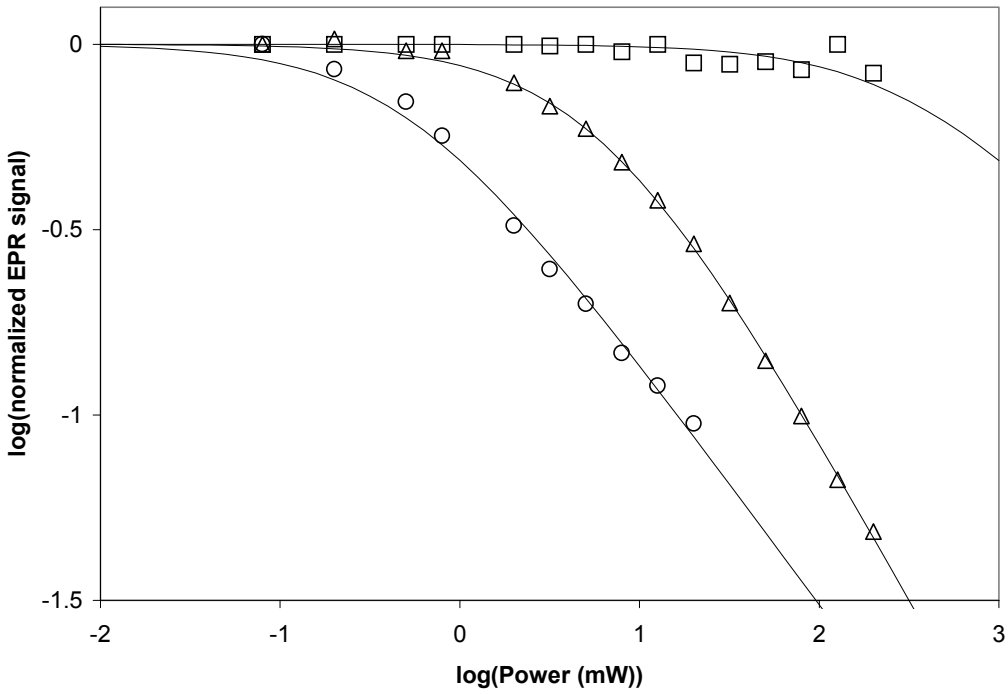

Figure 4. Saturation plot of *Pyrococcus furiosus* GAPOR W^V and $[4Fe\text{-}4S]^+$ S=1/2 signals at 19K. Trace A, $[4Fe\text{-}4S]^+$ S=1/2 signal (□). Trace B, $W_1{}^V$ signal (Δ). Trace C, $W_2{}^V$ signal (○). Normalized EPR signal ≡ (signal/√power)/(low-power signal/√low-power).

Table 1. EPR parameters of *Pyrococcus furiosus* GAPOR W^{5+} species.

species	g_z	g_y	g_x	A_z (mT)	A_y (mT)	A_x (mT)	W_z (mT)	W_y (mT)	W_x (mT)
W_1	1.923	1.882	1.813	7.0	6.0	6.0	0.09	0.10	0.20
W_2	1.948	1.887	1.831	7.0	8.0	6.0	0.20	0.07	0.15

Dye mediated redox titration

The results of the dye mediated titration with sodium dithionite is presented in Figure 5. The midpoint potentials of the $[4Fe\text{-}4S]^{2+/1+}$ and $W_2^{VI/V}$ couples have been determined and are given in Table 2. The standard deviations for the fits were between 5 and 15 mV for all the potentials given in table 2. The actual uncertainty may be larger depending on the number of samples in a titration curve. No reduction to W_2^{IV} was found. W_1^{V} was not found in the dye mediated redox titration. The S = 3/2 and S = 1/2 signals attributed to $[4Fe\text{-}4S]^{1+}$ have the same midpoint potential.

Substrate/product redox titration

In the GAP/3PG titration both W^{V} signals were found. No redox changes for the W_2 species was found (Figure 5). The E_m values of the W_1^{V} species can be seen in Table 2 and are consistent with two subsequent one electron reductions from W^{VI} to W^{IV}. The maximum quantity of W_1^{V} is 0.30 spins/molecule while the quantity of the W_2^{V} species is unchanged during the titration and amounts only 0.09 spins/mol (cf in Figure 5). W_2 is likely due to inactivated enzyme. The S = 1/2 and S = 3/2 signals of the cubane cluster are also observed. The GAP/3PG titration gives a much lower apparent E_m-value for the $[4Fe\text{-}4S]^{2+/1+}$ couple because electrons must flow via the tungsten in this titration (Figure 5). Therefore, the tungsten center has to be reduced before the cubane cluster can be reduced. This is of course not the case with the dye mediated titration. The results of the dye mediated and GAP/3PG titration are complementary.

Table 2. Reduction potentials of *Pyrococcus furiosus* GAPOR W center and [4Fe-4S] cluster. Reductive dye mediated and GAP/3PG titrations performed at 50°C in 30 mM Tris/HCl, pH 8.0.

Couple	Potential vs. NHE (mV)
$W_1^{VI/V}$	-506
$W_1^{V/IV}$	-491
$W_2^{VI/V}$	-329
$[4Fe\text{-}4S]^{2+/1+}$ S=1/2	-336
$[4Fe\text{-}4S]^{2+/1+}$ S=3/2	-333

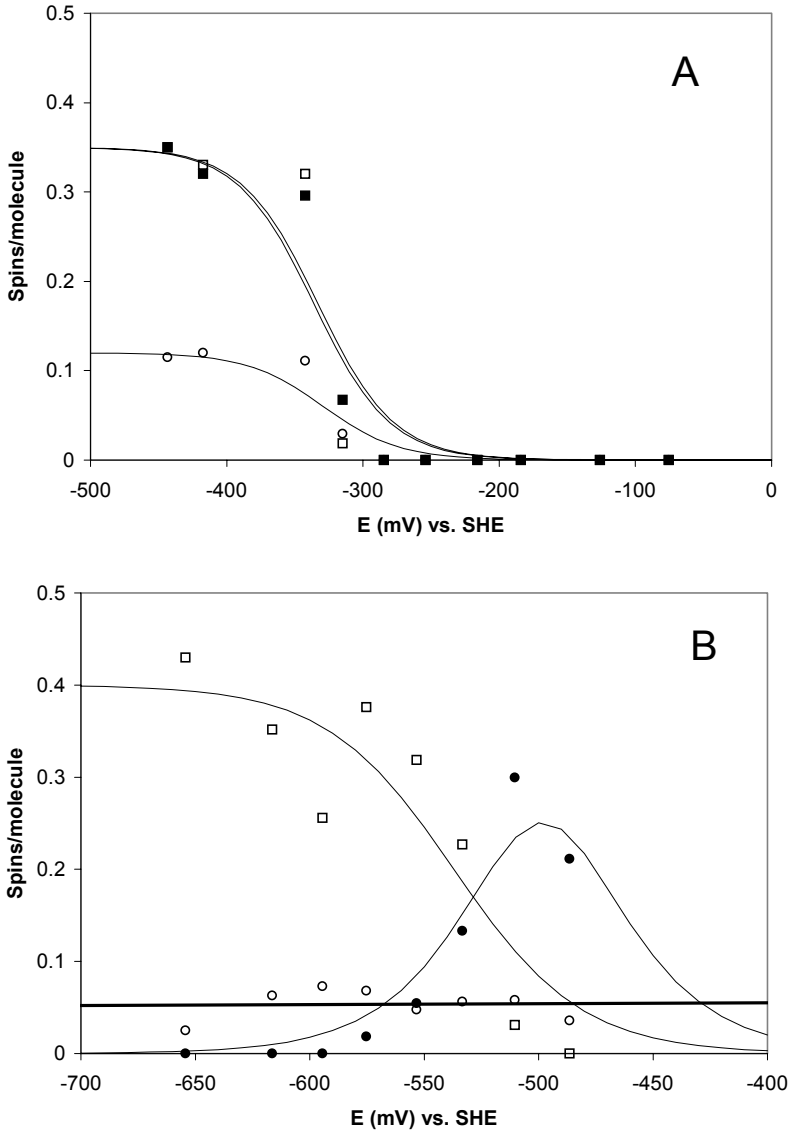

Figure 5. Redox titrations of *P. furiosus* GAPOR. Dye mediated redox titration (A) and GAP/3PG redox titration (B). The $[4Fe\text{-}4S]^{1+}$ S=3/2 signal (■) is monitored at g = 5.22 with the EPR conditions as in legend to figure 2. The $[4Fe\text{-}4S]^{1+}$ S=1/2 signal (□) is monitored as the amplitude at g_y = 1.890 with the same EPR conditions. The W_1^V signal (●) is monitored at g_z = 1.923 and the W_2^V signal (○) is monitored at g_z = 1.948 at 40K with EPR conditions as in legend to Figure 1. The solid lines are fits for n = 1 redox transitions with the midpoint potentials given in Table 2.

In vitro reconstitution of electron transfer chain

The cyclic voltammogram of Fd only shows a reversible electron transfer between the Fd and the electrode (Figure 6). The peak seperation is 60 mV which is close to the expected 63 mV for a fully reversible system at 55°C [105]. Diffusion of Fd from the bulk solution to the electrode and not the electron transfer from Fd to the electrode is rate limiting. Addition of GAP or GAPOR separately to Fd did not significantly change the voltammogram of Fd. However if GAP was added to GAPOR a catalytic wave appeared as a large increase of the anodic peak as can be seen in figure 6. The catalytic current increased with temperature, but was already detectable

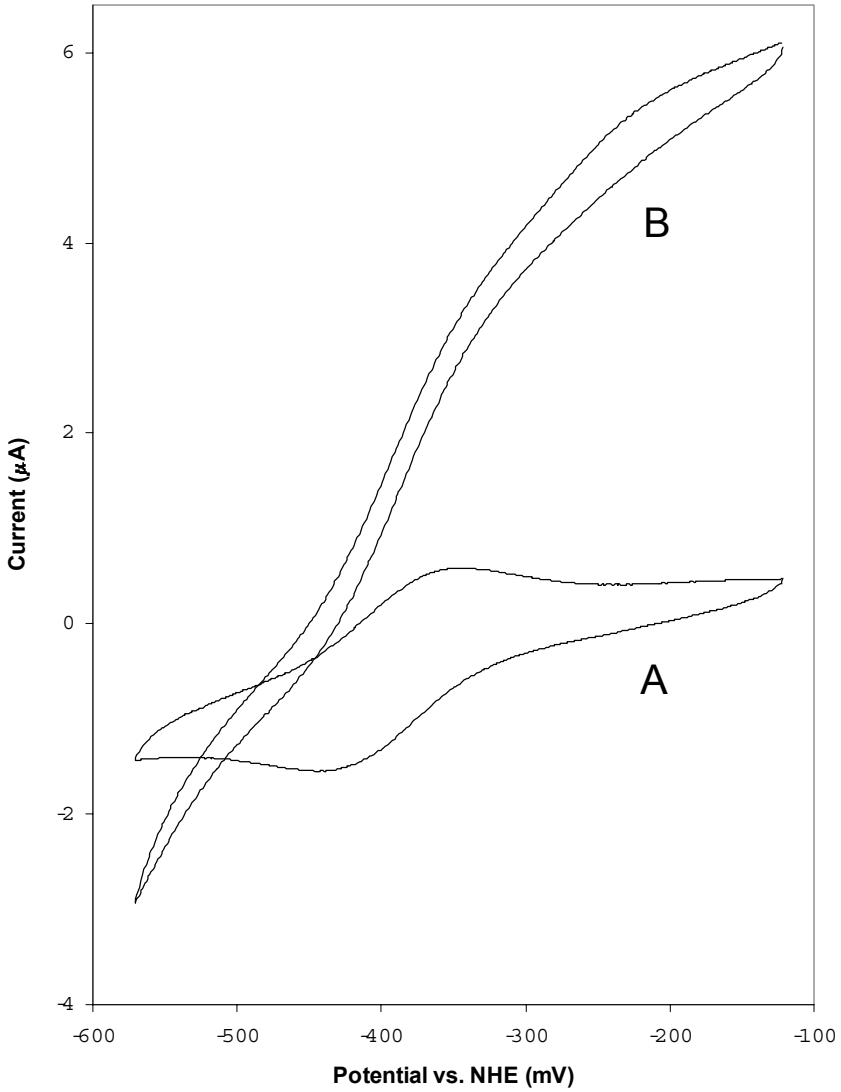

Figure 6. Cyclic voltammograms of *Pyrococcus furiosus* ferredoxin without (A) and with GAPOR and GAP (B) at 55°C. Trace A, *Pyrococcus furiosus* ferredoxin 0.15 mM in 25 mM Mops pH 7.2 with 6.7 mM neomycin, scan rate 10 mV/s. Trace B, same as in A with 3 µM GAPOR and 8 mM GAP.

at room temperature. Using the ratio of the catalytic and the diffusion-controlled current the pseudo first order rate constant of the rate determining step can be calculated. The rate determining step can be either the GAP oxidation or the Fd reduction by GAPOR because, as has been concluded from the Fd voltammogram, the Fd oxidation at the electrode is not rate limiting. At 55 °C and pH 7.25 a pseudo first order rate constant of 36 s^{-1} was found, which compares reasonably well to the value of 94.5 s^{-1} based on the V_{max} reported for GAPOR with Fd as electron acceptor at 70 °C and pH 8.4 (90 U/mg) [59]. The rate constant was not determined at 70 °C because GAP was unstable at that temperature.

Discussion

W_1^{5+} is an intermediate state of the tungsten during the catalytic cycle

The W_1 undergoes a two step one electron transfer, similar to the W in *P. furiosus* AOR and many molybdenum enzymes [46]. Both E_m values are low and close to the E_m value calculated for the GAP/3PG couple [102]. The quantity of the W_1^V is maximally 0.30 spins/mol. This can be explained assuming that the midpoint potential for the $W_1^{VI/V}$ couple is 15 mV more negative than for the $W_1^{V/IV}$ couple and that 90 % of the tungsten is W_1 (Figure 5 and Table 2). W_2 is a minority species of only 10 % of the tungsten and undergoes only a one-electron reduction from W_2^{VI} to W_2^V in the potential range tested. Although crossing of midpoint potentials of the $M^{VI/V}$ and $M^{V/IV}$ couples has been found for several molybdenum containing oxotransferases [106-108], this is the first example for a tungsten enzyme. GAPOR has only two different W^V species, not as many as have been found for AOR [46] and FOR [43, 101]. This confirms that the signals, other than the "low-potential" signals, that do not undergo a two step one electron transfer, do not represent catalytically relevant species. Even though the titrations have been performed at 50 °C, the E_m values may refer to a protein conformation at a much lower temperature. *P.furiosus* ferredoxin and rubredoxin have been shown to take their conformation corresponding to the freezing point of the solution upon rapid freezing [104]. However, temperature dependent redox titrations of *P. furiosus* AOR and FOR showed significant shifts in the midpoint potentials of the tungsten centers and cubane clusters, indicating that for complex enzymes the high temperature conformation may at least partially be

maintained in the frozen samples [Hagedoorn, P.L., Landa I., Hagen, W.R., unpublished results.]. Investigations in the temperature dependent redox chemistry of the tungsten enzymes of *P. furiosus* are in progress.

The [4Fe-4S]$^{+}$ exhibits an S = 3/2 and an unusual S = 1/2 EPR signal

As is common for many cubane clusters, the [4Fe-4S]$^{+}$ cluster of GAPOR exhibits both a S = 3/2 and a S = 1/2 EPR signal. The cubane in AOR, however, has been found to be S = 3/2 only [46]. The *Thermococcus litoralis* FOR cubane cluster exhibit both S = 3/2 and S = 1/2 signals [57]. The S = 3/2 signal of GAPOR [4Fe-4S]$^{1+}$ is rhombic with unknown D. A large D of +4 cm^{-1} has been found for the [4Fe-4S]$^{1+}$ S = 3/2 signal of *P. furiosus* AOR [46] and a small D of -0.7 cm^{-1} has been found for the A33Y mutant of *P. furiosus* Fd [109]. The signal also looks similar to the S = 3/2 signal found for *T.litoralis* FOR, of which only a low field feature at g = 5.39 was observed [57]. However no detailed analysis of that signal is currently available.

The S = 1/2 signal of GAPOR [4Fe-4S]$^{1+}$ is different from those of most other cubane clusters. All g-values are below 2.0, which is unusual. Similar EPR spectra have only been reported for putative [4Fe-4S] clusters in NADH reduced glutamate synthase [110] and NADPH reduced sulfide dehydrogenase (ferredoxin NADPH oxidoreductase) [111]. As can be seen in the saturation plot (Figure 4) the S = 1/2 species is relatively fast relaxing, which is normal for these type of clusters [112]. Therefore it is unlikely that it is a W^{5+} signal. The broad S = 1/2 signal appears to reflect dipolar interaction with another center. The only paramagnet close enough to interact with is W in the same molecule (GAPOR is monomeric). However the [4Fe-4S]$^{1+}$ S = 1/2 signal is already found at potentials were all the W_1 is expected to be W^{VI} which is diamagnetic (Figure 5), although the effect that dithionite may have on W_1 is not known.

The previous conclusion may not be valid if the midpoint potentials of W_1 would strongly shift towards more negative values as a response to the presence of substrate and/or product. In the dye mediated titration reduction of the [4Fe-4S] cluster may then coincide with the reduction of $W_1{}^{VI}$ causing the anomalous S = 1/2 signal. We consider this an unlikely possibility because in addition to the presumed interaction signal also the signals from non-interaction centers should be observable unless a strong positive cooperativety would occur.

Interaction of the cubane with W_2 is unlikely because it is a minority species of only about 10 % of the total enzyme. The immediate surrounding of the cubane cluster may contribute to the unusual EPR spectrum. Sequence alignment of the AOR family members has shown that between C334 and C338 there is a proline residue which is not present in AOR and FOR [60].

The electron transfer chain from GAP to Fd can be reconstituted in vitro

The electrochemical data clearly show that GAPOR can reduce Fd using GAP. The GAP/3PG titrations demonstrated that the tungsten has to be reduced before the cubane cluster can be reduced, even though dithionite reduces the cubane cluster first. Taken together with the values for the midpoint potentials obtained from the bulk titrations, an electron transfer pathway from GAP first to the W then to the [4Fe-4S] cluster and finally to the [4Fe-4S] cluster of Fd can be proposed. This pathway has already been proposed for *P.furiosus* FOR based on the position of the redox centers in the enzyme [55]. No evidence, e.g. pterin radical signals [113], has been found that the pterin cofactor participated in the redox chemistry of GAPOR.

Acknowledgments

We thank professor Michael Johnson for his useful comments on the original manuscript. This work was supported by the Gebiedsraad Chemische Wetenschappen with financial aid from the Nederlandse Organisatie voor Wetenschappelijk Onderzoek (NWO-CW)

Chapter 4

Steady-state kinetics and tungsten co-ordination of the glycolytic enzyme glyceraldehyde 3-phosphate oxidoreductase from the hyperthermophilic archaeon *Pyrococcus furiosus*

P.-L. Hagedoorn, J.M. Charnock, J.H. Slits, J.R. Freije, C.D. Garner, W.R. Hagen

Glyceraldehyde-3-phosphate oxidoreductase (GAPOR), aldehyde oxidoreductase (AOR), and formaldehyde oxidoreductase (FOR) are tungsten-containing aldehyde oxidoreductases from the hyperthermophilic archaeon *Pyrococcus furiosus*. GAPOR functions as a glycolytic enzyme, whilst AOR and FOR have been proposed to be involved in amino acid metabolism. D-GAP is the only substrate oxidized by GAPOR and a study of the steady-state kinetics of GAPOR has revealed partial substrate inhibition. This inhibition is alleviated by a relatively high concentration of salts, *e.g.* NaCl, and by the oxidation product 3-phosphoglycerate, resulting in increased enzyme activity at high substrate concentrations. GAPOR activity is strongly dependent on pH, with the optimum pH being 9. At pH 9, the substrate is a divalent anion and, therefore, positively charged amino acid residues are probably involved in the binding of the substrate. For GAPOR and AOR, only secondary kinetic isotope effects of the solvent have been found. However, for FOR, a significant primary kinetic isotope effect has been found for the substrate that is indicative of a rate-determining step involving hydride abstraction from formaldehyde. This represents the first experimental evidence for hydride transfer from the aldehyde, in the mechanism of the tungsten-containing aldehyde oxidoreductase. The tungsten L(III)-edge EXAFS recorded for GAPOR, poised at –454 mV (W^{VI}) and –645 mV (W^{IV}), is in each case, consistent with the tungsten being coordinated by four sulfur atoms that are presumed to be derived from the two pterin dithiolene groups. Furthermore, upon reduction from W^{VI} to W^{IV}, the tungsten coordination apparently changes from di-oxo to oxo(hydroxo). The implications of these new results, for the reaction mechanism of tungsten-containing aldehyde oxidoreductases, are discussed.

Introduction

Pyrococcus furiosus is a hyperthermophilic archaeon that grows optimally at 100ºC, pH 7.0, and 0.5 M NaCl [22]. Three different aldehyde oxidoreductases - aldehyde oxidoreductase (AOR), formaldehyde oxidoreductase (FOR), and glyceraldehyde-3-phosphate oxidoreductase (GAPOR) - have been isolated from *P. furiosus* and each contains a mononuclear tungsten centre bound to two pterin

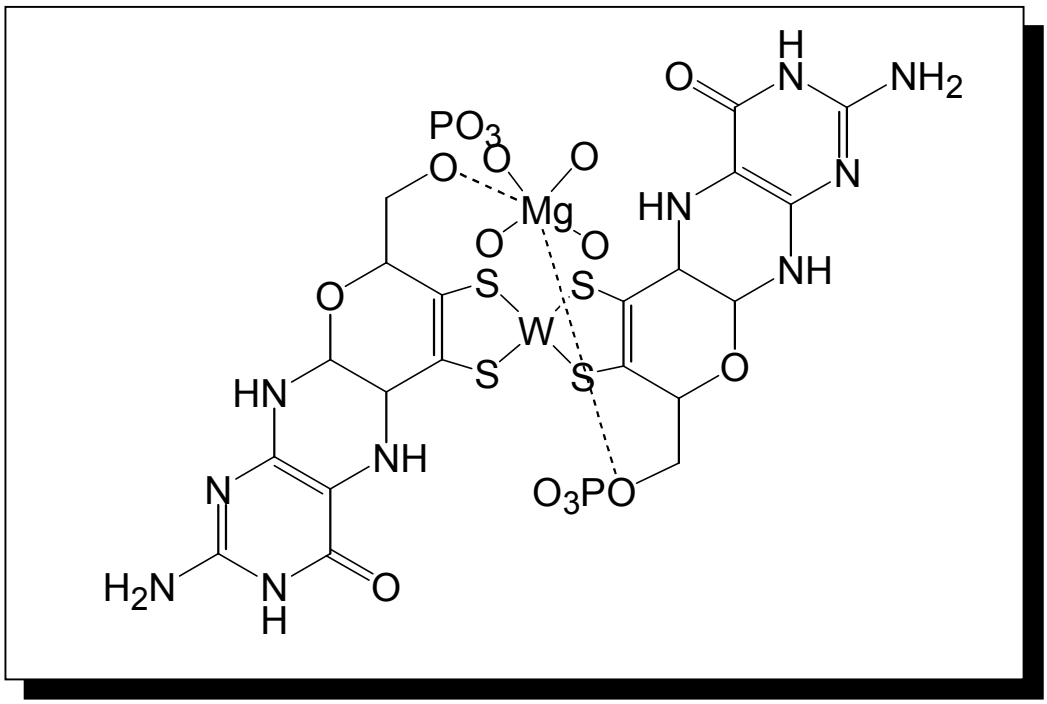

Figure 1. Chemical structure of the tungsten-(bis)pterin cofactor.

cofactors (see Figure 1) in their active site. A determination of the crystal structure of AOR and FOR, and a sequence comparison with the known genomes, have shown that AOR, FOR, and GAPOR are members of a family of enzymes that consist almost exclusively of tungsten enzymes [56]. The only exception is (2R)-hydroxycarboxylate-viologen-oxidoreductase, which is a molybdenum-containing enzyme [64]. It is anticipated that AOR and FOR oxidize aldehydes produced during amino acid breakdown; however, to date no physiological substrates have been identified for these enzymes. GAPOR is a key enzyme in the glycolysis of *P. furiosus*. The nature and properties of the tungsten centers of AOR, FOR, and GAPOR have been characterized by EPR and MCD spectroscopy [46, 47, 58, 61]. These studies have revealed that, in each of these enzymes, the tungsten center cycles

between the oxidation states VI, V, and IV with midpoint potentials between *ca.* –600 and –400 mV. Although some information on the kinetics of the activity of these tungsten enzymes has been obtained [44, 56, 59]**,** we have much to learn about the structure and function of these enzymes. Herein we present more information concerning the steady-state kinetics of the GAPOR that reveal aspects of the substrate inhibition and the enantioselectivity of this enzyme. The dependence of the activity of GAPOR on pH and temperature has been investigated and this behaviour compared with the corresponding aspects of AOR. Furthermore, kinetic isotope effects of incorporating deuterium into the solvent, for AOR and GAPOR, and the substrate, for FOR, have been determined. To complement the crystallographic information available for AOR and FOR [45, 55], we have determined tungsten L(III)-edge EXAFS of GAPOR for W^{VI}, W^{VI}, and W^{IV} forms of the enzyme. A mechanism for the catalytic action of GAPOR has been proposed, that incorporates the new kinetic and spectroscopic results obtained.

Materials and methods

Cultivation and enzyme purification

Pyrococcus fusiosus (DSM 3638) was cultivated in a 200 litre fermentor at 90°C, as described previously [88]. Aldehyde oxidoreductase (AOR), formaldehyde oxidoreductase (FOR), glyceraldehyde-3-phosphate oxidoreductase (GAPOR) were purified as described elsewhere [44, 57, 59].

Glyceraldehyde 3-phosphate stability

The degradation of glyceraldehyde 3-phosphate (GAP) at 60°C in 100 mM potassium phosphate buffer, pH 7.0, was studied by analyzing samples, drawn every minute, for aldehyde content using the Purpald method [114] - a colorimetric procedure that employs 3-hydrazino-5-mercapto-1,2,4-triazole (Purpald, as obtained from Sigma-Aldrich).

Substrate inhibition of GAPOR

GAPOR activity was assayed using benzyl viologen reduction, monitoring the optical absorbance at 580 nm (ε_{580} = 7,800 $M^{-1}cm^{-1}$) [59]. Activity measurements

with GAP concentrations of: 0.005, 0.01, 0.02, 0.03, 0.05, 0.1, 0.2, 0.5, 1.0 mM were measured in the presence of 1, 3, or 5 mM benzyl viologen. The data were analyzed using a model that assumed partial substrate inhibition of the enzyme, see equation {1} [115].

$$v = V_{max} \cdot [S] \cdot (1 + b \cdot [S]/K_I) \,/\, (K_M + [S] + [S]^2/K_I) \qquad \{1\}$$

The parameter *b* is the ratio between the v at infinite substrate concentration and V_{max} and, hence, represents the extent of the inhibition. If $b = 0$, the regular description of Michaelis-Menten kinetics with complete substrate inhibition is obtained; if $K_I \rightarrow \infty$, equation [1] becomes the regular, uninhibited, Michaelis-Menten equation.

Enantioselectivity towards D- and L-GAP

GAPOR activity was assayed as described above, using 3 mM benzyl viologen with D,L-GAP and D-GAP as substrates. The D-GAP content of commercially available D,L-GAP (Sigma) was measured enzymatically using rabbit muscle GAPDH [116]. D-glyceraldehyde-3-phosphate was produced from D-glyceraldehyde-3-phosphate diethyl acetal (Sigma-Aldrich) using Dowex 50W 4x200 (Supelco) [116]. The concentration D-GAP was determined enzymatically.

Effect of ionic strength, pH and temperature on GAPOR activity

GAPOR activity was assayed at 60°C as described above, using 3 mM benzyl viologen with 0.5 mM D,L-GAP as substrates. The activity was measured in: 50 mM Mes pH 5.3 and 6.0; Mops pH 6.9; EPPS/tricin pH 7.8; EPPS pH 7.9; Ches pH 8.3, 8.5, 8.8, 9.2, and 9.4; and TAPS pH 9.7 and 10.5 – these pH values are for 60°C. The GAPOR activity with EPPS/tricin pH_{60} 7.8 was measured between 20 and 80°C; at temperatures > 80°C, the lifetime of the substrate was too short to be measured. To investigate the effect of the ionic strength, the GAPOR activity was measured at 60°C, using 3 mM benzyl viologen in 50 mM EPPS/tricin pH_{60} 7.8 with 0.5 mM D,L-GAP in the presence of 0, 0.1, 0.2, or 1 M NaCl.

Deuterium kinetic isotope effects on AOR, FOR and GAPOR activity

For AOR and GAPOR, the deuterium kinetic isotope effect of the solvent at 60 ºC was measured using 3 mM benzyl viologen and 50 mM EPPS/tricin, prepared

in D_2O rather than H_2O. The activities of AOR (0.6 mM crotonaldehyde) and GAPOR (0.5 mM D,L-GAP) were measured as described above. The deuterium kinetic isotope effect of the substrate at 70ºC was measured for FOR in a non-deuterated assay buffer using formaldehyde-d_2 (20% solution in D_2O, Aldrich) as the substrate.

Tungsten L(III)-edge EXAFS of GAPOR

GAPOR was concentrated using a filter with a 30 kDa cutoff under argon atmosphere in an anaerobic glove box. The redox potential of GAPOR was poised at –454 mV and –645 mV vs. NHE by adding glyceraldehyde-3-phosphate (GAP) and 3-phosphoglyceric acid (3PG) and incubating at 50 °C for 10 minutes, noting that the potential of the GAP/3PG couple has been reported as –614 mV vs. NHE [102]. GAPOR samples (1.25 mM) were injected into aluminum sample holders and contained between Mylar windows and the cells were then frozen in liquid nitrogen. XAS data were collected in fluorescence mode at the W L(III)-edge on station 16.5 of the Daresbury Synchrotron Radiation Source, operating at 2 GeV with an average current of 150 mA. The temperature of the samples was maintained at 13 K using a closed-system helium exchange cryostat (further details are available at http://srs.dl.ac.uk/XRS/index.html, under Sample Stages). A Si(220) double crystal monochromator was used, calibrated using a 15μm tungsten foil. I_o was measured using an ion chamber filled with a mixture of Ar/He. Fluorescence data were recorded using an Ortec 30-element solid state detector. The signals from each individual element were recorded separately, but several were discarded due to spurious signals that were considered to represent diffraction peaks from crystalline ice in the samples. 24 scans were recorded and summed for the sample poised at –645 mV and 32 scans for the sample poised at –454 mV. The raw data were background subtracted using the Daresbury program EXBACK. The isolated EXAFS were analyzed using EXCURV98 [117], employing the exact spherical wave calculation [118, 119]. Phase shifts were derived from *ab initio* calculations using Hedin-Lundqvist potentials and von Barth ground states [120]. The EXAFS were simulated by considering the backscattering due to shells of atoms around the central absorber (W) and refining the Fermi energy, (E_f), the absorber-scatterer distances (r), and the Debye-Waller factors ($2\sigma^2$), in order to minimize the R-factor - the sum of the

square of the residuals between the experiment and the theoretical fit [121]. The number of backscattering atoms in each shell (N) was optimised as an integer or half-integer value. Only shells, the inclusion of which, led to a significant improvement in the R-factor, were included in the final fit.

Results

Glyceraldehyde 3-phosphate stability

Although the glyceraldehyde-3-phosphate is relatively stable in its free acid form, the dianion - which is the major species at ambient and basic pH - is highly sensitive towards non-enzymatic hydrolysis. This non-enzymatic reaction is likely more pronounced at high temperatures and, therefore, is of relevance to the *in vitro* activity assays of GAPOR and the metabolism of glyceraldehyde-3-phosphate in *P.furiosus*. Possible breakdown or isomerization products of glyceraldehyde-3-phosphate are glyceraldehyde, dihydroxyacetone phosphate and methylglyoxal [122]. We have found that GAP, when incubated at 60°C and pH 7, is hydrolyzed to methylglyoxal (Figure 2A and Figure 3); this degradation follows first order kinetics with $t_{1/2}$ = 7.2 min. at 60ºC (Figure 2B). Studies have shown that glyceraldehyde and dihydroxyacetone phosphate are not to be substrates or inhibitors of GAPOR [59], however, the interaction of methylglyoxal with this enzyme has never been investigated. Furthermore, commercially available D,L-GAP has been reported to contain 3-15% methylglyoxal [123]. Therefore, the effects of this compound on GAPOR are relevant to kinetic measurements accomplished using commercially available D,L-GAP. We have found that GAPOR cannot use methylglyoxal as a substrate, and that GAPOR activity is unaffected by 5.5 mM methylglyoxal (not shown).

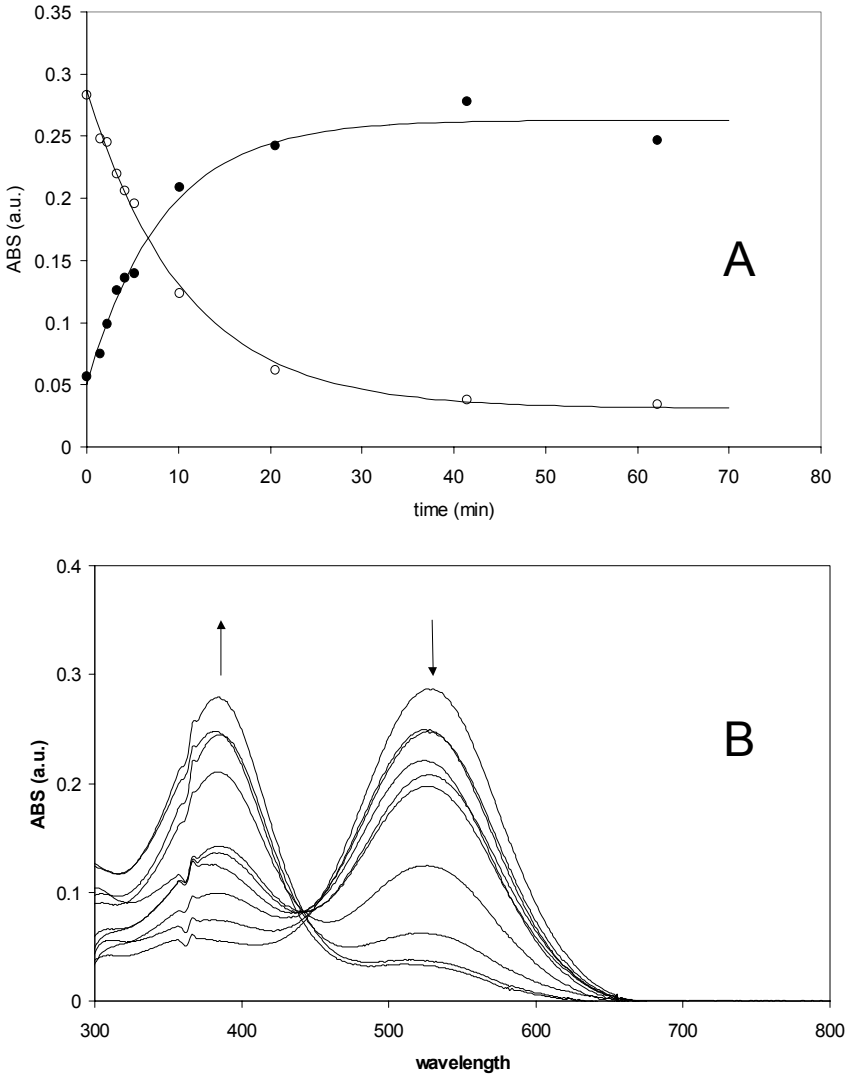

Figure 2A. First-order kinetics of the disappearance of glyceraldehyde-3-phosphate (○) and appearance of methylglyoxal (●) at 60°C and pH 7.0. **B.** Optical absorption of the purpald product during incubation of glyceraldehyde-3-phosphate after 0, 1, 2, 3, 4, 5, 10, 20, 40, 60 minutes incubation at 60°C and pH 7.0.

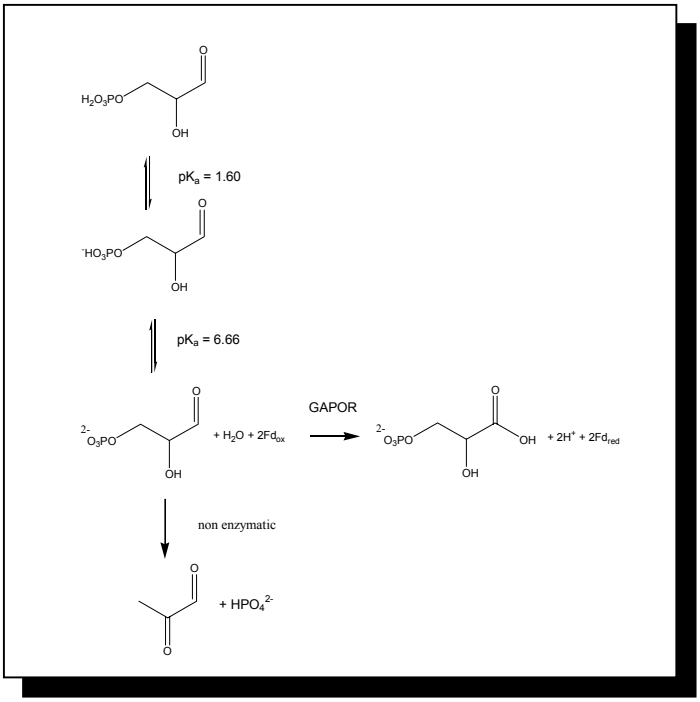

Figure 3. Fate of glyceraldehyde-3-phosphate under enzymatic assay conditions.

Substrate inhibition of GAPOR

As reported previously [59], GAPOR is significantly inhibited by GAP at concentrations > 0.5 mM, however, the K_m and V_{max} were determined without taking this substrate inhibition into account. Such substrate inhibition may cause large differences between the K_m and V_{max} values, determined from measurements at low substrate concentrations, and the actual K_m and V_{max} values. We have found that the inhibition of GAPOR by GAP is most prominent at low benzyl viologen concentration (see Figure) and decreases at higher benzyl viologen concentrations (Figure 4). We interpret these findings by assuming partial substrate inhibition of the enzyme: *i.e.* the substrate-inhibited form of the enzyme retains some activity.

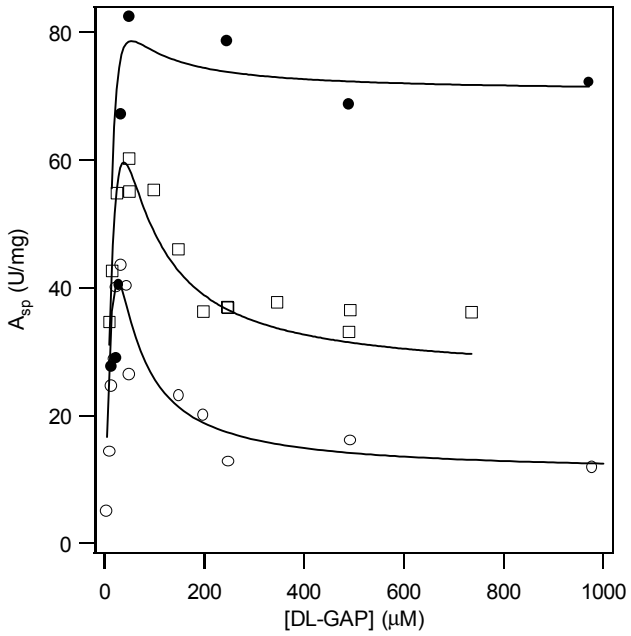

Figure 4. Substrate inhibition of *P.furiosus* GAPOR at 1 mM (○), 3 mM (□)and 5 mM (●) benzyl viologen. The solid lines represent fits to equation {1} assuming identical V_{max} and K_M values. V_{max}, 445 U/mg, K_M, 125 µM, K_I, 4, 2, 7 µM, b, 0.02, 0.06, 0.16 for 1, 3 and 5 mM benzyl viologen respectively.

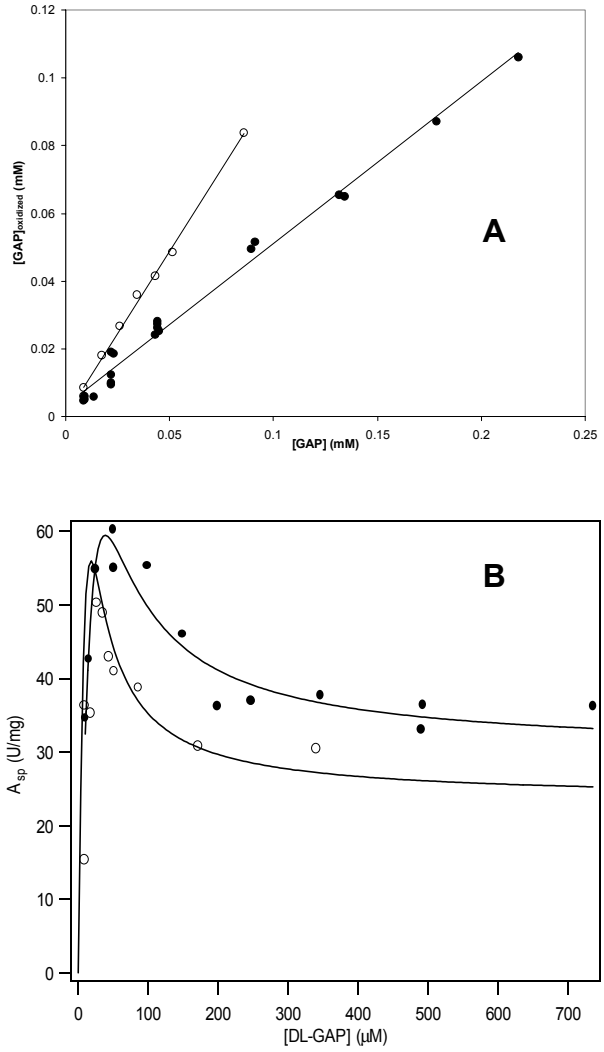

Figure 5. Enantioselectivity of *P.furiosus* GAPOR. **A.** Conversion of D-GAP (○) and DL-GAP (●) by GAPOR. **B.** Activity profile of GAPOR with D-GAP (○) and DL-GAP (●) as substrates. The solid lines represent fits to equation {1} with the following parameters: V_{max}, 445 U/mg, K_M, 63 µM, K_I, 3 µM, b, 0.05 for D-GAP and V_{max}, 445 U/mg, K_M, 125 µM, K_I, 6 µM, b, 0.07 for DL-GAP.

Enantioselectivity towards D- and L-GAP

Figure 5A shows the conversion of D-GAP and the racemic mixture D,L-GAP by GAPOR as indicated by the reduction of benzyl viologen at 60°C; *ca.* 100% of D-GAP and *ca.* 50% of D,L-GAP are oxidized. Apparently D-GAP is the only substrate of GAPOR, and L-GAP is not oxidized (or is oxidized at a much lower rate than D-GAP). The activity profiles of GAPOR with D-GAP and D,L-GAP are depicted in Figure 5B and a comparison of these profiles shows that the K_i and K_m values for the former are *ca.* half those of the latter while the V_{max} and b value are essentially

unchanged. Again this is consistent with D-GAP being the only substrate of GAPOR and it appears that L-GAP is not an inhibitor of GAPOR when present in equimolar quantities with D-GAP.

Effect of ionic strength, pH and temperature on GAPOR activity

The pH dependence of GAPOR activity can be described assuming two pK_a values, each of *ca.* 9 (Figure 6B). This pH dependence differs from that for AOR (Figure 6A), for which no pK_a values can be determined. The pK_a values of GAP at 50°C have been reported: (i) from free acid to monoanion, as 1.60; (ii) from monoanion to dianion, as 6.66 [122]. Therefore, it appears that the substrate for GAPOR is the glyceraldehyde-3-phosphate dianion. The pK_a values of figure 6B may represent amino acid residues close to the active site of the enzyme, however, in the absence of a three-dimensional structure of this enzyme, we cannot assign the pK_a's to particular residues.

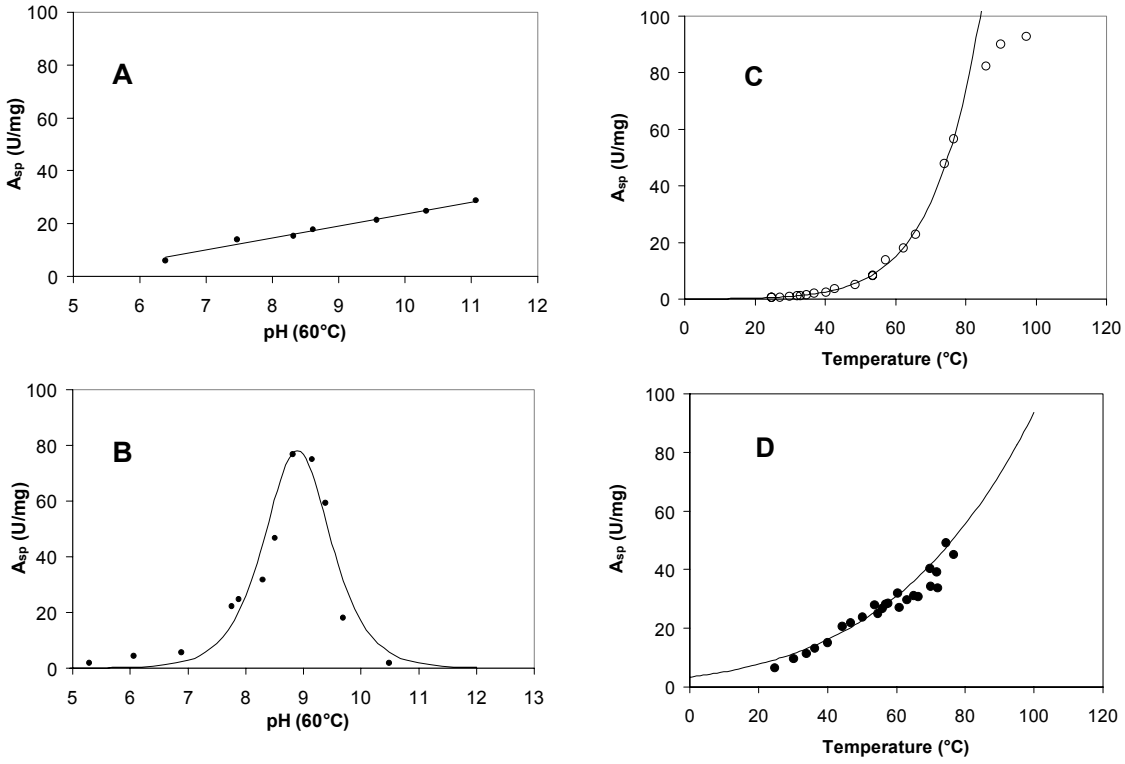

Figure 6. The pH dependent activities of (**A**) AOR and (**B**) GAPOR and the temperature dependent activities of (**C**) AOR and (**D**) GAPOR.

The temperature dependencies of AOR (Figure 6C) and GAPOR (Figure 6D) correspond to Eyring behaviour, involving a single activation enthalpy and entropy change from 20-80°C. The thermodynamic parameters $\Delta H^{\ddagger}$ and $\Delta S^{\ddagger}$ are: (i) 74.7 $kJ \cdot mol^{-1}$ and –5.42 $J \cdot K^{-1} \cdot mol^{-1}$, for AOR; and (ii) 39.7 $kJ \cdot mol^{-1}$ and –24.5 $J \cdot K^{-1} \cdot mol^{-1}$, for GAPOR. The relatively low enthalpy of activation for GAPOR may be due to the fact that the active center of this enzyme is ideally suited to the substrate GAP, whilst AOR has a broad substrate specificity.

Figure 7 shows the effect of ionic strength on the activity of GAPOR. Clearly the activity of GAPOR is strongly dependent on the [NaCl], however, this dependence is much less at lower [GAP]. The activity profiles show that the effect of substrate inhibition is reduced as [NaCl] increased and, at 1 M NaCl, the GAPOR activity profile accords to regular Michaelis-Menten kinetics. A global fit of the four traces of figure 7, assuming partial substrate inhibition and a common V_{max} and b values, resulted in values of K_m and K_I that were dependent on the ionic strength; thus high

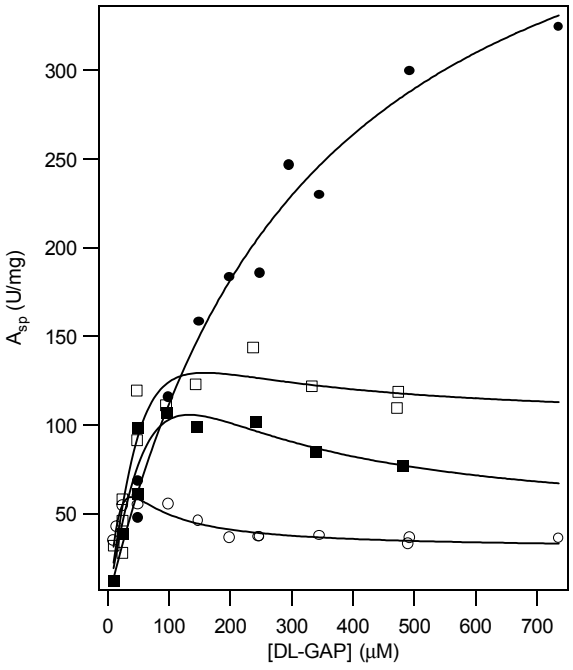

Figure 7. Effect of ionic strength on *P.furiosus* GAPOR activity. Sodium chloride concentrations of 0 (○), 0.1 (■), 0.2 (□) and 1 M (●). The solid lines represent fits to equation {1} assuming and identical V_{max} value for all four traces. The fit parameters were: V_{max}, 445 U/mg, K_M, 125, 213, 192, 306 µM, K_I, 6, 49, 28, 3600 µM, b, 0.07, 0.10, 0.23, 1 for 0, 0.1, 0.2 and 1 M NaCl respectively.

[NaCl] values decrease the affinity of GAP towards both its substrate (higher K_m) and product binding site (higher K_i).

Kinetic isotope effects

The solvent kinetic isotope effects, k_H/k_D, of GAPOR and AOR at pH 8.4 and 60°C were detemined as 1.66 and 2.25, respectively . These values are consistent with secondary kinetic isotope effects of the solvent; therefore, O-H/D bond breaking of a water molecule is not a rate determining step in the catalytic mechanism of GAPOR and AOR. The substrate kinetic isotope effect of FOR (Figure 8) is $k_H/k_D = 3.3$, at pH 8.4 and 70°C, and represents a significant primary isotope effect for C-H/D bond breaking at that temperature [124]. Therefore, it would appear that hydride abstraction from formaldehyde is the rate-determining step in the catalytic mechanism of FOR.

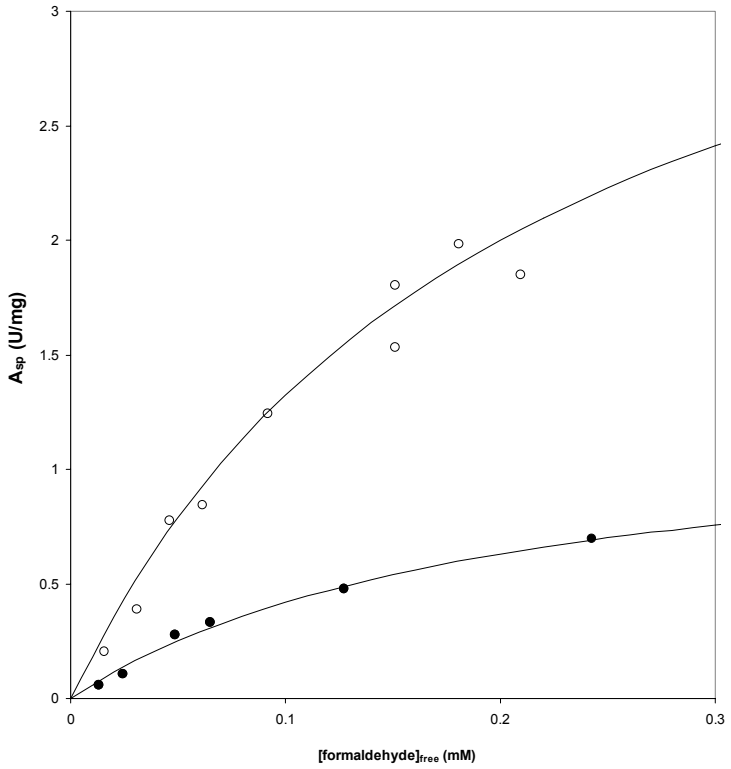

Figure 8. Kinetic isotope effect of *P.furiosus* FOR. FOR activity with formaldehyde (○) and formaldehyde-d_2 (●). The solid lines represent fits to the regular Michaelis-Menten equation with the following parameters: V_{max}, 4.1 U/mg, K_M, 0.2 mM for formaldehyde and V_{max}, 1.3 U/mg, K_M, 0.2 mM formaldehyde-d_2.

Redox dependent coordination of the tungsten center in GAPOR

Tungsten L(III)-edge EXAFS were collected for GAPOR poised at the redox potentials of –645 and –454 mV (vs. NHE). Since the data suffer from significant noise, the following analysis has to be approached with some caution. The best fit of the EXAFS recorded for the low potential sample (see Table 1; Figure 9A and 9B), involved backscattering from three shells: a) one oxygen at *ca.* 1.73 Å - a distance characteristic of W=O (oxo-groups) [125]; b) one oxygen at *ca.* 2.09 Å; and c) a shell of four sulfurs at *ca.* 2.42 Å. Coordination numbers higher than six cannot be excluded based on the EXAFS results, however five or six coordination is consistent with the present knowledge on the tungsten and molybdenum coordination chemistry in enzymes [126].

The best fit obtained for the tungsten L(III)-edge EXAFS recorded for GAPOR poised at higher potential (-454 mV)(Table 2 and Figure 9C and D) required two shells; a) a W=O shell at *ca.* 1.70 Å and b) a W-S shell at *ca.* 2.40 Å. The optimum fit was obtained with two W=O bonds and four W-S bonds. Addition of an extra W-O shell at 2.04 Å did not improve the fit.

Table 1. Analysis* of the tungsten L(III)-edge EXAFS recorded for GAPOR poised at –645 mV.

Residual	S atoms			O atoms		
	N	R/Å	$2\sigma^2$/Å^2	N	R/Å	$2\sigma^2$/Å^2
64.5	4	2.42	0.011	1	1.73	-0.002
				1	2.09	0.003
64.8	4	2.42	0.011	2	1.73	0.010
				1	2.09	0.003
65.8	3	2.42	0.006	1	1.73	-0.002
				1	2.10	0.002
67.8	4	2.42	0.011	1.5	1.73	0.003
				0.5	2.07	0.001
70.4	3	2.42	0.006	1.5	1.73	0.003
				0.5	2.07	0.002
73.2	4	2.40	0.012	2	1.73	0.008

*Estimated uncertainty in: N ≥ 10%; R ≥ 0.02 Å; $2\sigma^2 \geq 0.002$ Å^2.

Table 2. Analysis* of the tungsten L(III)-edge EXAFS recorded for GAPOR poised at –454 mV.

Residual	S atoms			O atoms		
	N	R/Å	$2\sigma^2$/Å^2	N	R/Å	$2\sigma^2$/Å^2
64.0	4	2.40	0.013	2	1.70	0.017
64.9	3	2.39	0.009	2	1.69	0.017
65.6	4	2.40	0.013	1	1.69	0.006
65.9	5	2.40	0.017	2	1.70	0.017
66.0	4	2.38	0.021	2	1.70	0.017
	1	2.43	0.004			
66.1	4	2.42	0.013	2	1.68	0.016
				1	2.04	0.040

*Estimated uncertainty in: N ≥ 10%; R ≥ 0.02 Å; $2\sigma^2 \geq 0.002$ Å^2.

The position of the tungsten L(III)-edge, measured as the top of the first major peak in the first derivative of the edge profile, relative to that for a tungsten foil at 10193.8 eV, was 10200.8 eV, for the sample poised at –645 mV, and 10201.2 eV, for the sample poised at –454 mV. This difference is consistent with the oxidation state of the tungsten in the latter sample being (on average) higher than that in the former.

However, this difference in the L(III)-edge positions is small and less than that (1-2 eV) reported [125] for W^{VI} vs. W^{IV} centers in low molecular weight tungsten complexes possessing an inner coordination sphere similar to that of tungsten centers in enzymes. Therefore, it is possible that the enzymes samples do not involve exclusively W^{VI} and W^{IV}.

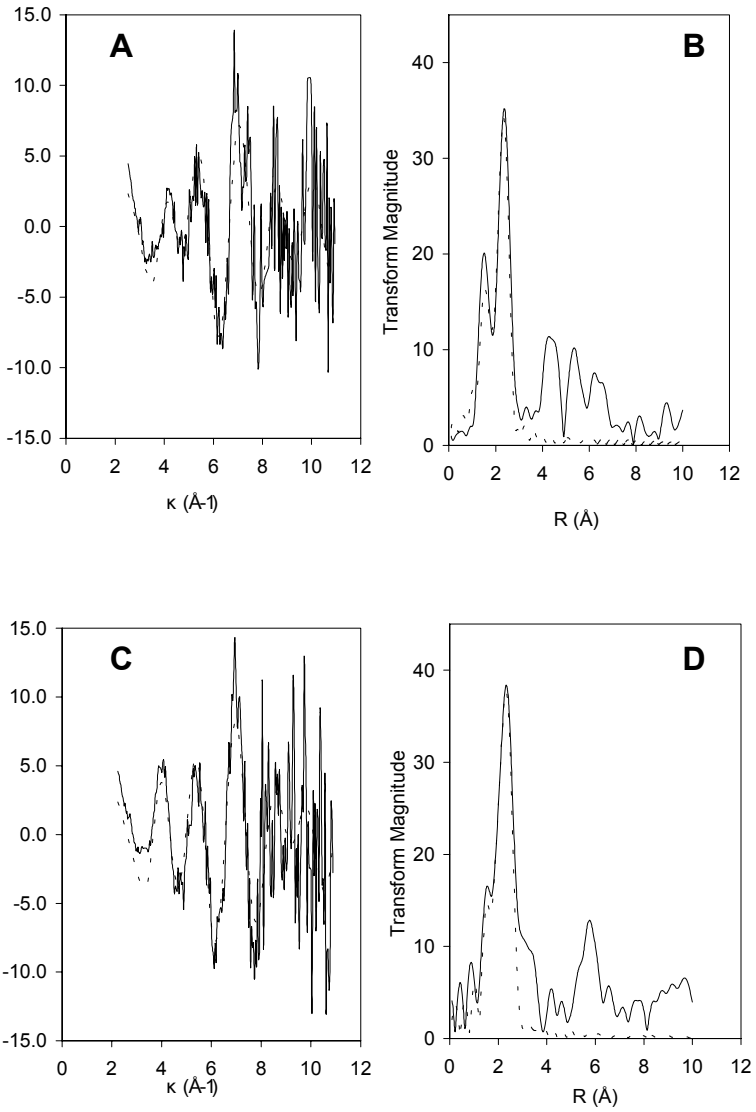

Figure 8. Tungsten L(III)-edge EXAFS data (solid lines) and curve-fitting results (broken lines) of *P.furiosus* GAPOR poised at –454 mV (A and B) and –645 mV (C and D). A and C show the EXAFS oscillations and B and D the corresponding EXAFS Fourier transforms.

Discussion

Glyceraldehyde 3-phosphate stability

The breakdown of GAP at high temperatures (>50°C) has not been investigated previously. We have found methylglyoxal to be the major product of the non-enzymatic degradation under assay conditions of GAPOR. Methylglyoxal does not interfere with GAPOR activity, however, it may have physiological consequences for *P. furiosus*, since it is toxic for most organisms [127]. There is no evidence yet for *in vivo* production of methylglyoxal by *P. furiosus*. However, we note that the boiling point of methylglyoxal is 70°C, which is also the minimum growth temperature of *P. furiosus* [128].

Steady state kinetics of GAPOR

We have found GAPOR to be subject to partial substrate inhibition by GAP. This inhibition may be a mode of regulation for this glycolytic enzyme. The nature of the inhibition by this substrate is not known, but it is possible that GAPOR has separate substrate and product binding sites. Since the substrate (GAP) has structural similarities with the product 3PG [129] and binding of the substrate (with low affinity) at the product binding site would result in partial inhibition of GAPOR activity. The pH and temperature dependence of GAPOR was determined at the relatively high substrate concentration of 0.5 mM GAP since substrate inhibition does not allow measurement under apparent V_{max} conditions. Although the enzyme is partially inhibited at this substrate concentration, the adopted procedure was convenient since the activity of GAPOR is relatively independent of substrate concentration in the range 0.3-0.6 mM GAP (Fig. 2 and 5).

GAPOR has a narrow substrate specificity and, in our investigations, we found only D-GAP to be oxidized with a significant rate by GAPOR. This is a property that this enzyme has in common with glyceraldehyde-3-phosphate dehydrogenase (GAPDH). GAPOR is not inhibited by L-GAP; therefore, a racemic mixture of D-GAP and L-GAP can be used for kinetic measurement.

The activity of the enzyme is pH dependent with an optimal activity occurring at pH 9. At this pH the substrate is exclusively present as the dianion, which suggests that positively charged groups (*e.g.* Lys or Arg) are necessary for substrate binding.

Clearly, the negatively charged phosphate group is important for recognition of the substrate, since GAPOR shows no activity towards glyceraldehyde or methylglyoxal. Furthermore, the dependence of GAPOR activity on the ionic strength of the solution reflects the influence of charged groups on the binding of the substrate and the release of the product.

The temperature dependence of GAPOR activity shows no indication for temperature-induced conformational changes, *e.g.* the presence of an "on-off" switch. The physiological temperature of *P. furiosus* is *ca.* 100°C and, as discussed above, at this temperature the substrate is unstable. Therefore, a mechanism to protect the substrate would appear to be necessary, to allow glycolysis to function effectively at this temperature; however, the nature of this mechanism is not known.

The steady state kinetics for GAPOR have not previously been clearly defined and the reported values of the V_{max} in the benzyl viologen reduction assay for this enzyme range from 25 U/mg [60] to 350 U/mg [59]. This large difference in V_{max} cannot be fully explained by the different assay temperatures of 50°C and 70°C, respectively (Fig. 6D), however, it may be explained by the differences in the benzyl viologen concentration (1 and 3 mM) and in the GAP concentration (1.5 and 0.4 mM), as can be seen in Figs. 4 and 6.

Although substrate inhibition has been suggested previously [59], it was disregarded in the determination of the V_{max} and K_m. Also, it has been reported, without explanation, that GAPOR activity is stimulated by the presence of potassium phosphate, sodium arsenate, potassium chloride, sodium citrate, or sodium sulfate [59]. In the studies reported herein, we have shown that the activity of GAPOR is affected by sodium chloride. We suggest that these salts decrease the binding of GAP to the product-binding site of GAPOR, thereby decreasing the inhibition of the enzyme activity by the substrate and, in consequence, cause higher activities at high concentrations of GAP. High ionic strength affects, the binding of GAP not only at the product binding site, but also at the substrate binding site, as manifest by the higher K_m value at 1 M NaCl than at 0 M NaCl. The stimulating effect of the product, 3-phosphoglycerate, on GAPOR activity can be understood by assuming it competes with GAP for the product binding site and therefore decreases the substrate inhibition.

Evidence for a hydride abstraction catalytic mechanism of tungsten aldehyde oxidoreductases

For the oxidation of formaldehyde, FOR exhibits a significant primary deuterium kinetic isotope effect, whereas the solvent k_H/k_D effects for AOR and GAPOR are secondary. Therefore, it appears that the breaking of the aldehyde C-H bond and not the breaking of the O-H bond of water is rate-determining step in the catalysis effected by the W-containing aldehyde oxidoreductases. Indeed, for the Mo-containing aldehyde dehydrogenase (Mop), based on crystallographic studies, a mechanism has been proposed involving nucleophilic attack by a molybdenum-bound water molecule on the α-carbon of the aldehyde, followed by hydride transfer to the sulfido-ligand of the molybdenum [130]. Although the crystal structures of AOR and FOR are ambiguous in respect of the oxo- or hydroxo- coordination of the tungsten, a mechanism similar to that proposed for Mop has been suggested, based on the structural similarity of the active sites [45, 55]. The work reported herein represents the first experimental evidence for hydride transfer from the aldehyde during aldehyde oxidation by tungsten enzymes.

We are not yet able to propose a complete reaction mechanism in the absence of a crystal structure of GAPOR. However we propose that following points to be part of such a mechanism: a) the W^{IV} is coordinated by 1 oxo-, 1 hydroxo- and 4 sulfur ligands; b) W^{VI} is coordinated by 2 oxo- and 4 sulfur ligands; c) hydride transfer from the aldehyde is involved; d) for a hydride transfer to occur a water molecule has to be activated so it can act as a base to attack the aldehyde α-carbon; e) from our previous EPR measurements a W^{V} species is likely an intermediate in the reaction mechanism [61].

Nature of the tungsten center in GAPOR

Some caution is required with the interpretation of the EXAFS data, since the data exhibit severe noise. The fact that we obtain six-coordinate tungsten centers in both the IV and VI oxidation state is consistent with what is presently known from crystallographic studies on mononuclear molybdenum and tungsten enzymes [126]. The crystal structures of AOR and FOR have been determined [45, 55]. In both cases no clear conclusions could be drawn about the oxygen coordination in different oxidation states of the tungsten, however, coordination of the four dithiolene-sulfurs to the tungsten, initially found with EXAFS, has been confirmed.

This work includes the first report of W-L(III) EXAFS for an active tungsten enzyme from *P. furiosus*. The observed length of the W=O, W-O and W-S bonds are similar to the corresponding distances reported for: *P. furiosus* inactive AOR (red tungsten protein) [131]; *P. furiosus* active AOR (unpublished results cited in [43]); *Moorella thermoacetica* formate dehydrogenase [132]; and *Rhodobacter capsulatus* W-DMSO reductase [80].

Acknowledgements

Dr. L. J. Stewart is acknowledged for her help with the EXAFS investigations. CLRC Daresbury is acknowledged for provision of beamtime. This research has been financially supported by the Council for Chemical Sciences of the Netherlands Organization for Scientific Research (CW-NWO)

Chapter 5

Redox characteristics of the tungsten DMSO reductase of *Rhodobacter capsulatus*

Peter-Leon Hagedoorn, Wilfred R. Hagen, Lisa J. Stewart, Arefa Docrat, Susan Bailey, C. David Garner

The DMSO reductase from *Rhodobacter capsulatus* is known to retain its three-dimensional structure and enzymatic activity upon substitution of molybdenum, the metal that occurs naturally at the active site, by tungsten. The redox properties of tungsten-substituted DMSO reductase (W-DMSOR) have been determined; at pH 7.0, $E_m(W^{VI/V})$ is –194 mV and $E_m(W^{V/IV})$ is –134 mV. Thus, as for the molybdenum in Mo-DMSOR, the tungsten center of W-DMSOR is poised for a two-electron redox change. At pH 7.0, each of the E_m values of W-DMSOR is *ca*. 335 mV lower than that of the corresponding couple of Mo-DMSOR. The maximum intensity of the EPR signal observed occurs at pH 5 and corresponds to *ca.* 40% of the total W; the amount of W^V decreases at pH>5.0, indicative of a pH dependence of the E_m ($W^{VI/V}$) and/or E_m ($W^{V/IV}$). Two different W^V EPR signals have been observed: W^V "split" (g_{xyz} = 1.888, 1.927, 1.960) with, and W^V "unsplit" (g_{xyz} = 1.860, 1.928, 1.958) without superhyperfine coupling to an adjacent proton; the ratio between these two signals is pH dependent and the "split" signal being more prominent at pH 5.0.

Introduction

Molybdenum enzymes occur in all living systems and, with the notable exception of the nitrogenases, involve the metal bound by one or two molecules of a special cofactor "molybdopterin" (MPT) [42, 133]. These enzymes catalyze the net transfer of an oxygen atom to or from the substrate. In each case, conversion is effected at the molybdenum center and the catalytic cycle involves interconversion between Mo^{VI} and Mo^{IV} with Mo^{V} appearing as an intermediate. Although less prominent than their molybdenum counterparts, several tungsten-containing enzymes have been isolated and characterized [43, 134, 135]. In general, these systems involve tungsten bound by two MPT moieties and - like their molybdenum counterparts – these enzymes catalyze a conversion, the net effect of which is the transfer of an oxygen atom to or from the substrate.

The chemical properties of molybdenum and tungsten are very similar [136]. The parallels in their biochemical behavior (*vide infra*) has stimulated comparisons of the nature and the properties of enzymes containing these two metals. For example, molybdenum, the naturally occurring metal in sulfite oxidase can be substituted by tungsten [137]. This substitution permitted the first direct comparison of the EPR spectrum of a Mo^{V} center of an MPT-dependent enzyme with that of its W^{V} counterpart; the nature of the EPR spectra suggested that the two metals were bound at the same site. However, whilst the molybdenum center of sulfite oxidase is readily reduced from Mo^{VI} to Mo^{V}, in the pH range 6-9, the corresponding W^{VI} center was found to be more difficult to reduce, however, a W^{V} EPR signal could be generated at pH<6. These observations are consistent with: (i) the preference for higher oxidation states, W>Mo, as is generally manifest in the chemistry of these two Group VI metals [136]; and (ii) the reduction of these M^{VI} centers involves coupled proton-electron addition [138].

For sulfite oxidase, as with several other molybdenum MPT-dependent enzymes, substitution by tungsten leads to a loss of activity [139]. However, recent studies of the molybdenum MPT-dependent enzymes dimethylsulfoxide reductase (DMSOR) from *Rhodobacter capsulatus* [80, 81] and trimethylamine N-oxide reductase (TMAOR) from *Escherichia coli* [82] have shown retention of some enzymatic activity upon substitution of the molybdenum by tungsten. X-ray crystallographic and X-ray absorption spectroscopic studies of the DMSOR from *R.*

capsulatus [80] have shown that tungsten is incorporated into the same site as molybdenum [140, 141] with virtually no change in the dimensions of the metal's inner co-ordination sphere.

We have performed redox titrations for W-DMSOR from *R. capsulatus*, to determine the potentials of the $W^{VI/V}$ and $W^{V/IV}$ couples over the pH range 5.0-8.0. A comparison of this information with the corresponding details for the molybdenum center of Mo-DMSOR [106, 142] will aid our understanding of the similarities and differences in behaviour, when molybdenum or tungsten act as the catalytic center of MPT-dependent enzymes [139].

Materials en methods

Growth and protein purification

As described previously [80], *Rhodobacter capsulatus* was grown on medium containing tungstate and the periplasmic W-DMSO isolated and purified. The tungsten content of samples of W-DMSO reductase samples was determined electroanalytically [143]. The samples employed for the redox titrations, possessed a tungsten content of *ca.* 0.6 W/molecule.

Redox titrations

The oxidation/reduction characteristics of W-DMSOR from *R. capsulatus* were investigated by a dye-mediated reductive titration as described previously [90]. These studies were accomplished at 25°C in 100 mM potassium phosphate buffer pH 6.0, 7.0, 8.0 or 100 mM citrate-phosphate buffer pH 5.0; each medium contained 60 μM W-DMSOR. Phosphate buffer or citrate-phosphate buffer was used because Hepes buffer has been shown to bind at the active site of Mo-DMSOR of *Rhodobacter sphaeroides* [141] and induce dissociation of the dithiolene sulfurs of MPT from the metal [144]. Sodium dithionite was used as the reductant and potassium ferricyanide as the oxidant; samples were frozen at 77 K, immediately upon attainment of the redox equilibrium.

Spectroscopy

X-band EPR spectra were recorded on a Bruker ER-200D spectrometer, using facilities and data handling as detailed elsewhere [103]. The W^V EPR signals observed during the course of the redox titration were simulated as described previously [47].

Results

W^V EPR signals observed for W-DMSOR

Both the shape and the intensity of the EPR spectrum of the W^V species observed at potentials from –250 mV to –50 mV was found to be pH-dependent (Figure 1.) The EPR spectra have been interpreted (Figure 2) on the basis of two different W^V species. One signal manifests a clear superhyperfine coupling, but the other does not; these signals are designated as "split" (g_{xyz} = 1.888, 1.927, 1.960) and "unsplit" (g_{xyz} = 1.860, 1.928, 1.958), respectively. The former is considered to arise due to the d^1 centre being coupled to a proton and, consitent with this, the "split" signal predominates at pH 5.0 and the "unsplit" signal at pH 7.0. The difference spectrum of the spectrum at pH 5.0 minus that at pH 7.0 (Figure 2 trace C) reveals the "split" signal. This "split" signal resembles the W^V EPR signal previously reported for dithionite reduced W-DMSOR enzyme [80].

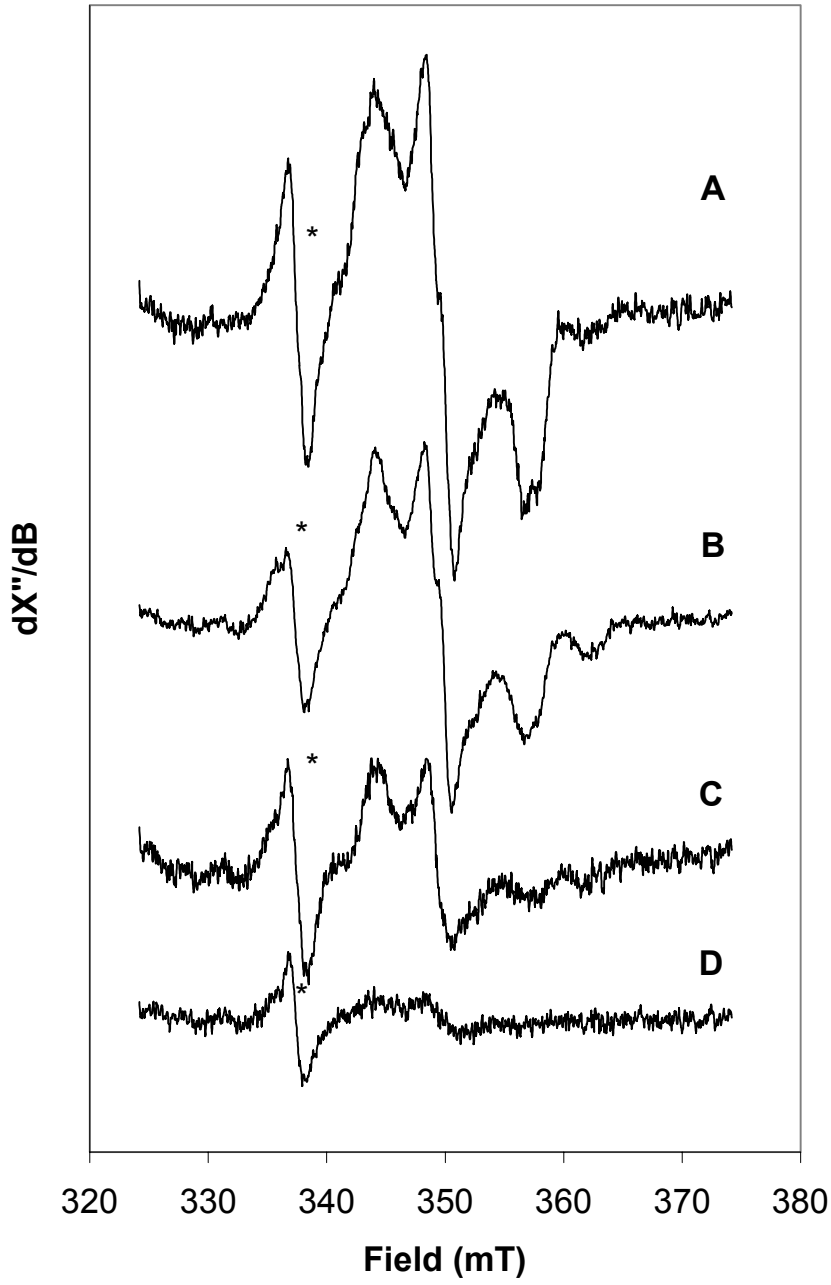

Figure 1. EPR spectra observed for W-DMSOR over the pH range 5.0 to 8.0. W-DMSOR in 100mM phosphate-citrate buffer, pH 5.0 (**A**); 100mM KPi buffer, pH 6.0 (**B**), 7.0 (**C**) or 8.0 (**D**). Sodium dithionite was used as the reductant. All spectra have been normalized with respect to the tungsten concentration of the sample. The signal labeled * is attibuted to radicals that derive from redox mediators used in the titration. EPR conditions: microwave frequency, 9.43 GHz; modulation frequency, 100 kHz; modulation amplitude, 1.0 mT; microwave power, 5.0 mW; temperature, 44 K.

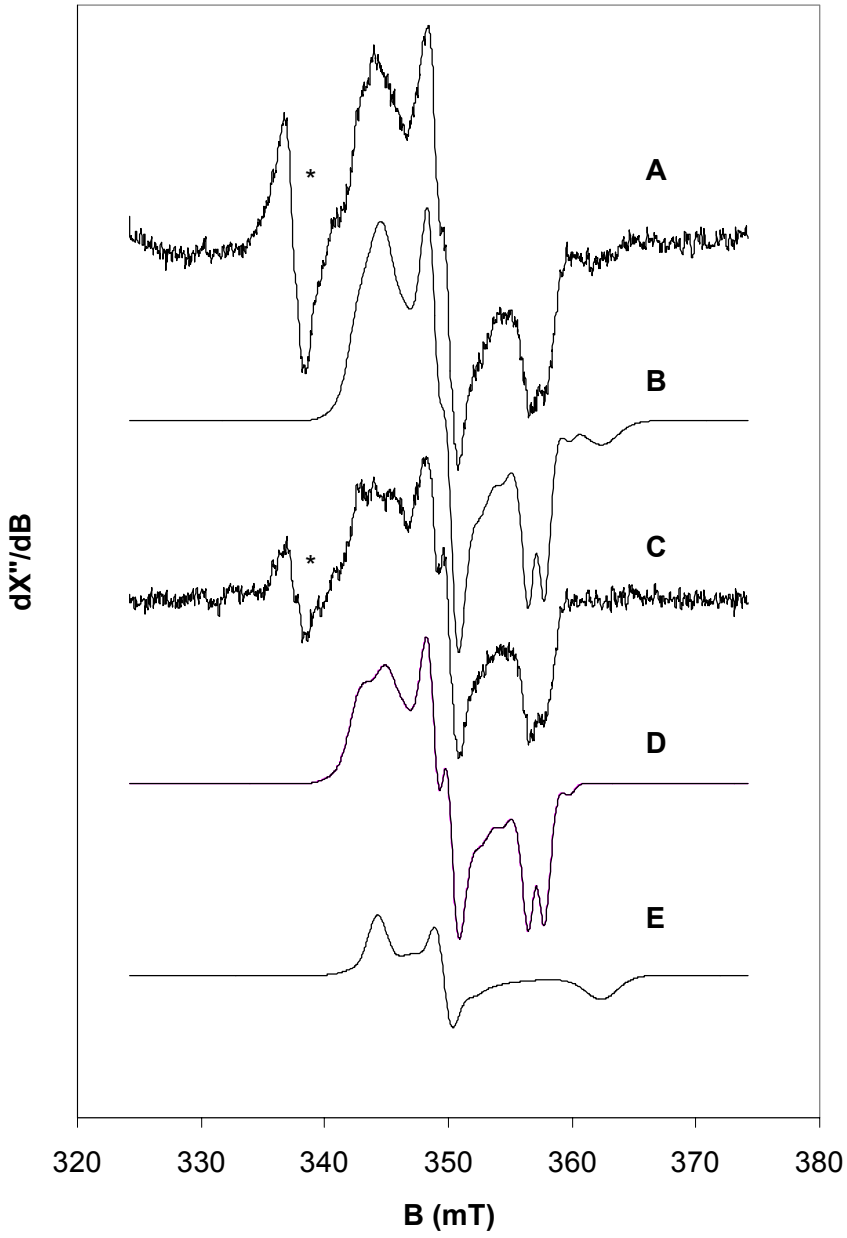

Figure 2. EPR spectra observed for W-DMSOR together with simulations of the "split" and "unsplit" signals. **A**: spectrum observed at pH 5.0; **B**: simulation produced by a combination of simulated spectra, 40% "split" and 60% "unsplit"; **C**: spectrum at pH 5.0 minus that at pH 7.0 revealing the "split" signal.; **D**: simulation of the "split" signal; **E**: simulation of the "unsplit" signal. The signal * is attributed to radicals that derive from redox mediators used in the titration. EPR conditions are the same as in legend to figure 1. Simulation parameters: "split" signal, g_{xyz} = 1.888, 1.927, 1.960; $A(^{183}W)_{xyz}$ = 4.0, 4.0, 4.0 mT, $A(^{1}H)_{xyz}$ = 1.3, 1.4, 2.0 mT, linewidth W_{xyz} = 0.8, 0.83, 1.5 mT; "unsplit" signal, g_{xyz} = 1.860, 1.928, 1.958; $A(^{183}W)_{xyz}$ = 4.0, 4.0, 4.0 mT, W_{xyz} = 2.0, 1.0, 1.3 mT.

$E_m(W^{VI/V})$ and $E_m(W^{V/IV})$ of W-DMSOR

The redox titration curves obtained for W-DMSOR at pH 5.0, 6.0, 7.0 and 8.0 are shown in figure 3. The maximum quantity of W^V, *ca.* 40% of the tungsten present in the sample, occurs at pH 5 and the amount decreases at higher pH. The redox titration curves were interpreted successfully on the basis of two redox couples, a pH-dependent $E_m(W^{VI/V})$ couple and a pH-independent $E_m(W^{V/IV})$ couple and the midpoint potentials obtained for these couples are given in table 1. However, it should be noted that the pH dependence of the $E_m(W^{VI/V})$ is only –31 mV/(pH unit), *i.e.* significantly lower than the –59 mV/(pH unit) expected for one-electron reduction coupled to stoichiometric uptake of a proton. Previously, determinations of $E_m(Mo^{VI/V})$ and $E_m(Mo^{V/IV})$ for Mo-DMSOR of *Rhodobacter sphaeroides* have been reported as +141 mV and +200 mV (pH 7.0) [106] and +37 and +83 mV (pH 8.5) [142].

Table 1. Midpoint potentials of the tungsten center in DMSO reductase.

pH	E_m (W^{6+}/W^{5+}) (mV)	E_m (W^{5+}/W^{4+}) (mV)
5.0	-133	-142
6.0	-167	-156
7.0	-194	-134
8.0	n.d.	n.d.

n.d. not determinable.

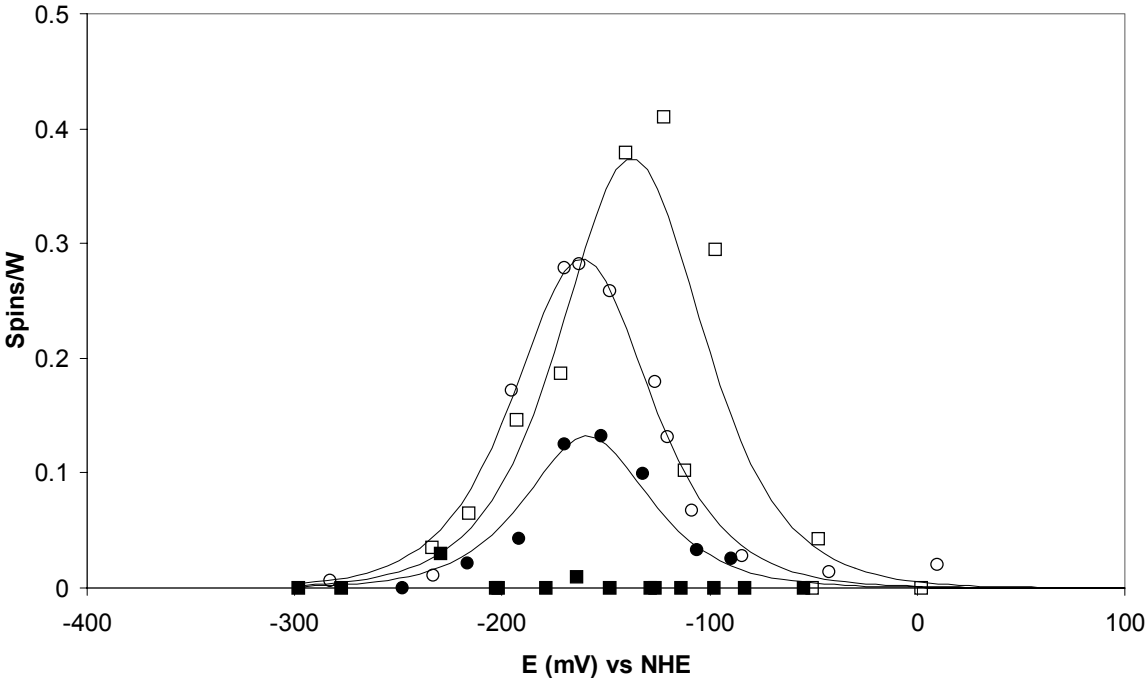

Figure 3. Amount of W^V (normalized with respect to the total amount of tungsten present in the sample) present in W-DMSOR as a function of the redox potential of the medium at pH 5.0 (□); pH 6.0 (○); pH 7.0 (●); pH 8.0 (■). The experimental data for each pH have been fitted (solid line) to the Nernst equation, on the basis of two one-electron couples, W^{VI}/W^V and W^V/W^{IV}, with the midpoint potentials given in Table 1.

Discussion

EPR properties of W-DMSO reductase

The "split" W^V-signal of W-DMSOR has a g_{av} = 1.925 and the "unsplit" W^V–signal has g_{av} = 1.916. In the oxidized state of W-DMSOR, the metal is bound to an oxo-group, one serine oxygen, and four dithiolene sulfurs [80]. We propose that the "split" signal is generated by coupled electron/proton addition, producing a $\{W^V(OH)(O_{Ser})(S_{dithiolene})_4\}$center. The "unsplit" signal is proposed to represent the deprotonated form.

Several Mo^V-signals have been reported for reduced forms of Mo-DMSOR, however, only the "high-g-unsplit" and "high-g-split" signals are considered to be biochemically relevant and each signal has g_{av} = 1.98 [145, 146]. The former has been attributed to a Mo^V center without a coordinating oxo- or hydroxo-group and the latter to a center posessing a Mo^V-OH moiety [146].

A Mo^V–compound generally possesses a g_{av}-value closer to the free-electron value than the corresponding W^V–compound and this is attributed to the spin-orbit coupling parameter of W^V ($\zeta = 2700$ cm^{-1}) being larger than that of Mo^V ($\zeta = 900$ cm^{-1}) [147, 148]. The spin-orbit coupling parameters of sulfur ($\zeta = 382$ cm^{-1} in SH [149]) and oxygen ($\zeta = 152$ cm^{-1} in OH [149]) further affect the g_{av}-value observed for Mo^V- and W^V-compounds.

The respective anisotropy (g_z-g_x) and rhombicity (g_z-g_y/g_z-g_x) are 0.071 and 0.44 for the "split" W^V-signal and 0.096 and 0.31 for the "unplit" signal; these values are 0.027 and 0.41 for the "high-g-split" Mo^V signal and 0.025 and 0.25 for the "high-g-unsplit" signal [106, 145]. Thus, the anisotropy for each W^V-signal is greater than that of the corresponding Mo^V-signal. However the rhombicity is similar for the corresponding W^V and Mo^V centers, as expected since the geometry of the site is essentially unchanged upon substitution of the molybdenum with tungsten in DMSOR. These results are similar to observations of the tungsten substituted sulfite oxidase [137] and to previous observations in inorganic model compounds [150, 151]. However, contrary to sulfite oxidase, DMSOR is known to retain catalytic activity and three-dimensional structure upon replacement of molybdenum with tungsten [80].

Redox properties of W-DMSO reductase

The $E_m(M^{VI/V})$ and $E_m(M^{V/IV})$ values of *R. capsulatus* W-DMSOR were determined by EPR-monitored redox titrations. The $E_m(M^{VI/V})$ and $E_m(M^{V/IV})$ values were obtained by fitting the variation in the amount of W^V (expressed as a percentage of the total amount of tungsten present) to the Nernst equation for two sequential one-electron processes. The intensity of the W^V EPR signal was observed to be a maximum at pH 5.0, decreasing with increasing pH. This observation can be explained by a pH dependence of $E_m(W^{VI/V})$ and/or $E_m(W^{V/IV})$. The values obtained for these couples are shown in table 1 and the former varies with pH (*ca.* –31 mV/pH unit); at pH 7.0, $E_m(W^{VI/V}) = -194$ mV and $E_m(W^{V/IV}) = -134$ mV.

Two previous redox titrations of *R. sphaeroides* Mo-DMSOR have been published: at pH 7.0, $E_m(Mo^{VI/V}) = +141$ mV and $E_m(Mo^{V/IV}) = +200$ mV [106]; at pH 8.5, $E_m(Mo^{VI/V}) = +37$ mV and $E_m(Mo^{V/IV}) = +83$ mV [142]. A decrease in the intensity of the Mo^V EPR signal with increasing pH was observed [106] and a pH dependence of –59 mV/pH for both couples was inferred [142, 146]. In each case, the

data were rather scattered around the fit and one [106] titration clearly deviated from Nernstian behaviour.

Determination of the $E_m(M^{VI/V})$ and $E_m(M^{V/IV})$ values from EPR-monitored redox titrations of molybdenum and tungsten enzymes is not trivial. The EPR detectable Mo^V (or W^V) species usually exists as an intermediate during the redox cycle that operates between the M^{VI} and M^{IV} states. The M^V usually comprises a relatively small fraction of the total metal content. Furthermore, often several different Mo^V (or W^V) species are found depending on the history and the nature of the sample. Also, the fit of the data to the Nernst equation for two sequential one-electron processes is very sensitive to the percentage of the M^V state present. Therefore, an accurate assessment is required of both the amount of M^V and the total amount of M present. The datapoints are fitted to the Nernst equation for two sequential one-electron reductions. Thus, the accuracy of the E_m values obtained are subject to significant uncertainty (±30 mV).

The crystal structure of oxidized *R.capsulatus* W-DMSOR [80] shows that the tungsten center is coordinated by the four dithiolene sulfurs from the MPT, one oxygen from Ser147 and one oxo-ligand. This structure is similar to the crystal structure of oxidized *R.capsulatus* Mo-DMSOR, although the latter shows an extra oxygen ligand to the metal center [140]. However, the 1.3 Å crystal structure of *R. sphaeroides* Mo-DMSOR revealed that the structure results from a superposition of two independent active site conformations: a “normal” hexacoordinate environment, and a distorted pentacoordinate environment due to binding of a Hepes molecule at the active site [141]. Given the structural similarity of the Mo and W sites in DMSOR, differences in the redox behaviour between Mo-DMSOR and W-DMSOR are directly attributable to the change in the metal, although MPT may modulate the redox potential [152].

Tungsten is more difficult to reduce than molybdenum in non-biological isostructural compounds [153]. As can be seen in Table 2, the redox potentials of tungsten compounds are 225-450 mV lower than their molybdenum counterparts [150, 154], depending on the acidity of the coordinating ligands. This report has shown that the same holds for DMSOR. Furthermore, the redox potential differences explain why W-DMSOR cannot oxidize DMS, in contrast to Mo-DMSOR, while W-DMSOR reduces DMSO *ca.* 17 times faster than Mo-DMSOR [80]. The midpoint potentials of Mo-DMSOR are close to the midpoint potential of the DMSO/DMS

couple (+160 mV [155]), while the midpoint potentials of W-DMSOR are *ca.* 335 mV lower. Clearly DMSO reduction, and not DMS oxidation, is thermodynamically favorable for W-DMSOR. Differences in the reduction potentials, and as a consequence altered reaction rates, may explain why certain organisms (e.g. *Pyrococcus furiosus* [156]) prefer tungsten over molybdenum enzymes.

pH dependence of the redox potentials of W in W-DMSOR

The maximum W^{V} EPR signal observed is the highest at pH 5.0 and decreases with increasing pH. This observation can be explained by a pH dependence of the $E_m(W^{VI/V})$ and/or $E_m(W^{V/IV})$. Furthermore the W^{V} "split" signal exhibits

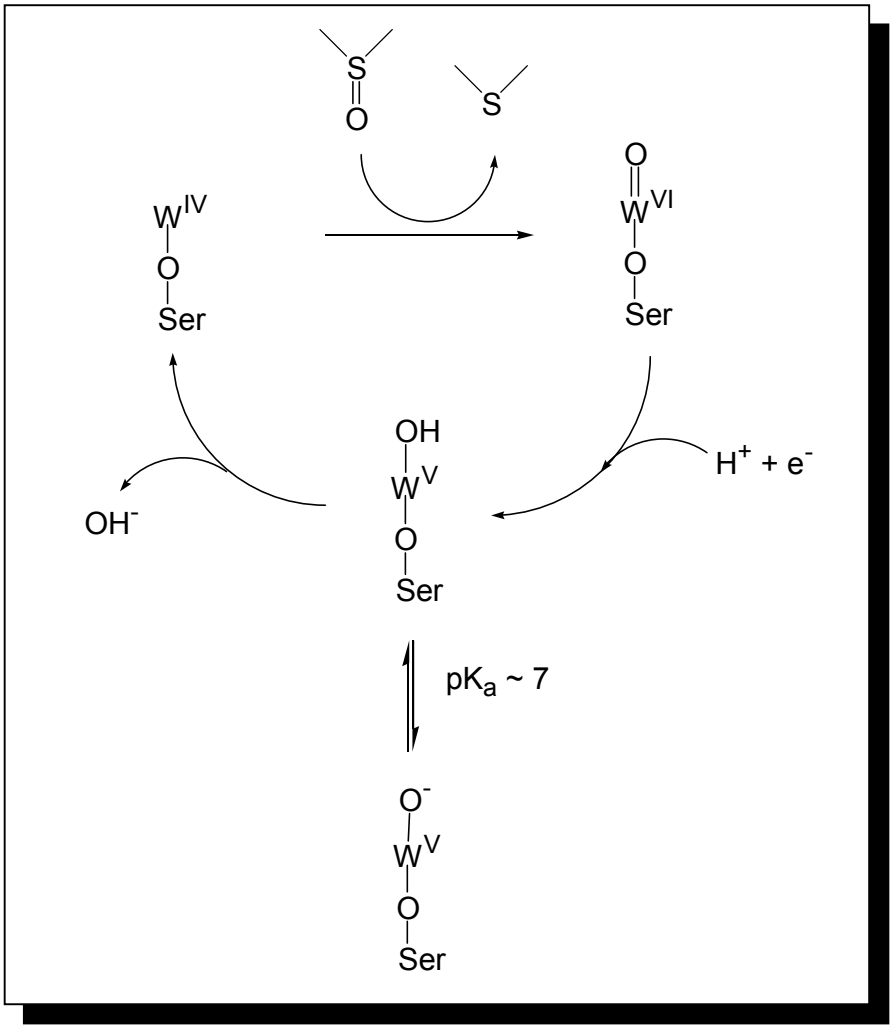

Figure 4. Schematic overview of a possible catalytic mechanism of the DMSO reduction by the tungsten substituted DMSO reductase. For simplicity the four dithiolene sulfurs from the MPT cofactors coordinating the tungsten center have been removed.

superhyperfine coupling to a nearby proton. These results are consistent with a coupled electron-proton addition involved in the second half reaction of DMSOR, i.e. regeneration of W^{IV} from W^{VI}-oxo (Figure 4) [150]. The W^{V}-hydroxo intermediate of this mechanism, may be represented by the "split" signal in figure 1. For Mo-DMSOR a gradual decrease in Mo^{V} EPR signal intensity with increasing pH has been observed previously [106]. Furthermore, a pH dependence of –59 mV/pH of both couples has been inferred based on two redox titrations [106, 142, 146].

Acknowledgments

This research was supported by the Council for Chemical Sciences of the Netherlands Organization for Scientific Research (CW-NWO) and the Engeneering and Physical Sciences Research Council (UK).

Chapter 6

Electroanalytical determination of tungsten and molybdenum in proteins

Peter -L. Hagedoorn, Petra van ‘t Slot, Herman P. van Leeuwen, Wilfred R. Hagen

Published in: Anal. Biochem. 297, pp. 71-78, 2001.

Recent crystal structure determinations accelerated the progress in the biochemistry of tungsten containing enzymes. In order to characterize these enzymes, a sensitive determination of this metal in protein containing samples is necessary. An electroanalytical tungsten determination has successfully been adapted to determine the tungsten and molybdenum content in enzymes. The tungsten and molybdenum content can be measured simultaneously from 1-10 µg of purified protein with little or no sample handling. More crude protein samples require precipitation of interfering surface active material with 10% perchloric acid. This method affords the isolation of novel molybdenum and tungsten containing proteins via molybdenum and tungsten monitoring of column fractions, without using radioactive isotopes. A screening of soluble proteins from *Pyrococcus furiosus* for tungsten, using anionic-exchange column chromatography to separate the proteins, has been performed. The three known tungsten containing enzymes from *Pyrococcus furiosus* were recovered with this screening.

Introduction

Tungsten has been found to be an essential element for bacteria, methanogenic and hyperthermophilic archaea (see [43, 134, 135] for reviews). It is chemically similar to molybdenum, which has been known to be a bioelement for decades. The biochemistries of tungsten and of molybdenum are also entangled. Tungsten, which is a bioelement for some organisms, is toxic towards many others as it can act as a molybdenum antagonist. Recent determinations of crystal structures of tungsten and molybdenum containing proteins accelerated the progress in elucidating the biological importance of these metals. Reliable analytical determinations for tungsten and molybdenum are important for the study of the proteins that contain these metals. However the analytical determination of tungsten in biological materials is not trivial. The most frequently used determinations of biological tungsten and molybdenum are inductively coupled plasma mass spectrometry (ICP-MS)[2] and colorimetry. The colorimetric methods suffer in resolution from the chemical similarity of molybdenum and tungsten and are relatively insensitive [157, 158]. And although the development of sensitive ICP-MS determinations of tungsten is in progress [159-161], stripping voltammetric techniques are still superior in sensitivity (see Table 1). Stripping voltammetric techniques are often used in environmental chemistry to analyze water samples for trace concentrations and speciation of heavy metals. In spite of the sensitivity, stripping voltammetric techniques have not been used to determine tungsten or molybdenum in proteins, although some applications to determine molybdenum in complex biological matrices (e.g. foodstuffs) have been described [162, 163]. Here we present a sensitive, selective and fast method to simultaneously determine tungsten and molybdenum in purified or crude protein samples. The electroanalytical method used is adsorptive stripping voltammetry (AdSV). The method consists of adsorption accumulation of molybdenum or tungsten, complexed with oxine and 3-methoxy-4-hydroxymandelic acid, on a mercury drop electrode surface at a potential of –100 mV with respect to NHE, followed by a voltammetric scan in the negative direction. The current response of the molybdenum or tungsten complexes is amplified by the catalytic reduction of chlorate by the metal complex [164]. The precise mechanism for this catalysis has not been established. A proposed mechanism is given below:

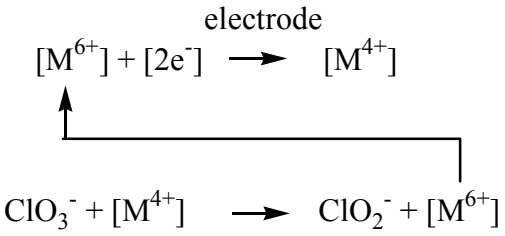

In which [M] is the tungsten or molybdenum complex.

Table 1. comparison different tungsten determinations.

method	detection limit W (nM)	Reference
AdSV	0.025[a,d]	[164]
ICP-MS	0.40[b]/272[a]	[160]/[159]
ICP-AES	98[b]	[160]
Colorimetry	435[b]/1666[c]	[158]/[157]

[a]detection limit defined as 3 times the noise level. [b]detection limit defined as 3 times the standard deviation. [c]detection limit defined as absorbance at 630 nm = 0.05 a.u. [d]with a 5 minutes deposition time.

Materials and methods

Equipment and chemicals

Electrochemical measurements were performed with a digitally controlled PSTAT10 potentiostat using GPES 4.8 software (Eco-chemie, The Netherlands) equipped with a hanging mercury drop working electrode (HMDE 663 VA stand, Metrohm Switzerland), a glassy carbon counter electrode, and a double-junction Ag/AgCl (3M KCl) reference electrode (Metrohm). Oxine, 3-methoxy-4-hydroxymandelic acid, sodium tungstate, sodium molybdate and sodium chlorate were obtained from Sigma. Mercury AR grade, perchloric acid, hydrochloric acid, sulfuric acid and formic acid were obtained from Merck. Bicinchoninic acid protein assay was obtained form Pierce. Bovine milk xanthine oxidase (EC 1.1.1.204) was used as obtained from Boehringer Mannheim. The xanthine oxidase concentration was determined using $\varepsilon_{450} = 72\ mM^{-1}cm^{-1}$ [108]. *Pyrococcus furiosus* glyceraldehyde-3-phosphate oxidoreductase was purified as described [61]. The glyceraldehyde-3-

phosphate oxidoreductase concentration was determined using the bicinchoninic acid protein assay and the molar mass of 80 kDa based on the amino acid sequence [60].

Electroanalytical determination of tungsten and molybdenum

Tungsten concentration was determined by catalytic-adsorptive stripping voltammetry according to [164]. Aliquots (1-100µl) of samples or standard solutions were added to a 20 ml blank solution containing 10 mM H_2SO_4, 0.5 mM oxine, 0.05 mM 3-methoxy-4-hydroxymandelic acid and 50 mM $NaClO_3$. The potentials are reported with reference to the normal hydrogen electrode. For the adsorptive stripping voltammetry (AdSV) the following conditions were used: pulse height 25 mV, step potential 5 mV, deposition potential –0.10 V, deposition time 120 s, stirring speed during deposition 1000 rpm, scan range –0.10 to –1.20 V. The mercury drop surface was approximately 0.52 mm^2. Sodium chlorate was used instead of potassium chlorate, because of its higher solubility in water.

Sample handling

The protein containing samples were digested with perchloric acid (final concentration 10% w/v). Precipitated protein was removed by centrifugation for 5 minutes at 9000 rpm. The supernatant was analyzed as described above. Prior to measurement the solution was purged with high-purity argon for 300 s.

Screening soluble proteins from Pyrococcus furiosus for tungsten

All buffers used were anaerobic and contained 1 mM dithiothreitol (DTT) and 1 mM cystein. *Pyrococcus furiosus* (DSM 3638) cells were grown and cell free extract was obtained as previously described [61]. Cell free extract was loaded using an FPLC system (Pharmacia) on a 300 ml DEAE Sepharose fast flow column (Pharmacia) equilibrated with 20 mM Tris-HCl buffer pH 8.0. Proteins were separated using an FPLC system (Pharmacia) by applying a 1 L gradient from 0 to 1 M NaCl 20 mM Tris-HCl pH 8.0. Fractions (25 ml) were collected anaerobically and monitored for tungsten content and tungstoenzyme (aldehyde oxidoreductase, formaldehyde oxidoreductase and glyceraldehyde-3-phosphate oxidoreductase) activity . Aldehyde oxidoreductase activity was monitored spectrophotometrically at 60°C as the crotonaldehyde oxidation with benzyl viologen as artificial electron acceptor. Stoppered anaerobic cuvettes contained assay buffer pH 8.4 consisting of 50

mM EPPS , 50 mM tricin, 50 μM deazaflavin and 1.0 mM benzyl viologen. The contents of the cuvettes were slightly pre-reduced using the photoreduction of deazaflavin, prior to addition of the enzyme sample [165]. The reaction was started by adding 0.6 mM crotonaldehyde, and the reduction of benzyl viologen was followed at 580 nm (molar absorption coefficient 7,800 $M^{-1}cm^{-1}$). The formaldehyde oxidoreductase activity assay was similar to the aldehyde oxidoreductase assay, however with using 0.2 mM formaldehyde as substrate and 5 mM methyl viologen as artificial electron acceptor. The methyl viologen reduction was followed at 600 nm (molar absorption coefficient 12,000 $M^{-1}cm^{-1}$). The glyceraldehyde-3-phosphate oxidoreductase activity assay was similar to the aldehyde oxidoreductase assay, however with 0.5 mM glyceraldehyde-3-phosphate as substrate. The tungsten content was measured as described above using standard additions.

Results

Performance of the molybdenum and tungsten determination

The performance of the tungsten determination was similar to that described by Wang and Lu[164] (see Figure 1.). The dependence of the peak current on the concentration (see Figure 2 traces A and B) fit a Langmuir adsorption isotherm (equation {1})

$$I_p = \frac{I_{p,\max} \cdot \beta \cdot c}{1 + \beta \cdot c} \qquad \{1\}$$

in which $\beta = \exp(-\Delta G°/RT)$, ΔG° is the free energy of adsorption, c is the bulk concentration of adsorbent, I_p is the peak current, and $I_{p,\max}$ is the peak current from a covered surface. The Langmuir isotherm describes the relation between the amount of adsorbed compound and the equilibrium concentration of adsorbate at a given temperature with the following assumptions: no interaction between adsorbed species on the electrode surface, no heterogeneity of the electrode surface, and saturation coverage of the electrode by the adsorbate at high bulk concentrations [166]. At relatively low concentrations (below 20 nM) the adsorption isotherm is approximately linear, defining a convenient range to use for analytical purposes. The peak current has been found to be directly proportional to the size of the electrode surface area (not

shown). These results suggest that the extent of adsorption of the complex at the mercury surface is limiting the peak current.

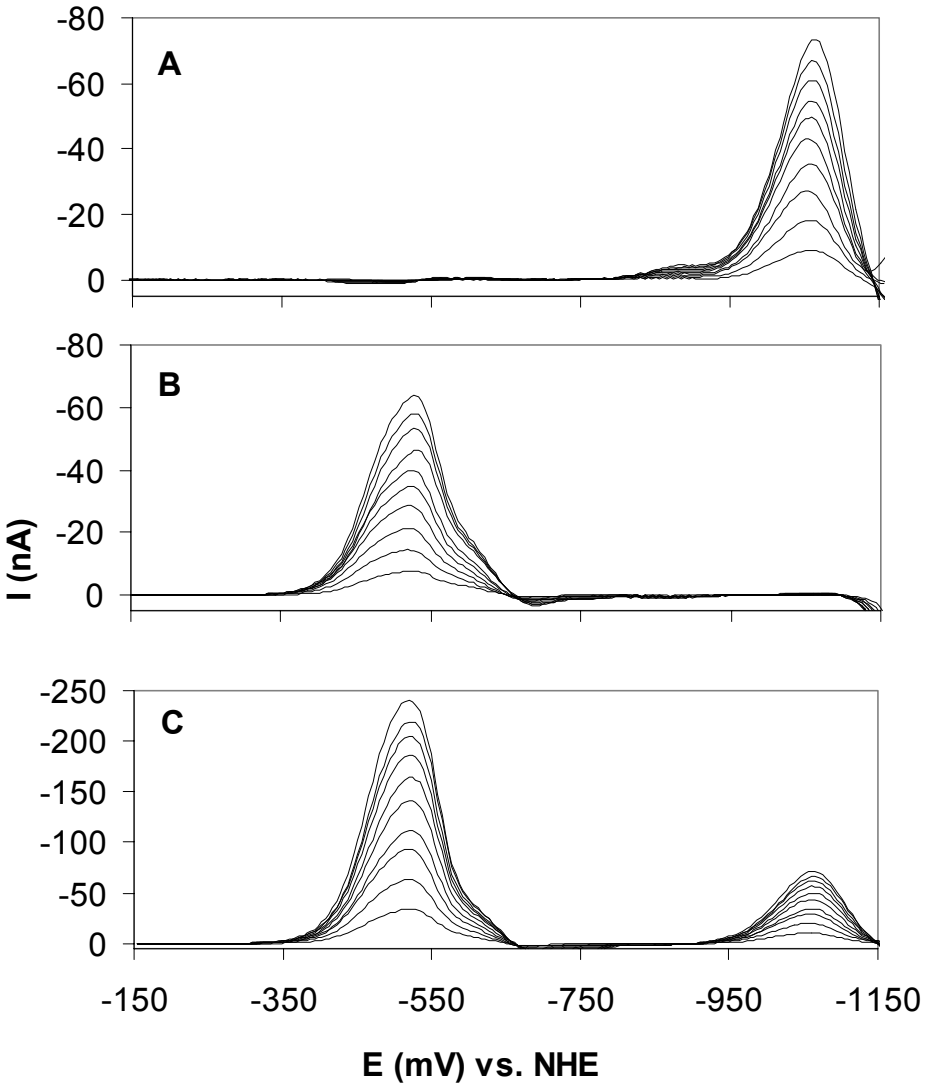

Figure 1. Simultaneous determination of tungsten and molybdenum
Trace A. 1.0-10 nM tungsten. Trace B. 0.25-2.5 nM molybdenum. Trace C. 1.0-10 nM molybdenum and tungsten 1:1. The voltammogram of the blank solution has been subtracted. The measurement solution consisted of 10 mM H_2SO_4, 0.5 mM oxine, 0.05 mM 3-methoxy-4-hydroxymandelic acid and 50 mM $NaClO_3$. Adsorptive stripping voltammetric (AdSV) conditions: deposition potential –0.10 V, deposition time 120 s, stirring speed during deposition 1000 rpm, equilibration time after deposition 20 s, pulse amplitude 25 mV, step potential 5 mV, scan range –0.10 to –1.20 V.

Simultaneous determination of molybdenum and tungsten

Wang and Lu reported a response of molybdenum at a peak potential of approximately 500 mV lower than that of tungsten, which is even more sensitive than the tungsten response[164]. However, no details about possible interference on the tungsten determination were given. Since we have found that adsorption to the electrode determines the electrochemical response of the molybdenum or tungsten complex, it is likely that molybdenum and tungsten will compete for the same electrode surface and thus complicate a simultaneous determination. However, as can be seen in figure 2 traces C and D, these metals only show a mutual interference at relatively high concentrations (> 10 nM). The peak currents do not longer fit a Langmuir isotherm. Competitive adsorption, however, is not a sufficient model to fit the peak currents. Apparently the interference between tungsten and molybdenum is more complex. When the method is used only in the range below 10 nM, molybdenum and tungsten can be determined simultaneously without interference.

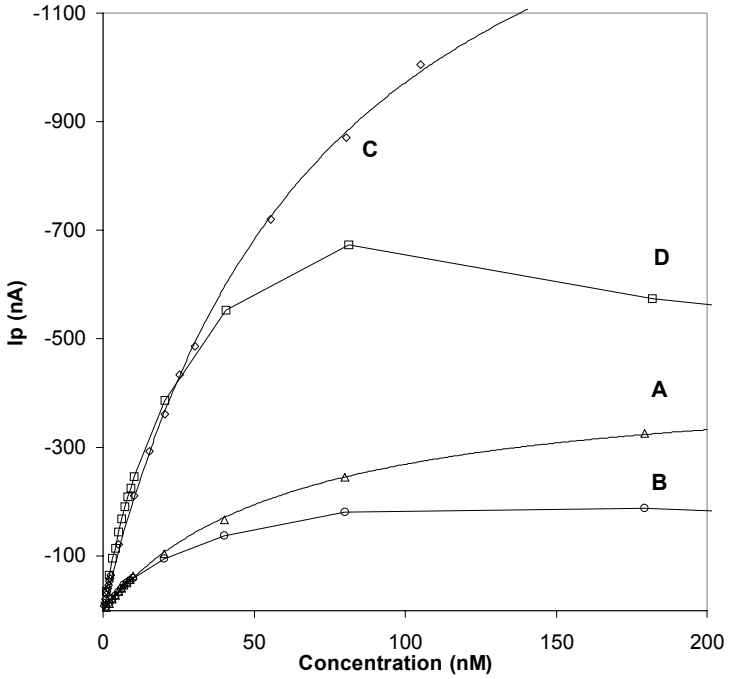

Figure 2. Tungsten and molybdenum peak currents fit to a Langmuir adsorption isotherm. Trace A. tungsten only. Trace B. tungsten in the presence of equimolar molybdenum. Trace C. molybdenum only. Trace D. molybdenum in the presence of equimolar tungsten. Measurement solution and AdSV conditions were as in Figure 1. Trace A and B are fitted to the Langmuir isotherm (equation {1}). Trace B and D do not fit to a Langmuir isotherms since the two metals mutually interfere.

Applicability to protein samples

It is important for a determination of biological tungsten and molybdenum that other bio-metals do not give significant interference. Wang and Lu have previously established that the response of 5 nM tungsten (with a 30 second deposition time) is not influenced by 1 $\mu g \cdot L^{-1}$ Mn^{2+}, Co^{2+}, Ni^{2+} or Zn^{2+} i.e. approximately 60 fold excess over tungsten [164]. Notably, iron is frequently present in molybdenum and tungsten containing proteins as iron-sulfur cluster prosthetic groups. We have found that up to 10000 fold excess of Fe^{2+} or Fe^{3+} does not influence the response of 5 nM tungsten or

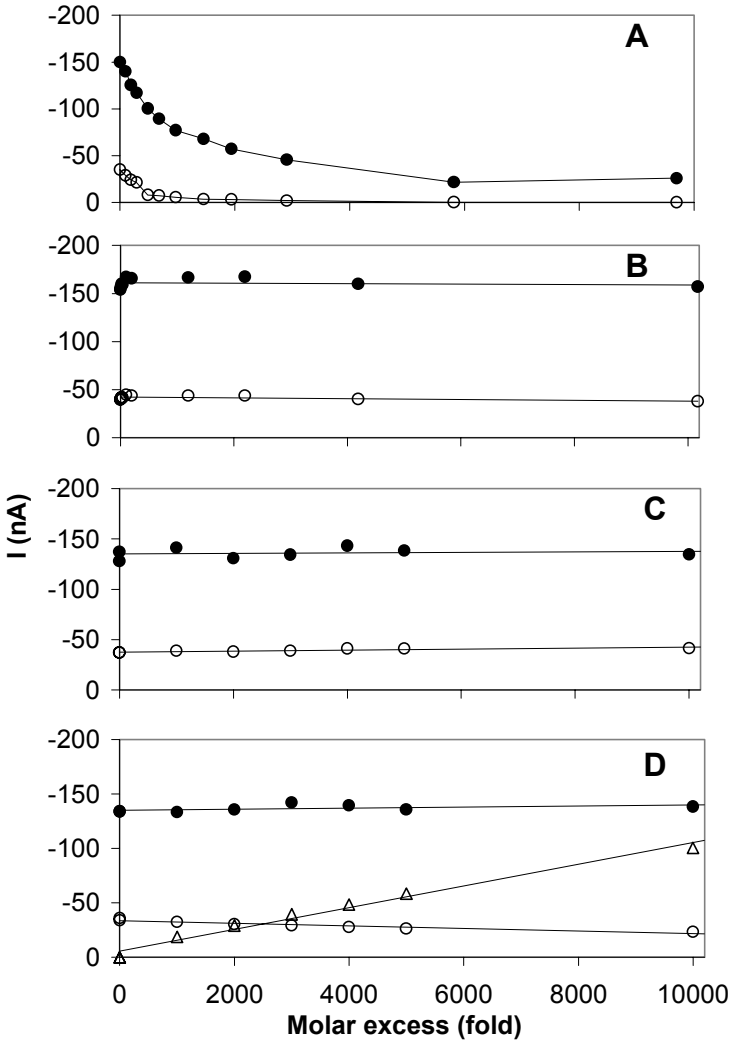

Figure 3. Effect of possible interfering metals on the determination of 5 nM tungsten and 5 nM molybdenum. Interfering ion in A, Ti^{3+}; B, Fe^{3+}; C, Fe^{2+}; D, Cu^{2+}. Measured ions are ● Mo, ○ W, Δ Cu. Measurement solution and AdSV conditions were as in Figure 1.

molybdenum (see Figure 3 B and C). Copper gives a response at –216 mV, which is at least 2000 times less sensitive than the molybdenum and tungsten responses. At 10000 fold excess of Cu^{2+} concentrations the tungsten response is 30% reduced. The molybdenum response, however, is unaffected. Ti^{3+} gives a response at -900 mV partially overlapping with the tungsten response. The responses of tungsten and molybdenum are significantly decreased if Ti^{3+} is present in high excess (>100 fold). Although titanium is not a bio-element, titanium(III)citrate is a reducing agent sometimes used in biochemistry. Results for Fe^{2+}, Fe^{3+}, Ti^{3+} and Cu^{2+} are presented in figure 3.

Interference of surface active materials

Surface active materials, such as proteins, are known to interfere in stripping

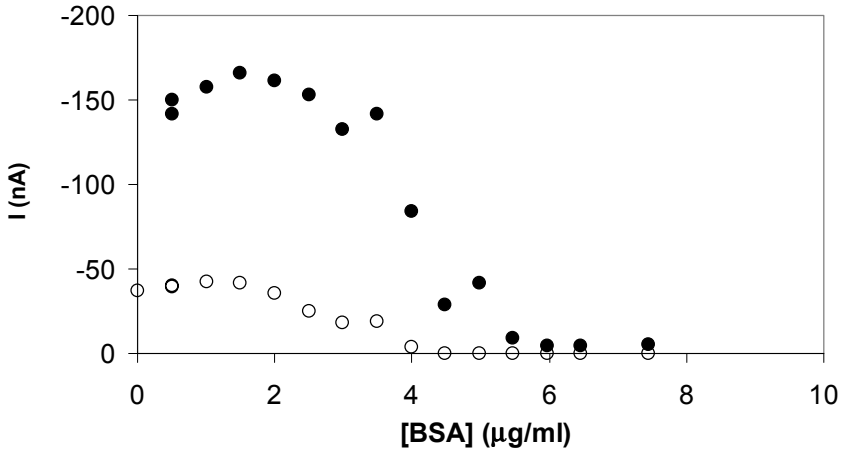

Figure 4. Effect of bovine serum albumin, a surface active material, on the determination of 5 nM tungsten and 5 nM molybdenum. ● Mo, ○ W. Measurement solution and AdSV conditions were as in Figure 1.

voltammetry. Wang and Lu reported significant interference of gelatin on the tungsten determination [164]. To test the effect of proteins on the molybdenum and tungsten determination, bovine serum albumin (67 kDa) was used as a model system. Since adsorption is the essential process in this determination, adsorption of the metal to the protein surface will interfere significantly with the determination. Proteins may also adsorb at the mercury surface and thus interfere at the electrode. As can be seen in

figure 4, BSA was found to result in reduced peak currents from 5 nM Mo and 5 nM W if present in concentrations above 2 µg/ml (=29.9 nM, 6 fold molar excess). Although at high concentrations of protein the responses collapse, at lower concentrations, ≤ 2 µg/ml, BSA does not interfere with the determination. This opens the possibility to determine the molybdenum and tungsten content of purified proteins without any sample pretreatment, assuming the metal is released from the protein in the measurement solution (pH 2). To analyze more crude protein samples digestion or removal of interfering protein material is necessary.

Perchloric acid precipitation of interfering protein material

In order to avoid laborious digestion of the protein samples, e.g. with wet ashing, precipitation with 10% perchloric was tested for removing interfering protein from the sample while leaving the metal in solution (see Figure 5). Perchloric acid precipitation is a common method to remove proteins form e.g. human serum [167].

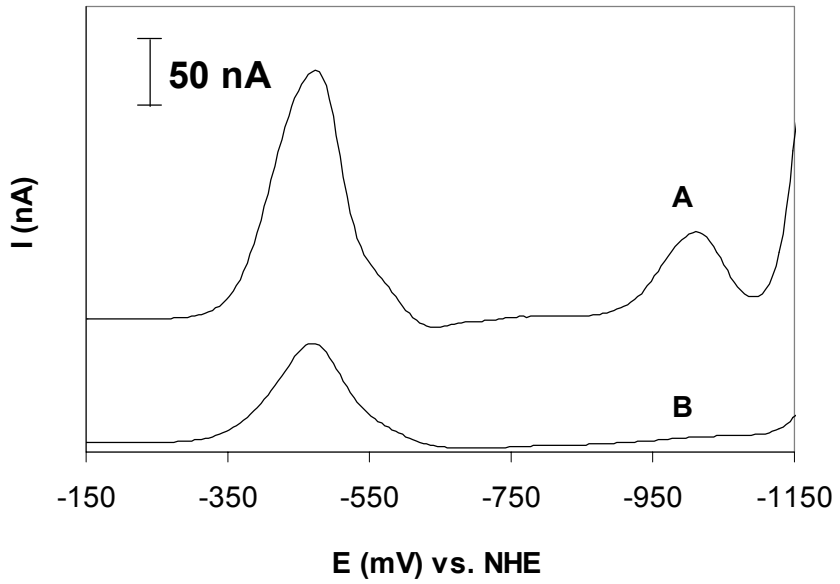

Figure 5. Effect of 10% perchloric acid precipitation on the interference of BSA.
Measurement of 8 nM Mo and W in the presence of 3.6 µg/ml BSA. Trace A. with precipitation prior to measurement. Trace B. without precipitation. Measurement solution and AdSV conditions were as in Figure 1.

Measurement of 8 nM Mo and W in the presence of 3.6 µg/ml BSA resulted in 98% reduction of the tungsten response and 60% reduction of the molybdenum response. Precipitation of protein in the same sample with 10% perchloric acid prior to measurement resulted in a recovery of 92% of the tungsten and 93% of the molybdenum. The AdSV method of Wang and Lu [164] is thus applicable to crude protein samples after precipitation with perchloric acid.

Mo and W content of purified proteins

Xanthine oxidase and glyceraldehyde-3-phosphate oxidoreductase are enzymes containing molybdenum and tungsten, respectively [59, 168]. Figure 6 shows the adsorptive stripping voltammograms of xanthine oxidase and glyceraldehyde-3-phosphate oxidoreductase. From this figure it is readily determined which enzyme contains molybdenum and which one tungsten. The molybdenum and tungsten contents of these enzymes have been determined as described above with

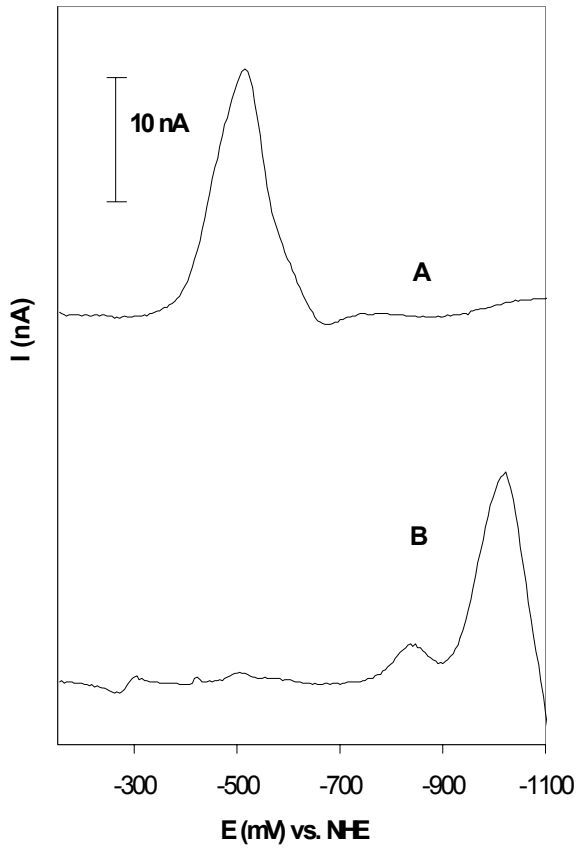

Figure 6. Molybdenum and tungsten determinations of enzymes.
Trace A. 0.77 nM xanthine oxidase. Trace B. 3.3 nM glyceraldehyde-3-phosphate oxidoreductase. Measurement solution and AdSV conditions were as in Figure 1.

four standard additions of a known concentration of molybdenum and tungsten. In total 7 µg xanthine oxidase and 10 µg glyceraldehyde-3-phosphate oxidoreductase have been used to take 4 samples well above the detection limit. The xanthine oxidase sample contained 1.7 ± 0.1 Mo/molecule and no detectable tungsten. Xanthine oxidase is expected to have 2 Mo atoms/molecule and no tungsten. Glyceraldehyde-3-phosphate oxidoreductase contained 0.6 ± 0.1 W/molecule and no detectable Mo. This is in reasonable agreement with the 1 W atom per molecule which is expected for this enzyme (assuming a 100% holoenzyme). Precipitation with perchloric acid did not increase the metal contents for these enzymes. These determinations illustrate the fact that purified proteins can be analyzed without sample pretreatment.

Screening of soluble proteins from Pyrococcus furiosus for tungsten

Pyrococcus furiosus is a hyperthermophilic archaeon from which three different tungsten containing enzymes have been isolated [44, 57, 59]. Although *Pyrococcus furiosus* prefers tungsten over molybdenum, even when molybdenum is present in 6,500 fold excess [156], no tungsten transport or storage proteins have been isolated. The electroanalytical tungsten determination was used to search for possible tungsten transport or storage proteins. During a protein purification step the three enzymatic activities of the known tungsten enzymes and the tungsten content were monitored. Figure 7 shows the elution profile of a linear gradient from 0-1 M NaCl from a DEAE-sepharose column. The peaks containing the different activities from the tungsten enzymes coincide with the tungsten peaks. Formaldehyde oxidoreductase activity shows two peaks in the elution profile, which are explained by the formaldehyde oxidizing ability of both formaldehyde oxidoreductase and aldehyde oxidoreductase [57]. The known tungsten enzymes can thus be recovered monitoring column fractions with the tungsten determination. Interestingly, several additional tungsten peaks are found, which may represent novel tungsten containing enzymes. Isolation of these putative tungsten containing proteins is in progress.

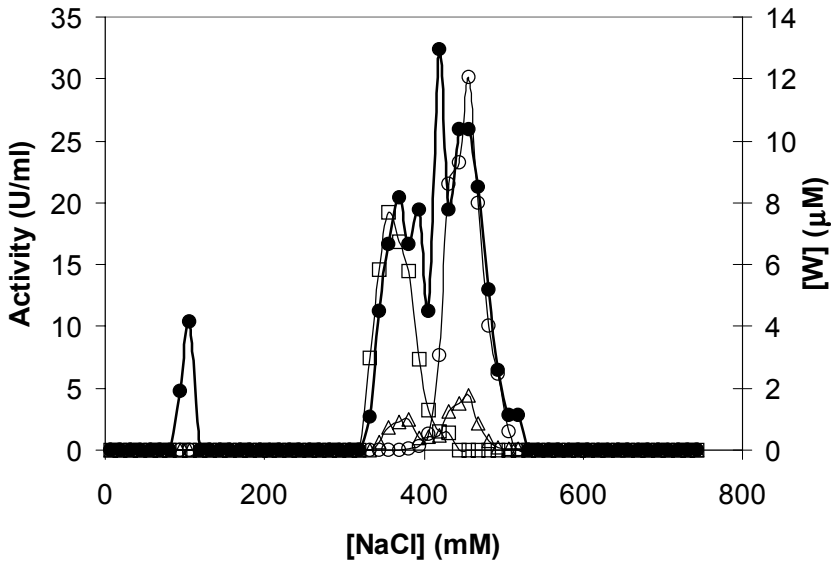

Figure 7. Biochemical application of the tungsten determination.● tungsten content determined by AdSV. ○ Aldehyde oxidoreductase activity. □ Glyceraldehyde-3-phosphate oxidoreductase activity. Δ Formaldehyde oxidoreductase activity. Measurement solution and AdSV conditions were as in Figure 1. Activity assayed at 60°C with benzyl viologen as an artificial electron acceptor.

Discussion

Performance of the molybdenum and tungsten determination

Wang and Lu have previously suggested that molybdenum and tungsten can be determined simultaneously with the method used in this report [164]. No significant interference was expected, based on the well-separated peak potentials of the molybdenum and tungsten responses. However, we have shown that this holds only at low concentrations (<10 nM) of molybdenum and tungsten. From the Langmuir isotherms of the molybdenum and tungsten responses (Figure 2, trace A and B) it can be concluded that the maximum current at saturation of the mercury surface is four times as high for molybdenum as for tungsten. Interestingly, the free energy of adsorption, calculated from the adsorption coefficient β using equation [1], is very similar for the two metals: 10.0 kJ/mol for tungsten and 10.5 kJ/mol for molybdenum. Apparently the affinity for the electrode surface is not much different

for tungsten and molybdenum. The chlorate catalysis, however, is much faster with molybdenum than with tungsten. The higher catalytic response for molybdenum is probably due to kinetic factors, because a faster catalysis for tungsten is expected based on the reduction potential [169]. The reduction potential for the molybdenum complex was found to be 500 mV higher than for tungsten. It is a common finding that tungsten compounds are more slowly reduced than their molybdenum counterparts [170]. This is the first report of an electrochemical method to determine the molybdenum and tungsten content of a protein. It is also the most sensitive determination described to date. Furthermore, tungsten and molybdenum can be determined in the presence of a high excess of other biochemically important metals, such as iron.

The mechanism of the electrochemical tungsten and molybdenum determination

Both the molybdenum and tungsten responses show overlapping major and minor peaks (Figure 1), which have not been mentioned by Wang and Lu [164]. Similar observations have been reported for several electroanalytical molybdenum determinations [162, 171, 172]. Three possible mechanisms have been proposed in the literature [163, 171, 173] for electroanalytical molybdenum determinations using one chelator and catalytic reduction of chlorate or nitrate. The three mechanisms involve a reduction of Mo^{VI} to Mo^{V} at the electrode as a first step. The proposed catalytic cycle, which follows, is different in all three cases. The species that have been proposed to reduce chlorate or nitrate are Mo^{III}, Mo^{IV} and Mo^{V}. The mechanism of the AdSV method by Wang and Lu is more complicated than the previously discussed ones, since it involves two different chelators [164]. The stoichiometry of the different chelators in the complex is not known. It may be that complexes are formed with different stoichiometries of the chelators. The different peaks found for molybdenum and tungsten can thus be the result of the different oxidation states of the metals and of different metal-chelate complexes formed with slightly different reduction potentials. For a complete understanding of the present data, these aspects would require a more detailed investigation.

Electroanalytical techniques as tools in biochemistry

The sensitivity of the method described in this report allows rapid screening of many protein containing samples for tungsten and molybdenum content, e.g. during a

protein purification. We have shown that we can recover the known tungsten enzymes from *Pyrococcus furiosus* during a protein purification with this method. The sensitivity of the method is competitive with the activity assays used for the tungsten enzymes, since we were able to find tungsten in all fractions containing tungstoenzyme activity. This electroanalytical determination can be an important tool to isolate new molybdenum and tungsten proteins, e.g. transport or storage proteins. Similar screenings have been performed for *Clostridium acidiurici* and *Clostridium cylindrosporum* using the radioactive isotope ^{185}W [68] and for *Clostridium pasterianum* [174, 175], *Klebsiella pneumoniae*, *Azotobacter vinelandii* [176] and *Rhodobacter capsulatus* using ^{99}Mo[177]. A molybdenum uptake investigation of *Escherichia coli* using ^{99}Mo has been reported [178]. The method presented in this report allows similar experiments to be performed without radioactive materials. Furthermore, the simultaneous determination of molybdenum and tungsten is attractive to screen proteins from organisms that contain both tungsten and molybdenum enzymes, such as *Clostridium formicoaceticum* [54].

Acknowledgments

W.F. Threels and S. Jansen from the Laboratory of Physical Chemistry and Colloid Science, Wageningen University (The Netherlands) are acknowledged for their help during this research. This research has been funded by the Nederlandse Organisatie voor Wetenschappelijk Onderzoek – Gebiedsraad Chemische Wetenschappen (CW-NWO).

Chapter 7

The effect of substrate, dihydrobiopterin and dopamine on the EPR spectroscopic properties and the midpoint potential of the catalytic iron in recombinant human phenylalanine hydroxylase

Peter–L. Hagedoorn, Peter P. Schmidt, K. Kristoffer Andersson, Wilfred R. Hagen, Torgeir Flatmark and Aurora Martínez

Published in: J. Biol. Chem. 276, pp. 22850–22856, 2001.

Phenylalanine hydroxylase (PAH) is a tetrahydrobiopterin (BH_4) and non-heme iron-dependent enzyme that hydroxylates L-Phe to L-Tyr. The paramagnetic ferric iron at the active site of recombinant hPAH, and its midpoint potential at pH 7.25 (E_m**(Fe(III)/Fe(II))), was studied by EPR spectroscopy. Similar EPR spectra were obtained for the tetrameric wild-type (wt-hPAH) and the dimeric truncated hPAH(Gly^{103}- Gln^{428}) corresponding to the "catalytic domain". A rhombic high spin Fe(III) signal with *g*-value 4.3 dominates the EPR spectra at 3.6 K of both enzyme forms. An E_m = + 207 ± 10 mV was measured for the iron in wt-hPAH, which seems to be adequate for a thermodynamically feasible electron transfer from BH_4 (**E_m *(quinonoid)*-BH_2/BH_4) = + 174 mV). The broad EPR features from *g* = 9.7 to 4.3 in spectra of the ligand-free enzyme decreased in intensity on addition of L-Phe, while more axial type signals were observed upon binding of 7,8-dihydrobiopterin (BH_2), the stable oxidized form of BH_4, and of dopamine. All three ligands induced a decrease in the E_m-value of the iron, to + 123 ± 4 mV (L-Phe), + 110 ± 20 mV (BH_2) and – 8 ± 9 mV (dopamine). On the basis of these data we have calculated that the binding affinities of L-Phe, BH_2 and dopamine decrease by 28-fold, 47-fold and 5040-fold, respectively, for the reduced ferrous form of the enzyme, with respect to the ferric form. Interestingly, an E_m-value comparable to that of the ligand-free, resting form of wt-hPAH, i.e. + 191 ± 11 mV, was measured upon the simultaneous binding of both L-Phe and BH_2, representing an inactive model for the iron environment under turnover conditions. Our findings provide new information on the redox**

properties of the active site iron relevant for the understanding of the reductive activation of the enzyme and the catalytic mechanism.

Introduction

Phenylalanine hydroxylase (PAH 1 , phenylalanine 4-monooxygenase, EC 1.14.16.1) is a tetrahydrobiopterin (BH_4) and non-heme iron dependent enzyme that hydroxylates L-Phe to L-Tyr using dioxygen. PAH is found mainly in the liver, and mutations in human PAH (hPAH) result in a dysfunction associated with the autosomal recessive disorder phenylketonuria, which is the most prevalent inborn error of amino acid metabolism. During the recent years important progress has been made in the elucidation of the crystal structure of the ligand-free PAH from human [179, 180] and rat [181], and of the homologous enzyme tyrosine hydroxylase (TH) [182]. PAH and TH are structurally and functionally closely related enzymes containing a 2-His-1-carboxylate facial triad motif [183, 184] anchoring the mononuclear non-heme iron atom. The crystal structure of the complexes of rat TH and hPAH with the oxidized cofactor analogue dihydrobiopterin (BH_2) have also been determined [185, 186]. Moreover, the structure of the ternary complex hPAH·BH_2·L-Phe has recently been studied by NMR spectroscopy and molecular docking [187]. These structural studies support the proposal that an iron-peroxo-tetrahydropterin complex forms during the catalytic cycle [188], and may either act as the hydroxylating intermediate itself or be the precursor of a ferryl oxo intermediate capable of aromatic hydroxylation [189, 190]. Thus, L-Phe seems to bind at the second coordination sphere of the iron with a distance between the hydroxylation sites (C4a in the pterin and C4 in L-Phe) of 6.3 Å, which is adequate for the intercalation of iron-coordinated molecular oxygen [187]. Moreover, the crystal structure of hPAH complexed with diverse catecholamines has revealed that the inhibitors bind to the iron by bidentate coordination through the catechol hydroxyl groups [191], as observed earlier by resonance Raman spectroscopy of PAH and TH [192, 193].

While these recent structural studies have provided further insight into the function of the iron and the pterin in the catalytic reaction of the aromatic amino acid hydroxylases, still little is known about the details of electron transfer reactions and the catalytic mechanism. It seems clear that no product or intermediate is released prior to the binding of all substrates and the first observable product of the pterin is a 4-hydroxytetrahydropterin which is dehydrated to *quinonoi*d-dihydrobiopterin *(q*-BH_2) either spontaneously or in a reaction catalyzed by pterin 4a-carbinolamine dehydratase [19, 194]. PAH isolated from rat liver and recombinant rat PAH contain

the catalytic iron in the ferric high-spin *(S* = 5/2) state [195-198]. In the catalytic reaction Fe(III) is reduced to Fe(II) by BH_4, termed "reductive activation" of the enzyme [199] and, *in vitro,* this reduction is an obligate step which occurs in the pre-steady state period [195]. Some experimental evidence has been presented in favor of Fe(II) during subsequent turnovers [19], but this has not been proven, and a redox cycling from the Fe(II) to Fe(III) and even Fe(IV) has alternatively been proposed [19, 200]. The reductive activation produces *q*-BH_2 directly [199] and, although some controversy exists in the early literature about the number of electron equivalents consumed in this reduction and the requirement for dioxygen, 1.2 ± 0.1 pterin derived electrons seem to be consumed per Fe(III) site, i.e. about 1 reduced tetrahydropterin/two Fe(III)-PAH subunits, under either aerobic or anaerobic conditions [19, 201].

Both BH_4 and the substrate L-Phe have also important regulatory functions, which seem to be of physiological significance [202], and inhibitory catecholamines regulate the activity of TH in an interplay with phosphorylation [203-205]. The conformational changes induced by the substrate, the natural pterin cofactor (and its inactive analogue) and the catecholamine inhibitors have been studied at the level of the tertiary and quaternary structure of both PAH and TH [202, 206, 207]. However, it is not known to what extent the binding of substrate, cofactor and catecholamines at the active site affects the coordination environment of the catalytic iron and its reactivity. Earlier EPR spectroscopic studies on rat PAH have revealed that the coordination geometry of the ferric iron depends on the buffer ions and the presence of ligands coordinating at the first and the second coordination sphere [197, 198]. Although the enzyme isolated from rat liver seems to contain a stoichiometric amount of iron per enzyme subunit, not all the iron has been found to be catalytically active [195-197]. Moreover, the same proportion of iron that coordinates to catecholamines is reduced by the tetrahydropterin cofactor and participates in catalysis [197].

In the present study we have further characterized the X-band EPR spectroscopic properties of both the tetrameric wild-type and a dimeric truncated form (corresponding to the catalytic domain) of human PAH corresponding to the catalytic domain, as well as the effect of the substrate L-Phe, reduced and oxidized pterin cofactor, and the inhibitor dopamine. We also report for the first time the midpoint potential of the iron in the wild-type human PAH as isolated, and its modulation upon the binding of substrate, oxidized pterin cofactor (BH_2) and dopamine.

Materials and methods

Expression and purification of the wild-type and truncated form of hPAH

Expression in *Escherichia coli* (TB1 cells) of human wild-type PAH (wt-hPAH) and the truncated hPAH(Gly^{103}-Gln^{428}), i.e. ΔN102/ΔC24-hPAH, as fusion proteins with maltose-binding protein (MBP), purification of the fusion proteins by affinity chromatography on amylose resin and their cleavage by the restriction protease factor Xa (New England Biolabs) was performed as described [208, 209]. The tetrameric form of wt-hPAH and the dimeric hPAH(Gly^{103}-Gln^{428}), corresponding to the "catalytic domain", were separated from aggregated/higher oligomeric forms and from MBP and factor Xa by size exclusion chromatography on HiLoad Superdex 200 HR prepacked column (1.6 cm x 60 cm) from Pharmacia [209]. Protein concentration was estimated spectrophotometrically using the absorption coefficients $A_{280\,nm}$ (1 $mg \cdot ml^{-1} \cdot cm^{-1}$) = 1.0 for wt-hPAH and 0.9 for hPAH(Gly^{103}-Gln^{428}) and the assay of PAH activity was performed as described [209].

Preparation of samples for EPR spectroscopy

Enzyme samples were initially prepared in 20 mM NaHepes, 0.2 M NaCl, pH 7.0. The iron content of the enzyme samples, measured by atomic absorption spectroscopy, was as previously reported (1.8-2.0 atoms Fe/tetramer for wt-hPAH and 0.8-0.9 atoms Fe/dimer for hPAH(Gly^{103}-Gln^{428})) [209]. In the experiments for the initial characterization of the iron center and the effect of ligands on the X-band EPR spectrum of hPAH, enzyme samples of either wt-hPAH or hPAH(Gly^{103}-Gln^{428}) were prepared in 20 mM NaHepes, 0.2 M NaCl, pH 7.0. Additions and incubations (5 min, pH 7.0, 25 °C) of either of the following compounds: L-Phe, dopamine, L-*erythr*o-7,8-dihydrobiopterin (BH_2, Dr. B. Schircks Laboratories) and 6-methyl-5,6,7,8-tetrahydropterin (6-MPH_4, Dr. B. Schircks Laboratories) in the presence of dithiothreitol (DTT), were performed in the EPR tubes prior to freezing the samples. We have previously shown that DTT alone does not reduce the Fe(III)in rat PAH in the presence of dioxygen [197]. For the EPR-monitored redox titrations the samples were prepared in 50 mM Mops buffer, 0.2 M KCl, pH 7.25, and the final enzyme (wt-hPAH) concentration was 100-120 μM subunit. Non-specifically bound Cu(II), giving rise to characteristic EPR signals round g = 2.0-2.3, was removed by incubation of the

enzyme with 5 mM EDTA, followed by 3 cycles of dilution and concentration in EDTA-free Mops buffer using Centricon 30 microconcentrators (Amicon). This treatment did not result in any significant change in the shape or the intensity of the Fe(III)-signal around $g = 4.3$.

EPR spectroscopy and redox titrations

A first series of EPR analysis was performed on the recombinant hPAH in the absence and presence of ligands at 9.64 GHz microwave frequency on a Bruker ESP300E equipped with an Oxford Instruments cryostat 900 at 3.6 K. Other EPR parameters are given in the figure legends. The EPR spectra were smoothed with the polynomial filter (n = 15), provided in the WINEPR software (Bruker), and were baseline corrected. Quantification of the Fe(III) EPR was performed by comparing the double integral of the spectra of hPAH with the double integral of a 500 µM transferrin standard at several temperatures (that excludes an error which might be introduced by very different D-values). In the cases in which quantification was performed using simulated spectra, similar results were obtained. Room temperature potentiometric titrations for subsequent EPR monitoring were performed in a 2 ml anaerobic cell under purified argon. The bulk potential of the stirred solution was measured using a platinum wire electrode with respect to the potential of a Radiometer REF201 Ag/AgCl reference electrode. Reported potentials were all expressed relative to the normal hydrogen electrode. 100 µM subunit hPAH in 50 mM Mops, 0.2 M KCl, pH 7.25 was poised at various potentials in the presence of 100 µM of each of the following mediators: N,N,N',N'-tetramethyl-p-phenylenediamine, 2,6-dichlorophenolindophenol, phenazine ethosulfate, methylene blue, resorufine, indigosulfonate, phenosafranin, safranin o, neutral red, benzylviologen and methylviologen. Sodium dithionite and $K_3Fe(CN)_6$ were used as reductant and oxidant, respectively. Redox equilibrium was obtained as judged by the attainment of a stable solution potential within a few minutes after addition of the titrant to the reaction mixture. The samples were transferred anaerobically to EPR tubes and directly frozen in liquid nitrogen. Midpoint potentials (E_m) were obtained from the experimental data points with a least square fit to the Nernst equation (n = 1). In addition to the titration of the ligand free enzyme, titrations in the presence of either L-Phe (5 mM), BH_2 (5 mM), both L-Phe (5 mM) and BH_2 (5 mM) or dopamine (1 mM) were also performed. The EPR-monitored titrations of hPAH samples were

performed at a microwave frequency of 9.41 GHz, a microwave power of 8 mW, with a 10 G (1.0 mT) modulation amplitude, and a modulation frequency of 100 kHz at 29 K. These temperature-values were used to optimize the signal-to-noise ratio under non-saturating conditions. Simulation of the spectra was performed as described [210].

Results

EPR spectra of recombinant human phenylalanine hydroxylase

Tris has been found to be an inhibitor of the enzyme, competitive to the pterin cofactor [199], and our previous EPR spectroscopic studies on rat PAH have demonstrated that Tris, in its base form, induces changes in the active site iron [197].

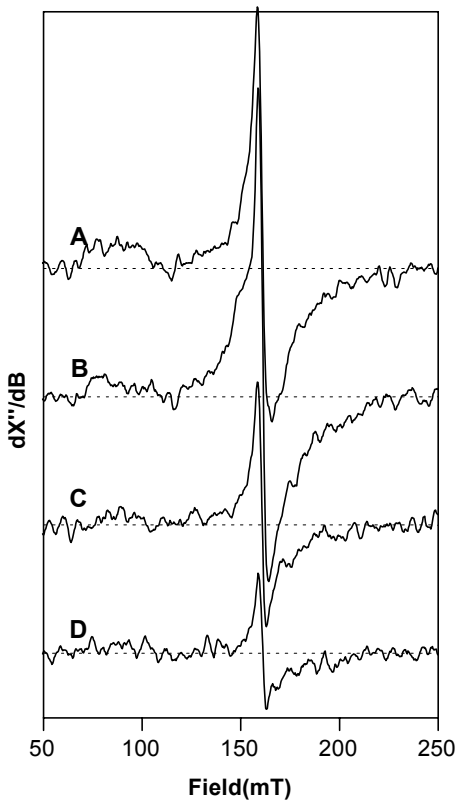

Figure 1. EPR spectra of wt-hPAH. A) wt-hPAH (100 µM subunit) as isolated, in 20 mM NaHepes, 0.2 M NaCl, pH 7.0; B) Sample A with 1mM L-Phe; C) Sample A with 0.5 mM 6-methyl-tetrahydropterin (6-MPH_4) and 5 mM dithiothreitol (DTT); D) Sample B with 0.5 mM 6-MPH_4 and 5 mM DTT (turnover conditions). All incubations of the enzyme samples were performed at 25 °C for 5 min prior to freezing the samples in the EPR tubes. EPR parameters were 9.64 GHz microwave frequency, 0.1 mW microwave power, 1 mT modulation amplitude, and a modulation frequency of 100 kHz at 3.6 K.

Consequently, we have used Hepes and Mops buffer in the present EPR studies. Recombinant wt-hPAH revealed a low temperature (3.6 K) EPR spectrum typical for high-spin *(S* = 5/2) Fe(III) (Figure 1, spectrum A). The spectrum is dominated by a resonance centered around *g* = 4.3, with an accompanying broad signal with g-value approximately 9.7, which is characteristic of ferric iron in a rhombic environment, with an E/D-value of approximately 1/3. Some minor iron species showing weak signals with *g*-values spread from 9.7 to 7.0 and 5.3 to 4.3 with various E/D-values between 0.05 and 0.33 are also present, indicating some microheterogeneity in the coordination geometry of the enzyme-bound iron. Nevertheless, the iron environment appears to be more homogenous in the recombinant hPAH than previously observed for the hepatic rat and bovine enzymes which are isolated through procedures including preincubation of the crude extracts with ferrous ions and DTT [211]. Those PAH preparations showed a split of the major resonance at *g* = 4.3 and a higher proportion of iron in a less rhombic environment (g_{max}-values in the range 7-6 and E/D < 0.05) [197].

Reduction of the high-spin (S = 5/2) Fe(III) by tetrahydrobiopterin and the effect of L-Phe

Quantification of the Fe(III) EPR in wild-type hPAH gave numbers which were in reasonable agreement with the the total iron content measured by atomic absorption spectroscopy, i.e. 0.45- 0.52 atoms iron/subunit for recombinant wt-hPAH [209]. This value is also similar to the catalytically active iron measured in rat PAH [196, 198, 212]. Thus, although the isolated rat and bovine liver enzyme preparations contain about 1 atom iron/subunit, only a fraction of it has been found to be reduced by the cofactor and thus to participate in catalysis [196, 197].

The effect of preincubation of the samples with either L-Phe or 6-MPH_4 as well as with both compounds simultaneously (turnover conditions) on the EPR spectrum of wt-hPAH is shown in figure 1. For a better estimation of the amount of iron that is not in the completely rhombic environment (E/D = 1/3, g = 4.3, resonance at 160 mT), the corresponding zero line for every spectrum is shown. The area enclosed by the recorded spectra between 70 and 100 mT and this zero line correlates with iron in a less rhombic environment. Comparing these areas in spectra 1A and 1B shows that preincubation of wt-hPAH (spectrum A) with the substrate L-Phe (spectrum B) results in a decrease of these signals. Moreover, a concomitant increase

of the intensity of the major signal at g = 4.3 is observed. Quantification, performed by double integration of the spectra shown in 1A and 1B between 60 and 240 mT, reveals that the total intensity of both spectra is identical within the error range of the method (10 %). By contrast, when the reducing cofactor analogue 6-MPH_4 is added to the resting form of the enzyme, the amount of ferric iron decreases to 35 %, as judged by the decrease of the double integral of the major signal at g = 4.3 (Figure 1, spectrum C). This reduction is slightly enhanced (only 28 % of the iron is in the ferric state) if 6-MPH_4 is added to the enzyme preincubated with L-Phe, i.e. at turnover conditions (Figure 1, spectrum D).

Effect of truncation of the enzyme and the addition of oxidized cofactor analogue (BH_2) on the EPR spectrum

The deletion of the N-terminal regulatory and C-terminal tetramerization domains of hPAH results in an activated (about 3-fold) dimeric hPAH(Gly^{103}-Gln^{428}) form which does not show any significant further activation by prior incubation with L-Phe, and, contrary to the full-length wt-hPAH, it does not bind L-Phe with positive cooperativity [209]. As seen by the crystal structures of this truncated form [179] and of rat PAH containing the catalytic and regulatory domains [181], the negative effect exerted by the regulatory domain on the catalytic activity is not accompanied by significant structural changes around the 6-coordinating iron site. Accordingly, no significant differences were observed in the main features of the X-band EPR spectra of the full-length and truncated hPAH forms, neither in the absence nor in the presence of L-Phe (Figure 1, spectra A and B and Figure 2, spectra A and B). However, there seem to be differences in the coordination environment between the iron in the full-length and the isolated catalytic domain as indicated by the decreased P½-values for the microwave power saturation behavior of the truncated PAH (Table 1), which may indicate a more homogenous iron coordination environment for this form.

Table 1. Microwave power saturation (P½) of the iron signal at $g = 4.3$ of different forms of hPAH at different temperatures.

Sample	P½ (mW)		
	4 K	6 K	10 K
wt-hPAH	0.93 ± 0.14	3.50 ± 0.17	58 ± 8
hPAH(Gly^{103}-Gln^{428})	0.90 ± 0.13	1.47 ± 0.12	10.3 ± 0.7
hPAH(Gly^{103}-Gln^{428}) + 1 mM L-Phe	1.3 ± 0.1	9.4 ± 1.6	n.d.

n.d., not determined

The oxidized cofactor analogue BH_2 inhibits both wt-hPAH and hPAH(Gly^{103}-Gln^{428}) by a competitive type of inhibition *versus* the natural pterin cofactor BH_4, with a K_i of 120 µM for wt-hPAH and of 100 µM for the truncated form [187]. The

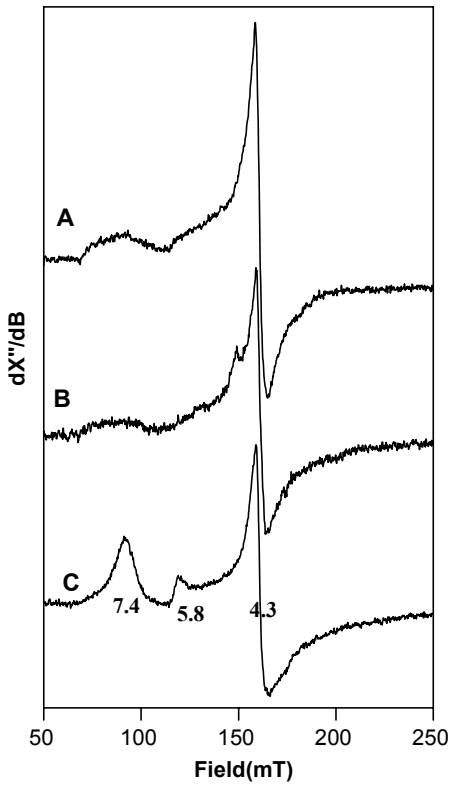

Figure 2. EPR spectra of the double truncated form of hPAH. A) hPAH(Gly103-Gln428) (or ΔN102/ΔC24) (533 µM subunit) in 20 mM NaHepes, 0.2 M NaCl, pH 7.0. B) hPAH(Gly103-Gln428) (480 µM subunit) with 2 mM L-Phe. C) hPAH(Gly103-Gln428) (600 µM subunit) with 600 µM 7,8-dihydrobiopterin (BH_2). EPR parameters were 9.64 GHz microwave frequency, 0.1 mW microwave power, 1 mT modulation amplitude, and a modulation frequency of 100 kHz at 3.6 K.

structure of the complex between hPAH(Gly^{103}-Gln^{428}) and BH_2 has recently been solved both by NMR spectroscopy and docking in the ligand-free crystal structure of the enzyme [187] and by X-ray crystallography [186]. We have here examined the effect of BH_2 on the EPR spectrum of this double truncated form.

The addition of BH_2 at concentrations of 500 μM results in the appearance of a less rhombic type high-spin ferric species with *g*-values of 7.4, 4.3 and (1.8) from the lowest and 5.8, (1.7) and (1.5) from the middle Kramers doublet with E/D = 0.07 (Figure 2, spectrum C). The g-values below 2 (in parentheses) can only be estimated from rhombograms as any g- or D-strain has severe broadening effects in these g-value regions. It seems that spectrum 2C consists of two major species, i.e. one with E/D=0.07 and one with E/D=0.33, and some minor species with intermediate E/D-values which distort the signal at g-value 5.8.

Determination of the midpoint potential (E_m) of the catalytic iron in hPAH and the effects of ligand-binding at the active site

Studies intended to determine the E_m(Fe(III)/Fe(II)) for the active site iron in hPAH by direct electrochemistry using activated glassy carbon as the working electrode were unsuccessful with all the promoters used. Thus, EPR-monitored redox titrations of the iron in wt-hPAH (100-120 µM enzyme subunit in Mops buffer at pH 7.25) were performed in the absence of ligands, and in the presence of L-Phe (Figure 3, spectrum A), BH_2 (Figure 3, spectrum B), and L-Phe and BH_2 simultaneously bound (Figure 3, spectrum C), at 29 K. For the samples with BH_2 the ratio of the intensities of the signals with g-values 5.8 and 7.4 is higher in the EPR spectra taken at 29 K (Figure 3, spectrum B) than in those taken at 3.6 K (Figure 2, spectrum C),

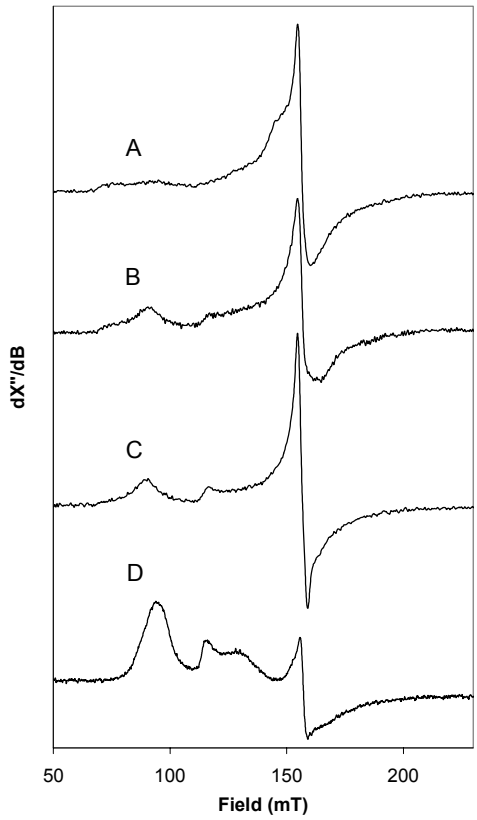

Figure 3. EPR spectra of the samples used in the redox titrations. The samples contained wt-hPAH (100 µM subunit) in 50 mM Mops buffer, 0.2 M KCl, pH 7.25, with: A) 5 mM L-Phe; B) 5 mM 7,8-dihydrobiopterin (BH2); C) 5 mM L-Phe and 5 mM BH2; D) 1 mM dopamine. Spectra were taken at a microwave frequency of 9.41 GHz, a microwave power of 8 mW, with a 1 mT modulation amplitude, and a modulation frequency of 100 kHz at 29 K.

substantiating the assignment of the signal at g-value 7.4 to the lowest and of the signal at g-value 5.8 to the middle Kramers doublet.

We have also studied the effect of dopamine both on the EPR spectrum of wt-hPAH and the E_m. The crystal structure of the complexes between the catalytic domain of hPAH and several catecholamines shows that these inhibitors bind to the iron by bidentate coordination through the catechol group [191], in agreement with earlier resonance Raman spectroscopic studies [192, 193, 213]. The resulting elimination of two coordinating water ligands and the changes in coordination geometry of the active site iron upon addition of dopamine are accompanied by an increase of the less rhombic type EPR signals with *g*-values at 7.0-7.2, 4.7-4.9, (1.90-1.92) from the lowest and at 5.8 from the middle Kramers doublet, corresponding to an E/D value 0.045-0.055, and a decrease of rhombic EPR signal at $g = 4.3$ (Figure 3, spectrum D).

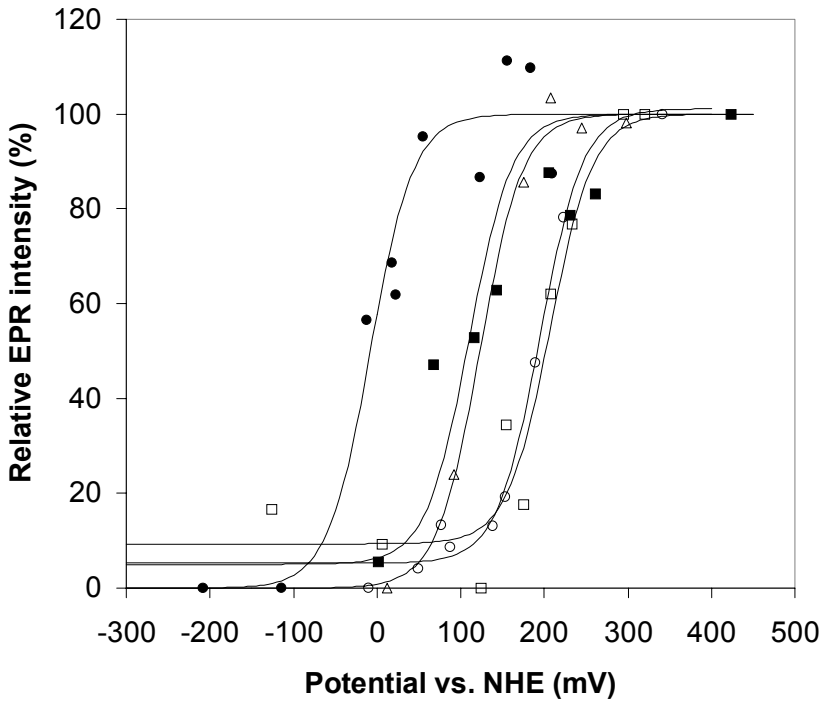

Figure 4. EPR monitored redox titrations. Samples: wt-hPAH (100 µM subunit) in 50 mM Mops buffer, 0.2 M KCl, pH 7.25, in the absence of ligands (□), with 5 mM L-Phe (Δ), 5 mM 7,8-dihydrobiopterin (BH2) (■), 5 mM L-Phe and 5 mM BH2 (○) and 1 mM dopamine (●). See also Table II and legend to Figure 3.

In order to determine the E_m, the intensity of the signals at g = 4.3 (spectra A-C) and at g= 7.09 (spectrum D) was followed during the titrations. As shown in figure 4, the Fe(III) in all the samples was reduced in the range – 200 to + 300 mV. The values of the estimated midpoint potential E_m at pH 7.25 in the absence and presence of ligands binding at the active site are summarized in Table 2. The E_m = + 207 ± 10 mV for the resting form of the enzyme in the absence of ligands was found to be decreased by about 84 mV, 100 mV and 210 mV upon the binding of L-Phe, BH_2 and dopamine, respectively. Moreover, when L-Phe and BH_2 were bound simultaneously, forming an inactive analogue (PAH-Fe(III)·L-Phe·BH_2) of the turnover active complex (PAH-Fe(II)·L-Phe·BH_4), the estimated E_m-value was 191 ± 11 mV. On the basis of the E_m-values in the absence (E_m(free)) and the presence of the ligands added separately (E_m(bound)), and by using the following equation [214]:

$$K_{d,red} = 10^{-[(E_m(bound)-E_m(free))nF/(2.303RT)]} K_{d,ox} \quad \{1\}$$

we calculated the apparent dissociation constants for the binding of L-Phe, BH_2 and dopamine to the reduced ferrous form of PAH ($K_{d,red}$), using the reported values for the binding of the ligands to the oxidized form of the enzyme ($K_{d,ox}$) [21, 215, 216]. As seen in Table 2, it is predicted that the binding affinities of L-Phe, BH_2 and dopamine decrease by 28-fold, 47-fold and 5040-fold, respectively, for the reduced ferrous form of the enzyme, with respect to the ferric form.

Table 2. Midpoint redox potential E_m(Fe(III)/Fe(II)) at pH 7.25 in samples of wt-hPAH in the absence and presence of L-Phe (5 mM), BH_2 (5 mM) and dopamine (1 mM), and apparent K_d-values for ligand binding to the enzyme.

Sample	E_m	$K_{d,ox}$[a]	$K_{d,red}$[b]
	mV	mM	mM
wt-hPAH[c]	+ 207 ± 10[d]		
wt-hPAH[c] + L-Phe	+ 123 ± 4[d]	0.10[e]	2.79
wt-hPAH[c] + BH_2	+ 110 ± 20[d]	0.01[f]	0.47
wt-hPAH c + L-Phe + BH_2	+ 191 ± 11[d]		
wt-hPAH[g] + dopamine	- 8 ± 9[h]	0.25 x 10^{-3}[i]	1.26
The q-BH_2 / BH_4 couple	+ 174[j]		

[a]Experimental values. [b]Calculated using equation {1}. [c]100 µM subunit. [d]Measured on the g = 4.3 signal. [e][215, 216]. [f][21]. [g]120 µM subunit. [h]Measured on the g = 7 signal. [i][217]. [j]The midpoint potential for the biological active BH_4/q-BH_2 couple is included for comparison [21].

Discussion

The low temperature (4 K) X-band EPR spectra obtained for recombinant hPAH, both wt-hPAH and its N-terminal and C-terminal truncated form ("catalytic domain"), are very similar to those previously obtained for the hepatic rat and bovine PAH when the enzyme samples are prepared in buffers which do not interact with the active site non-heme iron, i.e. potassium phosphate, NaHepes and Mops [197, 198]. However, an important difference was observed between the isolated hepatic and the recombinant enzyme forms. Whereas isolated rat liver PAH seems to contain more than 50 % of the iron which does not participate in catalysis [195-197], in hPAH the major EPR signal at g = 4.3, characteristic of high-spin (S = 5/2) ferric iron in a rhombic coordination geometry, is largely reduced (to almost a quarter of the intensity in the enzyme as isolated) in the presence of both L-Phe and tetrahydropterin (turnover conditions) (Figure 1D). The larger homogeneity of the iron population in the recombinant hPAH makes it possible to determine the midpoint potential (E_m) of the active site iron, an important novel finding in the present study.

The apparent E_m at pH 7.25 for the catalytic iron was measured both in the absence and presence of substrate, pterin cofactor analogue and catecholamine inhibitor, all compounds binding at the active site. Previously, the E_m-value of the

natural cofactor, i.e. (*quinonoid*-dihydrobiopterin (q-BH_2)/BH_4 couple), has been determined to be +174 mV at pH 7 [21], and the literature values vary from + 140 to + 184 mV for cofactor analogues with various substituents at the 6-position [21, 218, 219]. Thus, the E_m-value of + 207 ± 10 mV for the catalytic iron in the resting enzyme (Table 2) is in agreement with a thermodynamically feasible electron transfer from the reduced cofactor to the iron site and explains the observed reductive activation of the enzyme by the tetrahydropterin cofactors [199].

As seen from the EPR spectrum of the resting form of wt-hPAH, with a major broad peak around g = 4.3 and minor features with g-values stretching from 9.7 to 4.5, the coordination geometry of the active site iron seems to be rather flexible. This conclusion is further supported by the crystal structure showing three water molecules in the first coordination sphere of the iron [179, 181]. A sharpening of the g = 4.3 signal and an increase of the P½-value for the microwave power saturation behavior was observed in the presence of L-Phe, indicating a change in coordination environment of the active site iron in the substrate-activated enzyme form. This effect is in good agreement with our previous finding that the binding of L-Phe at the active site is accompanied by a dissociation of one of the ferric iron-coordinating water molecules [220, 221]. The recent structural study on the ternary PAH-Fe(III)·L-Phe·BH_2 complex [187] supports the conclusion that the binding of L-Phe may result in a five-coordinated iron in the ferric form of the enzyme. Even larger changes in the EPR spectra and the midpoint potential were encountered on addition of the tetrahydrobiopterin cofactor analogue BH_2 and the inhibitor dopamine. Thus, a less rhombic type of signal is observed in the presence of these inhibitors (g_{max}-values 7.4 and 7.0 for BH_2 and dopamine, respectively) (Figure 2C and Figure 3) indicating a decrease of the E/D-value (from 0.33 to approximately 0.07 and 0.05, respectively) and a change in the coordination geometry of the iron. These spectroscopic changes were also accompanied by a decrease of the E_m-value of the iron to numbers which are significantly lower than those of the pterin cofactor redox couple (Table 2). Notably for the hPAH-dopamine complex it is clear that reduction of the Fe(III) by the cofactor is not possible to achieve due to a ~200 mV negative shift of the E_m-value, and that this effect could be of physiological significance in the case of TH which is regulated by feed-back inhibition by catecholamines and phosphorylation [190, 203, 204]. The inhibition of PAH by catecholamines appears to be competitive with respect to the tetrahydropterin cofactors [222]. Paramagnetic relaxation NMR

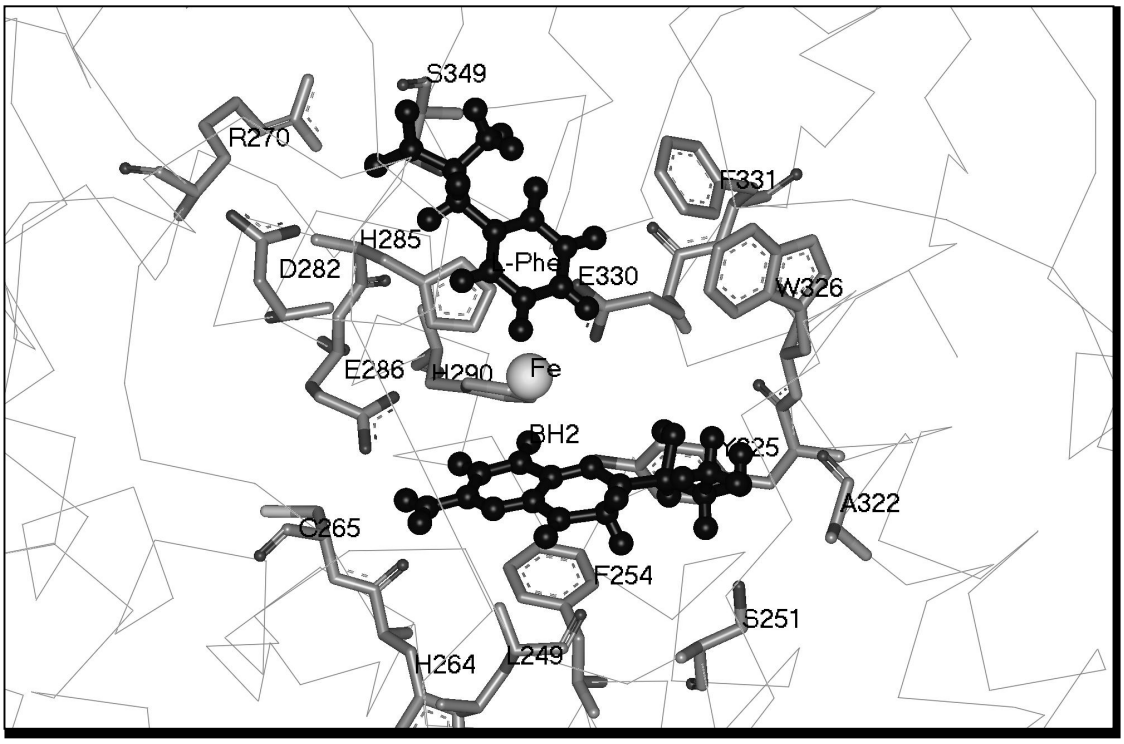

Figure 5. The structure of the active site of hPAH (PDB accession number 1PAH [179]) with L-Phe and BH_2 bound according to the structure of the ternary complex as resolved by NMR and molecular docking [187].

experiments have shown that catecholamines do not compete for the cofactor binding site in hPAH and that both noradrenaline and dopamine can be bound simultaneously with the cofactor analogue BH_2 [187]. Thus, the apparent competitive type of inhibition by catecholamines *versus* the pterin cofactor may rather be due to changes in ligand field geometry of the active site iron as a result of formation of the tight bidentate catecholate-Fe(III) complex [191], lowering the E_m-value and thus stabilizing the ferric state. The ~200 mV negative shift of the midpoint potential on dopamine binding also explains the experimental finding that recombinant human TH reconstituted with Fe(II) is rapidly oxidized upon the addition of catecholamines forming a ferric blue-green complex [223]. Moreover, based on the large decrease of E_m upon dopamine binding, we estimated that the K_d-value for the binding of this inhibitor to the reduced enzyme was increased by about 5040-fold (Table 2). This large decrease in affinity is in agreement with the calculated K_d-values for catecholamine binding to both the ferric and ferrous forms of TH [224]. The changes in the midpoint potential of the active site iron induced by the binding of L-Phe and

BH_2, both when bound independently (reduction in E_m) and when bound simultaneously (comparable E_m to the enzyme as isolated) may be explained using as a frame the modeled structure of the ternary complex of hPAH(Gly^{103}-Gln^{428}) with L-Phe and BH_2 [187] (Figure 5) and the crystal structure of the binary hPAH(Gly^{103}-Gln^{428})-BH_2 complex [186]. Thus, the amino group of L-Phe seems to interact with the enzyme through a hydrogen bond with Ser^{349}, and this residue is hydrogen bonded with the $N^{\delta 1}$ of the iron-coordinating His^{285} in the resting unbound form of the enzyme [179, 187]. Hence, the binding of the substrate may disrupt the initial hydrogen-bonding network of His^{285}, resulting in a modulation of the coordination geometry of the iron and a decrease of the E_m-value, as observed in this work. The disruption of the hydrogen bond between Ser^{395} and His^{331} in TH has also been related to a change in the reactivity of Fe(II) with oxygen [225]. The oxidized, inactive cofactor analogue BH_2, which inhibits the rat and recombinant human PAH competitive to the cofactor BH_4, appears to bind at the same or overlapping sites to BH_4 [21, 187, 226, 227]. In the structure of the binary complex of hPAH(Gly^{103}-Gln^{428}) and BH_2 determined either by NMR/molecular docking [187] (Figure 5) or X-ray crystallography [186], BH_2 binds at the bottom of the wide active site crevice structure. The pterin ring -stacks with Phe^{254} and interacts with Glu^{286}, Gly^{247}, His^{264} and Leu^{249}, while the dihydroxypropyl side-chain at C-6 establishes interactions with Ala^{322}. Although a similar binding site for BH_2 was found in the crystal structure and the NMR study, some important differences in the detailed interactions were encountered. Thus, in the NMR/docking structure, the N-3 and the amine group at C-2 hydrogen bond with the carboxyl group of Glu^{286} and the distance between the O-4 atom of BH_2 and the iron (2.6(±0.3) Å) is compatible with coordination [187]. In the crystal structure, however, the N-3 and the O-4 of BH_2 interact with Glu^{286} and the iron, respectively, through bridging water molecules, resulting in location of the pterin ring at distances not compatible for coordination to the iron. The reasons for these discrepancies are not clear, although alternative explanations have been proposed [186]. The less rhombic type of signals which appear in the EPR spectra of both the truncated form hPAH(Gly^{103}-Gln^{428}) and the wt-hPAH in presence of BH_2, are compatible with a coordination of BH_2 to the iron, as indicated by the solution structure [187]. Nevertheless, the interaction of the pterin ring with an iron-coordinated water molecule might as well result in a loss of flexibility and a change of the water-iron bonding distance, and thereby in a less rhombic coordination geometry.

Regardless of the detailed interactions between the pterin ring and the iron it seems clear that BH_2 changes the coordination geometry of the metal and decreases its midpoint potential (Table 2). However, when bound simultaneously at opposite sides in the coordination environment of the iron in the ternary PAH-Fe(III)·L-Phe·BH_2 complex [187] (Figure 5), L-Phe and BH_2 may exert compensatory changes in the electronic environment of the iron, in agreement with the finding that the midpoint potential in the ternary complex is more similar to that in the resting unbound enzyme than in the binary complexes (Table 2). The L-Phe induced conformational change at the protein level is well documented on the basis of intrinsic tryptophan fluorescence spectroscopy, limited proteolysis and dynamic light scattering (reviewed in [19] and [194]). Furthermore, it has been shown that in the double truncated form of hPAH BH_2 binds by an induced fit mechanism, involving a conformational change in the protein at the active site [186] as well as in the dihydroxypropyl side-chain of the cofactor [187]. All the structural and kinetic data obtained so far are compatible with the proposed four-state conformational model [228]; i.e. a resting state, a L-Phe activated state, a BH_4/BH_2 inhibited state and a state of catalytic turnover. In this model the resting state and the turnover state were found to be very similar by different indirect conformational probes.

The inactive ternary PAH-Fe(III)·L-Phe·BH_2 complex seems to provide a good model for the coordination environment of the iron under turnover conditions. Although the midpoint potential for the BH_4/q-BH_2 couple may change when the cofactor binds to the enzyme, the +81 mV increase in E_m obtained when both ligands are added simultaneously with respect to that obtained in the presence of BH_2 alone is in agreement with a thermodynamically favorable electron transfer from the cofactor to the iron at turnover conditions. As seen in Figure 1, a larger reduction is obtained with 6-MPH_4 when wt-hPAH is also complexed with L-Phe (spectrum 1D; turnover conditions) than in the absence of the substrate (spectrum 1C). Accordingly, although the affinity for tetrahydropterin cofactors is decreased for the L-Phe activated enzyme [227], it has been previously reported that the reduction seems to be facilitated by the presence of L-Phe [201]. This modulation of the E_m-value upon ligand binding also agrees with a type of mechanism for PAH involving the formation of a complex of all reactants prior to catalysis. Thus, only when both the substrate and the tetrahydropterin cofactor are simultaneously bound to ferrous PAH, dioxygen may bind and be activated at the open coordination position, as indicated by magnetic

circular dichroism spectroscopic studies with the cofactor analogue 5-deaza-6-methyltetrahydropterin [229]. Moreover, the K_m-values obtained for L-Phe and BH_4 with the ferrous form of PAH [206] resemble the $K_{d,ox}$ (Table 2), indicating that the decrease in affinity estimated for the independent binding of substrate and cofactor analogue with respect to the binding to the oxidized form of the enzyme, is reversed when the ligands bind forming the ternary complex. The midpoint reduction potential of the heme iron in the BH_4-dependent enzyme nitric oxide synthase has also been shown to be similarly modulated by substrate and active site inhibitors [214]. However, the absolute values for the midpoint potentials determined for this enzyme are about 400-500 mV lower than that determined in this work for hPAH, reflecting the different roles of BH_4 in the reactions. The E_m-values measured for nitric oxide synthase have been found to be adequate for a thermodynamically feasible reduction of the heme by the flavin cofactors [230] and neither 4-hydroxytetrahydropterin nor *quinonoi*d-dihydrobiopterin *(q*-BH_2) have been detected in the reaction of this enzyme. Recently, a protonated trihydrobiopterin radical [231] has been shown to be formed in the redox cycling of BH_4 in nitric oxide synthase [232, 233]. Formation of such a radical has been proposed but not detected for any of the aromatic amino acid hydroxylases [190]. Although the details of the electron transfer reactions in the catalytic process of the aromatic amino acid hydroxylases are not yet clear [19], our present findings represent new information on the redox properties of the active site iron which is relevant for our understanding of their catalytic mechanism.

Acknowledgments

We are very grateful to Dr. Per M. Knappskog for the preparation of bacterial strains expressing human phenylalanine hydroxylase and to Ali. J. S. Muñoz and Randi M. Svebak for the expression, purification and the kinetic characterization of the recombinant human phenylalanine hydroxylase. This work was supported by the Research Council of Norway, L. Meltzers Hoyskolefond, The Norwegian Cancer Society, the Norwegian Council on Cardiovascular Diseases, Rebergs legat, the Novo Nordisc Foundation, Marie-Curie Grant ERBFMBICT 961892, and the Training and Mobility of Researchers and Biotechnology Programs of the European Union (ERBMRFXT 980207 and BIO4-98-0385).

Chapter 8

Spectroscopic characterization and ligand binding properties of chlorite dismutase from the chlorate respiring bacterial strain GR-1

Peter-L. Hagedoorn, Daniel C. de Geus, Wilfred R. Hagen

Accepted for publication in: Eur. J. Biochem., 2002

Chlorite dismutase (EC 1.13.11.49), an enzyme capable of reducing chlorite to chloride while producing molecular oxygen, has been characterized using EPR and optical spectroscopy. The EPR spectrum of GR-1 chlorite dismutase shows two different high spin ferric heme species which we have designated as "narrow" g_{xyz} = 6.24, 5.42, 2.00 and "broad" g_{zyx} = 6.70, 5.02, 2.00. Spectroscopic evidence is presented for a proximal histidine coordinating the heme iron center of the enzyme. The UV-vis spectrum of the ferrous enzyme and EPR spectra of the ferric hydroxide and imidazole adducts are characteristic for a heme protein with an axial histidine coordinating the iron. Furthermore, substrate analogs nitrite and hydrogen peroxide have been found to bind to ferric chlorite dismutase. EPR spectroscopy of the hydrogen peroxide adduct shows the loss of both high spin and low spin ferric signals and the appearance of a sharp radical signal. The NO adduct of the ferrous enzyme exhibits a low spin EPR signal typical for a five-coordinate heme iron nitrosyl adduct. Apparently the bond between the proximal histidine and the iron is weak and can be broken upon binding of NO. The midpoint potential, $E_m(Fe^{3+/2+})$ = -23 mV, of chlorite dismutase is higher than for most heme enzymes. Spectroscopic features and redox properties of chlorite dismutase are more similar to the gas sensing hemoproteins, such as guanylate cyclase and the globins, than to the heme enzymes.

Introduction

Chlorate and chlorite are degradation products of the commonly used bleaching agent chlorine dioxide. Recently, microorganisms have been used to remove these oxyanions from wastewater. Many denitrifying bacteria can reduce chlorate to chlorite, however the latter compound is toxic to these cells. To date only six different bacterial species have been isolated that can grow using chlorate or perchlorate as a terminal electron acceptor. Strain GR-1 (DSM 11199), belonging to the β-subdivision of the *Proteobacteria*, is among the best studied of these organisms [234]. Two enzymes, a chlorate reductase (EC 1.97.1.1) and a chlorite dismutase (EC 1.13.11.49), have been found to be responsible for the respiration on (per)chlorate [234]. Together they can reduce chlorate or perchlorate to chloride and molecular oxygen (see below).

Chlorate reductase

$$ClO_3^- + 2e^- \longrightarrow ClO_2^-$$

Chlorite dismutase

$$ClO_2^- \longrightarrow Cl^- + O_2$$

Previous characterization of these enzymes has shown that the chlorate reductase is a molybdenum and iron sulfur containing enzyme [235] and the chlorite dismutase is an iron protoheme IX containing enzyme [16]. However, little is known about the mechanism of action of these enzymes. The name chlorite dismutase is unfortunate, since the enzyme does not dismutate or disproportionate chlorite, but it reduces chlorite to chloride while producing molecular oxygen. A more correct name would be chloride:oxygen oxidoreductase or chlorite oxygen-lyase. However since the name chlorite dismutase has been used in all references describing this enzyme, we will also use it until formal renaming.

Recently EPR spectra of *Ideonella dechloratans* chlorite dismutase have been reported [7]. As for most heme enzymes the EPR spectrum shows an axial high spin ferric signal and a minor low spin signal from a hydroxide adduct. Here we present the EPR spectroscopic and redox properties of GR-1 chlorite dismutase. Furthermore the binding of hydroxide and imidazole to the ferric enzyme and of NO to the ferrous

enzyme has been investigated in order to establish the nature of the proximal ligand to the heme iron center. The binding of the substrate analogs hydrogen peroxide and nitrite to chlorite dismutase has been studied in order to obtain information to formulate a possible reaction mechanism. WF10 is a chlorite based promising anti-AIDS drug. In a recent paper it was shown that the pharmacological activity ofWF10 is based on its interaction with heme iron proteins [236]. Interaction of WF10 with heme proteins has been proposed to generate an oxoferryl species and hypochlorite. The reaction mechanism of WF10 with hemoproteins may be similar to the enzymatic reaction of chlorite with chlorite dismutase. Thus, the study of chlorite dismutase may provide information of medical relevance.

Materials and methods

Cell cultivation and protein purification

GR-1 was grown on a mineral medium containing chlorate and acetate as described previously [234], however, the batch culture was scaled-up in a 200 L fermentor (Bioengeneering). The cells were harvested at OD_{600nm} = 0.3 and yielded typically between 70-100 g of wet cells. Anaerobicity of the culture was indicated by decolorization of the redox indicator resazurin (0.5 mg/L). Cells were broken using a Manton Gaulin press. Cell free extract was obtained as the supernatant after 1 hour centrifugation with 26000×g at 4ºC. Subsequently, cell free extract was clarified from membranes by centrifugation for 1 hour at 110000×g at 4ºC. Chlorite dismutase was purified as reported previously with minor modifications [16]. The purified enzyme has a specific activity of 2000 U/mg at pH 7.2 and 30°C, which is close to the value reported previously [16].

Activity measurements and spectroscopy

Chlorite dismutase activities were measured in 100 mM potassium phosphate buffer pH 7.0 at 25ºC using a thermostatted Clark-type electrode (model 5331 YSI Inc.). Sodium chlorite, the substrate, was added to 6 mM final concentration and gave no background response. The stock solution of sodium chlorite was prepared daily. Oxygen was removed from the measurement solution by bubbling with high purity argon. The reaction was started by adding enzyme solution. UV/visible absorption

spectra were recorded on a HP-8452A diode-array spectrophotometer (Hewlett-Packard). X-band EPR spectra were recorded on a Bruker ER-200D spectrometer with peripheral equipment and data handling as has been described previously [103]. The E/D ratios of the high-spin signals were calculated from the effective g-values by numerical diagonalization of the energy matrix for S = 5/2 [237].

Determination of the midpoint potential of the iron center in chlorite dismutase

A dye mediated redox titration was performed as described [90]. The titration cell contained 26 μM monomer chlorite dismutase with equimolar concentrations of each redox mediator in a 50 mM potassium phosphate buffer pH 7.2 containing 10 % (v/v) glycerol. The redox potential was poised by adding substoichiometric amounts of sodium dithionite as the reducing agent or potassium ferricyanide as the oxidant. EPR samples at different potentials were drawn and were frozen in liquid nitrogen. EPR spectra were recorded at 17 K and a titration curve was made using the amplitude of the high spin ferric EPR signal. The EPR spectrum with maximum signal intensity was quantified by double integration according to [210].

Determination of the pK_a value of the optical spectrum of chlorite dismutase

Chlorite dismutase, 2 μM monomer, was exchanged into 100 mM of each of the following buffers: Citrate-phosphate pH 5.0, Mes pH 6.0, Mops pH 7.0, Epps pH 8.0, Ches pH 9.0, Caps pH 10.0, Caps pH 11.0. Of each pH sample the UV-vis spectrum was recorded using a HP-8452A diode-array spectrophotometer. The absorbance difference between 394 nm (low pH form) and 409 nm (high pH form) was plotted versus the pH.

Determination of the K_d values of chlorite dismutase for nitrite, hydrogen peroxide and imidazole

To a solution of 2 μM monomer chlorite dismutase in 0.1 M potassium phosphate buffer pH 7.0 aliquots of either nitrite, imidazole or hydrogen peroxide were added. The UV-vis spectrum was recorded using a HP-8452A diode-array spectrophotometer. The absorbance difference between 394 nm (no ligand) and 412 nm (ligand bound form) was plotted versus the concentration of free ligand in solution. In the case of nitrite binding the absorbance difference at 390 nm was

monitored. The dissociation constant K_d was determinded using a least-square fit to the following equation:

$$A_{obs} = A_0 - B[L]/(K_d+[L]) \quad \{1\}$$

B is the maximum absorbance difference, [L] is the ligand concentration, A_{obs} is the observed absorbance and A_0 is the absorbance without ligand.

Preparation of NO adduct of chlorite dismutase

Chlorite dismutase (50 μM heme) in 50 mM potassium phosphate buffer pH 7 and 10% glycerol was incubated with 0.17 M sodium dithionite and 0.44 M sodium nitrite anaerobically under argon. To 50 μM monomer chlorite dismutase 172 mM sodium dithionite and 440 mM sodium nitrite were added under argon. NO is formed by reduction of the nitrite. After 10 minutes incubation at room temperature the sample was frozen in liquid nitrogen.

Results

Optical spectroscopy of chlorite dismutase and adducts

Figure 1 shows the UV-vis spectra of native chlorite dismutase and derivatives. The five-coordinate iron heme center of chlorite dismutase, found at pH 7.0, exhibits a broad Soret band at 394 nm. At higher pH the OH^- adduct of the enzyme is formed, exhibiting a much sharper soret band at 409 nm, characteristic for a six coordinate ferric heme center. By monitoring the absorbance spectral change with the Soret band shifting from 394 nm to 409 nm with increasing pH, a $pK_a = 8.2$ was found (Figure 2), which is close to the $pK_a = 8.5$ found for Ideonella dechloratans chlorite dismutase. Furthermore we have found the Soret band to decrease dramatically when the pH is raised above pH 10. At pH 11 chlorite dismutase did not show any detectable activity. Apparently the enzyme is unstable above pH 10. The imidazole and hydrogen peroxide adducts of the enzyme all exhibit a Soret band at 412 nm (Figure 1). Using these optical transitions the following K_d values were obtained: 8.8 μM for imidazole, and 42 μM for hydrogen peroxide (not shown). At higher hydrogen peroxide concentration the Soret band decreases due to further oxidation of the heme by the excess hydrogen peroxide.

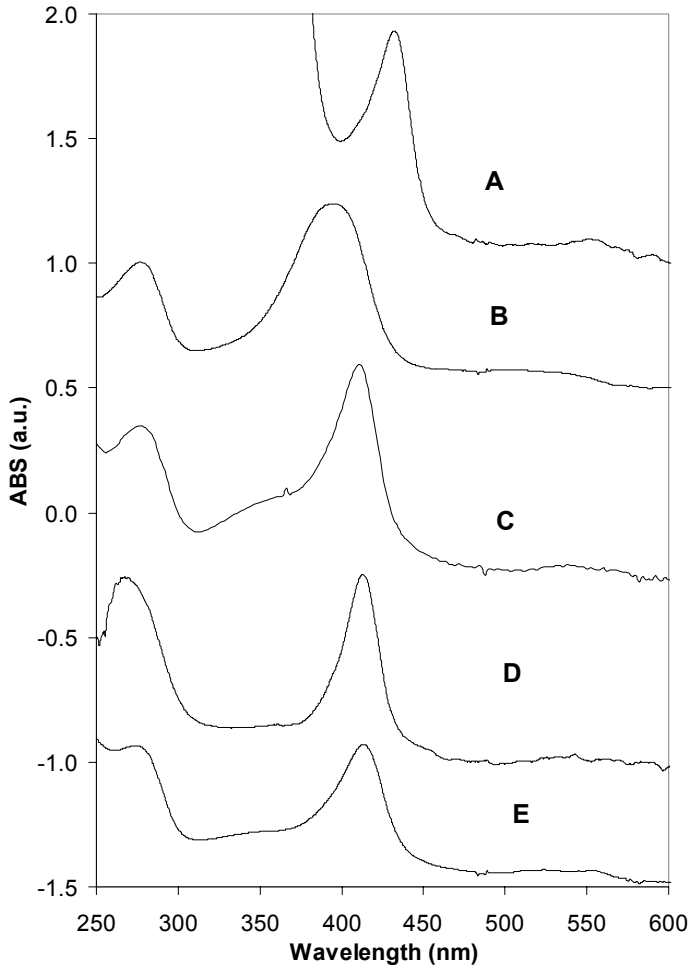

Figure 1. Optical spectra of 17 μM (monomer) chlorite dismutase and adducts. Trace A. ferrous chlorite dismutase at pH 7.0. Trace B. ferric chlorite dismutase at pH 7.0. Trace C. ferric chlorite dismutase at pH 10.0. Trace D. ferric chlorite dismutase with imidazole at pH 7.0. Trace E. ferric chlorite dismutase with hydrogen peroxide at pH 7.0.

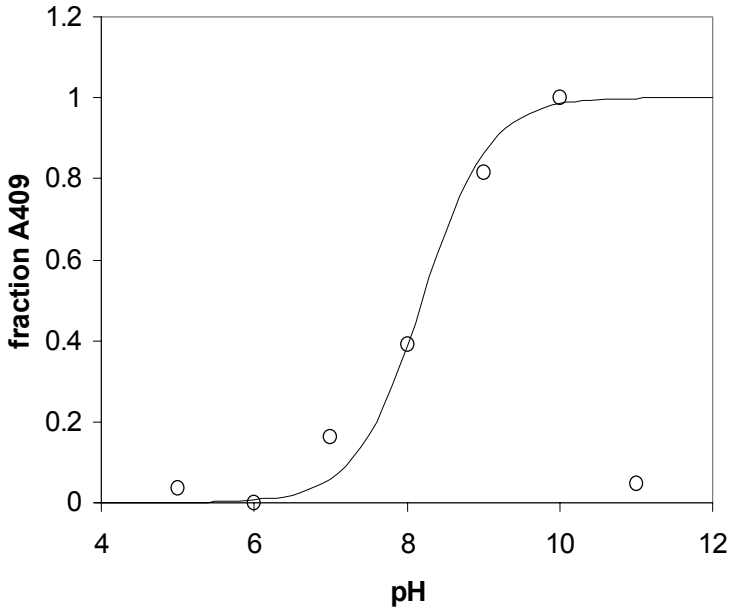

Figure 2. The dependence of the UV-vis spectrum on the pH. Fraction A409 represents the fraction of enzyme having the Soret band at 409 nm. The solid line represents a fit to the following equation which can be derived from the Henderson-Hasselbach equation:

$$\text{fraction A409} = 10^{pH-pK_a}/(1+10^{pH-pK_a})$$

EPR spectroscopy of chlorite dismutase and adducts

Ferric chlorite dismutase exhibits a mixture of two high spin and one low spin EPR signals with a ratio high spin: low spin of 4:1 at pH 7.0 (Figure 3). These EPR characteristics are similar to those of Ideonella dechloratans chlorite dismutase [7]. Since the low spin species is not found at pH 6, we attibute this species to the hydroxide adduct of the enzyme. The two different high spin signals are found in different ratios depending on the history of the sample. Both high spin species represent $m_s = \pm 1/2$ ground state doublets of S = 5/2 systems. We have designated these species as "narrow" and "broad" according to the rhombicity as determined by the ratio of the rhombic (E) and axial (D) zero-field parameters E/D, which is between 0.01-0.02 for the "narrow" species and 0.03-0.04 for the "broad" species. Since we have found that two samples with a different ratio of "broad" and "narrow" high spin signals gave almost identical activity (not shown), we attribute both high spin species

to active forms of the enzyme. High spin ferric heme species usually represent a pentacoordinate iron center or a hexacoordinate one with a weak sixth ligand, e.g. H_2O. In both cases the iron center is thus accessible for the substrate, and for other ligands such as: hydroxide, imidazole, nitrite and hydrogen peroxide. The EPR parameters are given in table 1.

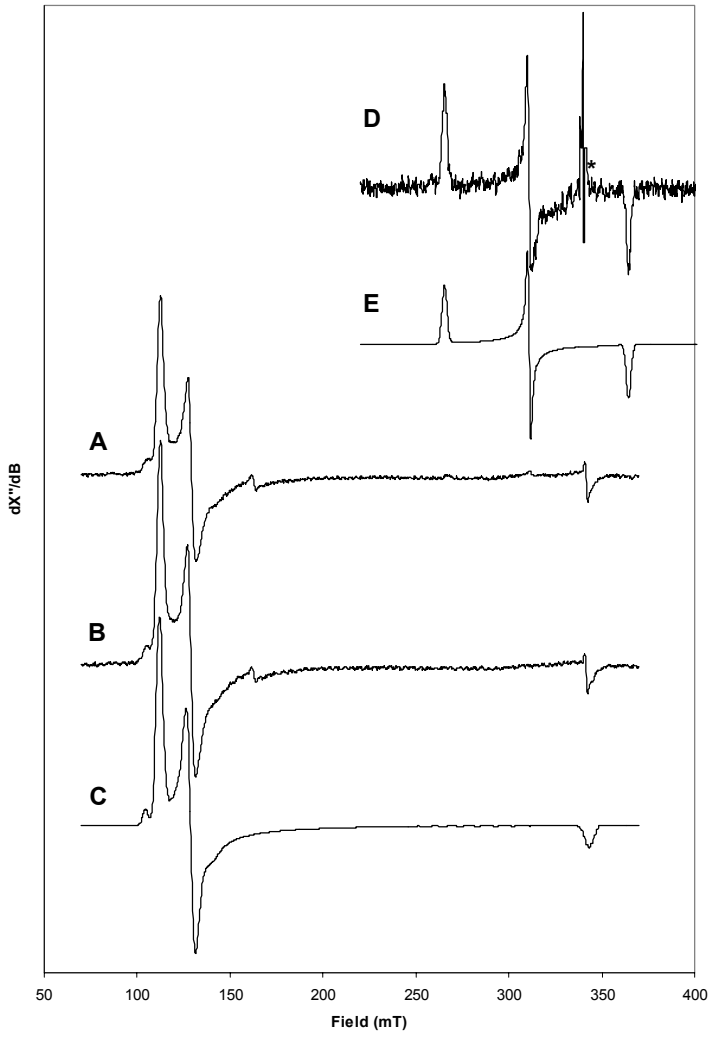

Figure 3. EPR spectroscopy of 0.18 mM monomer ferric chlorite dismutase at pH 6 and pH 9. Trace A: 50 mM Ches, pH 9. Trace B: 50 mM potassium phosphate, pH 6. Trace C: simulation of Trace B. Trace D: difference spectrum of pH 9 – pH 6. Trace E: simulation of Trace D. EPR conditions: microwave frequency, 9.39 GHz; microwave power, 80 mW for trace A and B, 0.8 mW for trace D; modulation frequency, 100 kHz; modulation amplitude, 1.25 mT, temperature 17 K. EPR simulation parameters are given in table 1. *radical signal

Table 1: EPR simulation parameters of chlorite dismutase and derivatives.

Species	g_z	g_y	g_x	W_z	W_y	W_x	A_z	A_y	A_x
Fe(III) High spin narrow	6.24	5.42	2.0	3.0	4.0	4.0			
Fe(III) High spin broad	6.70	5.02	2.0	2.7	5.0	4.3			
Fe(III) OH^- adduct	2.543	2.181	1.866	2.2	1.5	2.2			
Fe(III) Imidazole adduct	2.96	2.25	1.51	5.0	5.0	10.0			
Fe(III) NO_2^- adduct	2.93	2.18	1.55	2.5	2.3	8.0			
Fe(II) NO adduct	2.005	2.034	2.083	0.5	1.3	1.5	1.6	1.9	2.0

Line width W and ^{14}N hyperfine interaction A expressed in mT units.

Furthermore in all chlorite dismutase preperations a radical with $g_{iso} = 2.002$ and a peak width of 1.3 mT was found. This radical represents 0.05 spins/monomer chlorite dismutase as determined by double integration of the signal recorded under non-saturating conditions. Nitrite, a substrate analog for chlorite, binds to the ferric form of the enzyme producing a low spin species (Figure 4). However, unlike chlorite, it forms a stable complex and no turnover takes place. Since nitrite binds to the ferric form of the enzyme, we expect binding of chlorite to ferric chlorite dismutase to be the first step in the reaction mechanism. Furthermore, this nitrite adduct may be an interesting subject for crystallization studies.

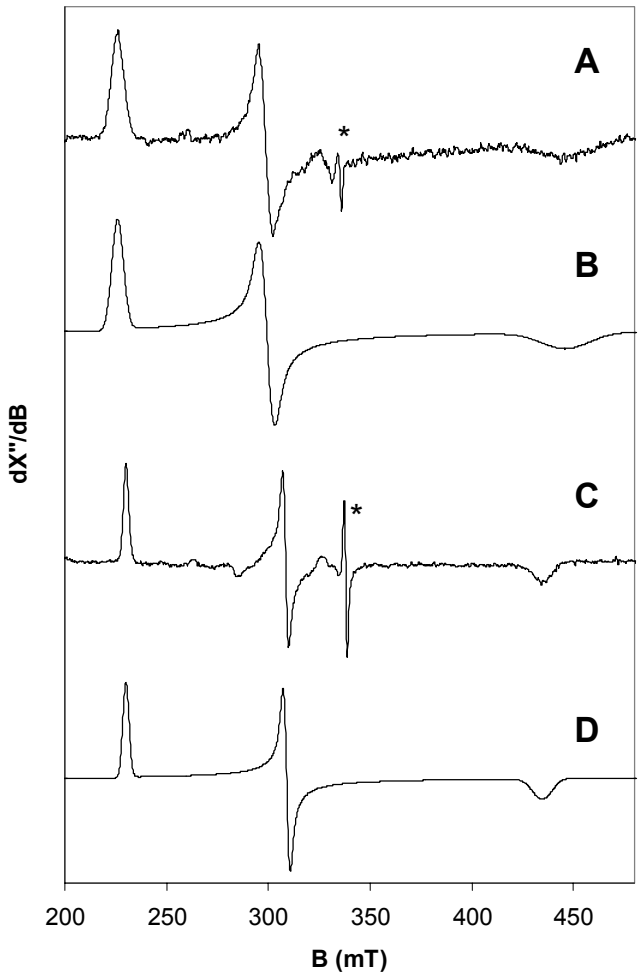

Figure 4. EPR spectroscopy of the imidazole and nitrite adducts of chlorite dismutase. Trace A. 90 μM monomer chlorite dismutase with 10 mM imidazole in 100 mM potassium phosphate buffer pH 7.0. Trace B. simulation of trace A. Trace C. 90 μM chlorite dismutase with 1 mM sodium nitrite in 100 mM potassium phosphate buffer pH 7.0. Trace D. simulation of trace C. Simulation parameters are given in table 1.EPR conditions: microwave frequency, 9.430 GHz; microwave power, 50 mW; modulation frequency, 100 kHz; modulation amplitude, 2.0 mT; temperature, 26.5 K.

We have found optical evidence for the formation of a complex with hydrogen peroxide (Figure 1, trace E). The EPR spectrum of the hydrogen peroxide complex, however, shows the decrease of the high spin signal of the enzyme and the appearance of an additional radical with g_{iso} = 2.00 and peak width of 0.54 mT (Figure 5). This radical represents 0.01 spins per monomer chlorite dismutase. Apparently the iron does not remain ferric when hydrogen peroxide binds. Possibly hydrogen peroxide oxidizes the ferric iron center of chlorite dismutase, as it does in metmyoglobin [238]. In the case of myoglobin, as with many heme proteins, the ferric iron center is oxidized to an oxoferryl complex (S = 1) and an additional protein radical [238].

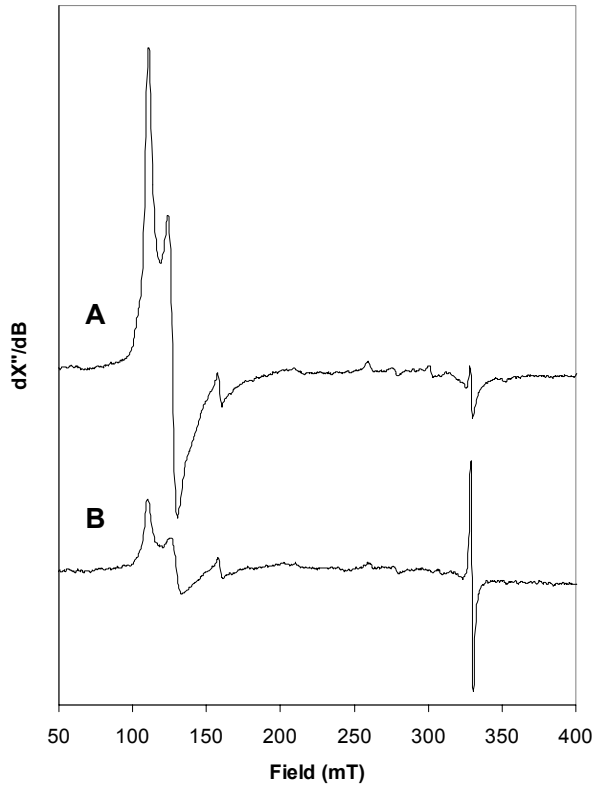

Figure 5. EPR spectroscopy of the H_2O_2 oxidized ferric chlorite dismutase. Trace A. 0.18 mM monomer ferric chlorite dismutase in 50 mM Ches buffer pH 9.0. Trace B. the same as in trace A except with 1.2 mM hydrogen peroxide. EPR conditions: 9.224 GHz; microwave power, 126 mW; modulation frequency, 100 kHz; modulation amplitude, 1.0 mT; temperature, 26.5 K.

The EPR spectrum of the NO adduct to ferrous chlorite dismutase (Figure 6) shows an S = 1/2 species with hyperfine splitting from the ^{14}N (I=1) of NO: $A_{z, y, x}$ = 1.6, 1.9, 2.0 mT. The simulation in Figure 6 deviates from the experimental spectrum in the 320-330 mT region. Attempts to improve the simulation by assuming hyperfine splitting from two ^{14}N nuclei or assuming two spin species with a slightly different g_x-value were not successful. Possibly the NO adduct has a low symmetry for which the co-linearity of the hyperfine- and g-tensors, assumed in our simulation program, does not hold. The EPR spectrum in Figure 6, however, is not detailed enough to allow simulation assuming a rotation between the principal axes of the hyperfine- and g-tensors. Additional hyperfine splitting would be expected from the ^{14}N of a proximal histidine. Clearly chlorite dismutase either contains a different proximal ligand, or the NO binding has resulted in the bond break between the iron and the proximal histidine. The EPR spectrum is similar to the signals found for NO bound to catalase

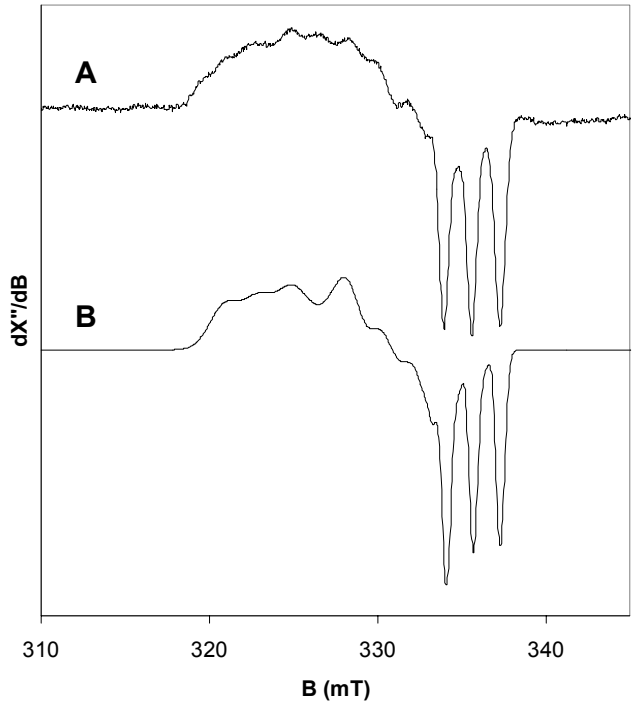

Figure 6. EPR spectroscopy of the NO adduct of ferrous chlorite dismutase. Trace A: experimental spectrum. Trace B simulated spectrum assuming the parameter values given in table 1. EPR conditions: microwave frequency, 9.418 GHz; microwave power, 2.0 mW; modulation frequency, 100 kHz; modulation amplitude, 1.0 mT; temperature, 16.5 K.

[239], the heme domain of guanylate cyclase [240] or low-pH myoglobin [241], which all do not have a proximal histidine (anymore) attached to the heme iron center. EPR spectra of the hydroxide and imidazole adducts of ferric chlorite dismutase exhibit low spin ferric signals with EPR characteristics as presented in table 1. The rhombic and tetragonal components of the crystal field have been calculated from the g-values [242]. Comparison with other heme proteins indicates a similar crystal field in the hydroxide adducts of chlorite dismutase (in dimensionless coefficients normalized with the spin-orbit coupling parameter λ: tetragonal field $\Delta/\lambda = 7.16$ and rhombicity $V/\Delta = 0.52$), horseradish peroxidase (5.15 and 0.38), cytochrome c peroxidase (7.29 and 0.49), myoglobin (6.92 and 0.46), and hemoglobin (6.61, 0.53) [243-246]. A similar crystal field is also found in the imidazole adduct of chlorite dismutase (3.37 and 0.55) and bis-His coordinated hemoproteins, such as hemoglobin (3.71 and 0.51) [245].

Redox characteristics of chlorite dismutase

An EPR monitored redox titration of chlorite dismutase of the high spin species resulted in an $E_m(Fe^{3+/2+}) = -23 \pm 9$ mV vs. NHE at pH 7.0 and 25°C (Figure

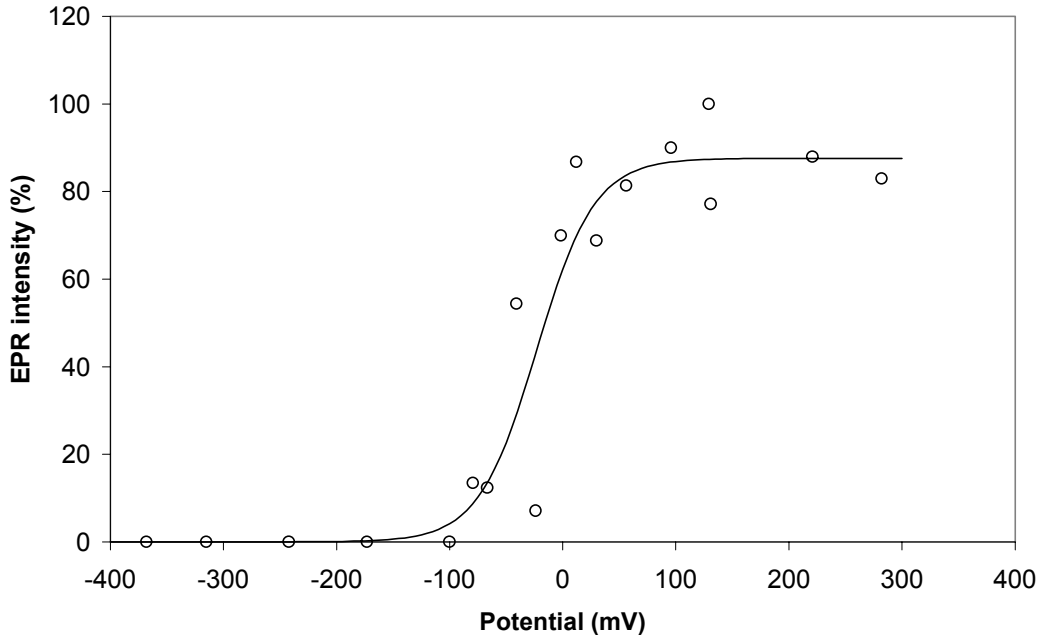

Figure 7. Reductive titration of the high spin ferric chlorite dismutase. The solid line represents a least square fit of the data points according to the Nernst equation for n = 1 and T = 25 °C resulting in an $E_m = -23 \pm 9$ mV vs. NHE.

7). This midpoint potential is close to the value of –21 mV found for *Ideonella dechloratans* chlorite dismutase measured in an optically monitored titration [7]. The UV-vis absorbance spectrum of ferrous chlorite dismutase exhibits a Soret band at 432 nm and a single α/β-band around 560 nm (Figure 1. Trace A), which are characteristics of a five coordinate high spin ferrous heme with an axial histidine, such as the ferrous hemes of deoxy-myoglobin [247] and soluble guanylate cyclase [248]. Ferrous chlorite dismutase rapidly auto-oxidizes to the ferric form in the presence of air (not shown). This was expected since we have found chlorite dismutase to be easily accessible to exogenous ligands.

Discussion

Spectroscopic properties of chlorite dismutase

The EPR spectroscopic properties of chlorite dismutase have been studied in detail. The published EPR spectra on chlorite dismutase from *Ideonella dechloratans* are similar to our results on the enzyme from GR-1 [7]. However the existence of a second high spin species, that we have designated as the "broad" signal, had not been reported previously. The nature of the multiplicity of these high spin signals is not known, however it does not reflect a difference in enzymatic activity. As is expected for heme enzymes, the ferric heme in the enzyme is primarily five-coordinate at the pH of optimal activity. Thus the ferric iron center is readily accessible to the substrate to form a six coordinate complex, as has been shown for the substrate analog nitrite.

Spectroscopic evidence for a histdine proximal ligand

Since the optical absorbance spectrum of the ferrous chlorite dismutase is characteristic of a five coordinate high spin ferrous heme center with an axial histidine and since the EPR spectra of the imidazole and hydroxide adducts of chlorite dismutase clearly indicate an axial histidine ligand, we propose chlorite dismutase to have a histidine proximal ligand to the iron center. This proximal histidine can be released from the iron coordination sphere upon binding of NO. As a consequence we attribute the EPR spectrum presented in Figure 6 to a five coordinate heme-NO complex. A study of NO binding to the myoglobin cavity mutant H39G with imidazole as proximal ligand has shown that NO reduces the binding constant of the

imidazole with several orders of a magnitude [249]. Furthermore binding of NO trans to the histidine has been found to result in breaking of the HisN-Fe bond in guanylate cyclase [250]. In the case of guanylate cyclase the HisN-Fe bond break is thought to be important for initiation of a structural change which triggers the enzymatic activity [250]. A thiolate proximal ligand has been ruled out for *Ideonella dechloratans* chlorite dismutase, based on the Soret band at 420 nm of the CO adduct of ferrous chlorite dismutase [7]. *Ideonella dechloratans* chlorite dismutase has similar optical and EPR spectroscopic properties and redox characteristics as GR-1 chlorite dismutase. Thus we propose that both *Ideonella dechloratans* and GR-1 chlorite dismutase, have a histidine as the proximal ligand.

Redox properties of chlorite dismutase

The $E_m(Fe^{3+/2+})$ = -23 mV found for GR-1 chlorite dismutase is higher than that of most heme enzymes, e.g. cytochrome P450 E_m ~ -200 mV, horseradish peroxidase E_m = -250 mV and catalase E_m < -500 mV [12, 13, 15]. However it is close to the E_m = + 50 mV found for myoglobin [4], to E_m = +24 mV of myeloperoxidase [5] and to E_m =-21 mV found for *Ideonella dechloratans* chlorite dismutase[7]. In contrast to what has been claimed previously [7] we find that GR-1 chlorite dismutase is readily reduced by sodium dithionite. The EPR spectra and the redox properties of chlorite dismutase are remarkably more similar to those of the globins than of the heme enzymes. The midpoint potential value of chlorite dismutase seems to confirm that the iron center has no cysteinyl or phenolate coordination, since the only known heme enzymes with cysteinyl or phenolate proximal ligands have an E_m < -200 mV. However peroxidases do have a proximal histidine ligand to the iron center and have an E_m around –200 mV. Basicity, or imidazolate character, of the proximal histidine modulates the redox potential of the $Fe^{3+/2+}$ [251]. As for metmyoglobin, chlorite dismutase appears to have a proximal histidine with is less basic than the proximal histidine of peroxidases. Since metmyoglobin can be oxidized by chlorite [252], we expect a similar oxidation as part of the reaction mechanism of chlorite dismutase. Furthermore, the helix containing the proximal histidine in the globins is located more directly under the heme plane but further from the iron than in peroxidases [1]. This stuctural difference allows greater flexibility of the proximal histidine in globins compared to peroxidases. Possibly, the localization of the proximal histidine in

chlorite dismutase is more similar to the globins than to peroxidases. This may also explain the His-Fe bond break upon binding of NO to the ferrous enzyme. The high midpoint potential of chlorite dismutase was unexpected, since it seems likely that the five-coordinate ferric species is the active form of the enzyme. The low midpoint potential of the peroxidases stabilizes this ferric state, while for the globins the ferrous state has to be stabilized. Possibly a low midpoint potential is not necessary for chlorite dismutase since the enzyme uses such a highly oxidizing substrate ($E_{m,\ pH\ 7.0,\ 25°C}$ (ClO_2^-/Cl^-) = +1175 mV).

On the mechanism of chlorite dismutase

Several considerations are important in order to determine a reaction mechanism of chlorite dismutase. First of all the valence of Cl in ClO_2^- is reduced from +3 to -1 in the product Cl^-. As a consequence during the reaction mechanism in

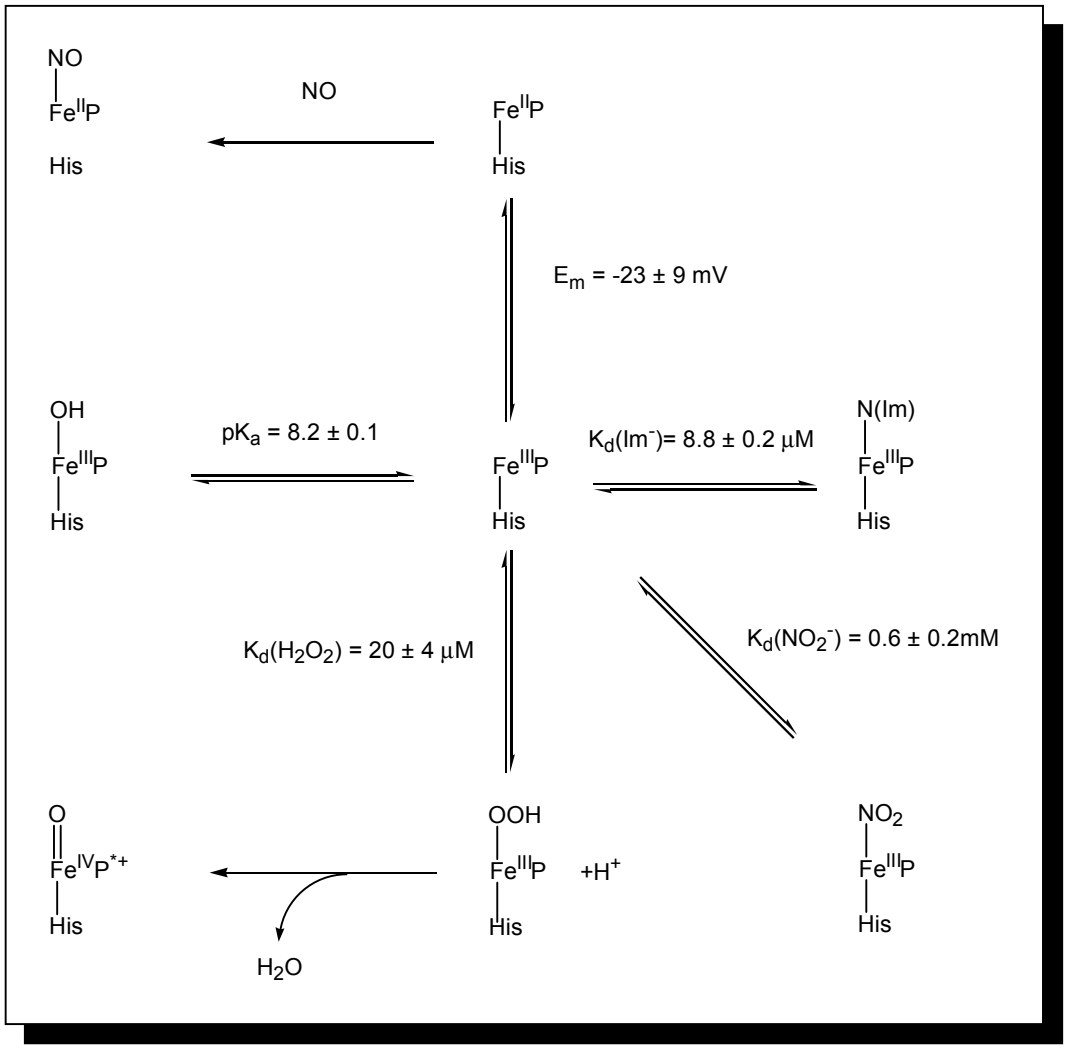

Figure 8. Schematic view of the formation of the different heme iron species described in this report.

total four electrons have to be transferred, likely via the heme iron center. High valence states of the heme iron, such as Fe^{4+}, seem necessary to facilitate the redox reactions. An important question that needs to be answered is whether or not H_2O is one of the substrates of the enzyme. And to put this question in a practical form: do both oxygen atoms in the dioxygen product of chlorite dismutase come from chlorite? An investigation to elucidate this problem is in progress.

The evidence from the spectroscopic and ligand binding studies of chlorite dismutase suggest binding of chlorite to the five coordinate high spin ferric form of the enzyme as the first step of the catalytic mechanism. Possible the second step would involve oxidation of the ferric iron to an oxoferryl π-cation radical species (compound I), as happens when hydrogen peroxide binds (Figure 8). The proximal His-Fe bond has been found to be relatively weak as in guanylate cyclase. Perhaps, as in guanylate cyclase, an Fe-His bond break is part of the catalytic mechanism of chlorite dismutase.

Acknowledgements

We thank Dr. Servé W.M. Kengen from Wageningen University for providing strain GR-1. This research has been financially supported by the Council for Chemical Sciences of the Netherlands Organization for Scientific Research (CW-NWO).

References

1. Poulos, T.L. (1996) The Role of The Proximal Ligand in Heme Enzymes, *J. Biol. Inorg. Chem. 1*, 356-359.
2. Goodin, D.B. & McRee, D.E. (1993) The Asp-His-Fe Triad of Cytochrome C Peroxidase Controls the Reduction Potential, Electronic Structure, and Coupling of the Tryptophan Free Radical to the Heme, *Biochemistry. 32*, 3313-3324.
3. Choudhury, K., Sundaramoorthy, M., Hickman, A., Yonetani, T., Woehl, E., Dunn, M.F. & Poulos, T.L. (1994) Role of the Proximal Ligand in Peroxidase Catalysis. Crystallographic, Kinetic, and Spectral Studies of Cytochrome c peroxidase Proximal Ligand Mutants, *J. Biol. Chem. 269*, 20239-20249.
4. Taylor, J.F. & Morgan, V.E. (1942) Oxidation-Reduction Potentials of the Metmyoglobin-Myoglobin System, *J. Biol. Chem. 144*, 15-20.
5. Ikeda-Saito, M. & Prince, R.C. (1985) The Effect of Chloride on the Redox and EPR Properties of Myeloperoxidase, *J. Biol. Chem. 260*, 8301-8305.
6. Arnhold, J., Furtmuller, P.G., Regelsberger, G. & Obinger, C. (2001) Redox Properties of the Couple Compound I/Native Enzyme of Myeloperoxidase and Eosinophil Peroxidase, *Eur. J. Biochem. 268*, 5142-5148.
7. Stenklo, K., Thorell, H.D., Bergius, H., Aasa, R. & Nilsson, T. (2001) Chlorite dismutase from *Ideonella dechloratans*, *J. Biol. Inorg. Chem. 6*, 601-607.
8. Hagedoorn, P.L., De Geus, D.C. & Hagen, W. R. (2002) Spectroscopic Characterization and Ligand Binding Properties of Chlorite Dismutase from the Chlorate Respiring Bacterial Strain GR-1, *Eur. J. Biochem. in press.*
9. Millis, C.D., Cai, D., Stankovic, M.T. & Tien, M. (1989) Oxidation-Reduction Potentials and Ionization States of Extracellular Peroxidases from the Lignin-Degrading Fungus *Phanerochaete chrysosporium*, *Biochemistry. 28*, 8484-8489.
10. Conroy, C.W., Tyma, P., Daum, P.H. & Erman, J.E. (1978) Oxidation-Reduction Potential Measurements of Cytochrome c Peroxidase and pH Dependent Spectral Transitions in the Ferrous Enzyme, *Biochim. Biophys. Acta. 537*, 62-69.
11. Mondal, M.S., Fuller, H.A. & Armstrong, F.A. (1996) Direct Measurement of the Reduction Potential of Catalytically Active Cytochrome c Peroxidase

Compound I: Voltammetric Detection of a Reversible, Cooperative Two-Electron Transfer Reaction, *J. Am. Chem. Soc. 118*, 263-264.

12. Gunsalus, I.C., Meeks, J.R., Lipscomb, J.D., Debrunner, P. & Münck, E. (1974) Bacterial monooxygenases. P 450 cytochrome system. in *Molecular Mechanism of Oxygen Activation* (Hayaishi, O., ed) pp. 559-613, Acedemic Press, New York.
13. Yamada, H., Makino, R. & Yamazaki, I. (1975) Effects of 2,4-Substituents of Deuteroheme upon Redox Potentials of Horseradish Peroxidases, *Arch. Biochem. Biophys. 169*, 344-353.
14. Farhangrazi, S.S., Fosset, M.E., Powers, L.S. & Ellis, W.R. Jr. (1995) Variable-Temperature Spectroelectrochemical Study of Horseradish Peroxidase, *Biochemistry. 34*, 2866-2871.
15. Williams, R.J.P. (1974) Heme Proteins and Oxygen. in *Iron in Biochemistry and Medicine* (Jacobs, A. & Worwood, M., eds) pp. 183-219, Acedemic Press, London.
16. Ginkel, C.G. van, Rikken, G.B., Kroon, A.G.M. & Kengen, S.W.M. (1996) Purification and Characterization of Chlorite Dismutase: a Novel Oxygen-Generating Enzyme, *Arch. Microbiol. 166*, 321-326.
17. Coates, J.D., Michaelidou, U., Bruce, R.A., O'Connor, S.M., Crespi, J.N. & Achenbach, L.A. (1999) Ubiquity and Diversity of Dissimilatory (Per)chlorate-Reducing Bacteria, *Appl. Environ. Microbiol. 65*, 5234-5241.
18. Jenney, F.E. Jr., Verhagen, M.F., Cui, X. & Adams, M.W.W. (1999) Anaerobic microbes: oxygen detoxification without superoxide dismutase, *Science. 286*, 306-309.
19. Kappock, T.J. & Caradonna, J.P. (1996) Pterin-Dependent Amino Acid Hydroxylases, *Chem. Rev. 96*, 2659-2756.
20. Shiman, R., Mortimore, G.E., Schworer, C.M. & Gray, D.W. (1982) Regulation of Phenylalanine Hydroxylase Activity by Phenylalanine In Vivo, In Vitro, and in Perfused Rat Liver, *J. Biol. Chem. 257*, 11213-11216.
21. Haavik, J., Døskeland, A.P. & Flatmark, T. (1986) Stereoselective Effects in the Interactions of Pterin Cofactors with Rat-Liver Phenylalanine 4-monooxygenase, *Eur. J. Biochem. 160*, 1-8.

22. Falia, G. & Stetter, K.O. (1986) *Pyrococcus furiosus* sp. nov. represents a Novel Genus of Marine Heterotrophic Archaeabacteria growing Optimally at 100°C, *Arch. Microbiol. 145*, 56-61.

23. Herriott, J.R., Sieker, L.C., Jensen, L.H. & Lovenberg, W. (1970) Structure of Rubredoxin: an X-Ray Study to 2.5 Å Resolution, *J. Mol. Biol. 50*, 391-406.

24. Blake, P.R., Park, J.B., Bryant, F.O., Aono, S., Magnuson, J.K., Eccleston, E., Howard, J.B., Summers, M.F. & Adams, M.W.W. (1991) Determinants of Protein Hyperthermostability: Purification and Amino Acid Sequence of Rubredoxin from the Hyperthermophilic Archaebacterium *Pyrococcus furiosus* and Secondary Structure of the Zinc Adduct by NMR, *Biochemistry. 30*, 10885-10891.

25. Bau, R., Rees, D.C., Kurtz, D.M. Jr., Scott, R.A., Huang, H., Adams, M.W.W. & Eidsness, M.K. (1998) Crystal Structure of Rubredoxin from *Pyrococcus furiosus* at 0.95 Å Resolution, and the Structures of N-terminal Methionine and Formylmethionine Variants of Pf Rd. Contributions of N-terminal Interactions to Thermostability., *J. Biol. Inorg. Chem. 3*, 484-493.

26. Ma, K. & Adams, M.W.W. (1999) A Hyperactive NAD(P)H:Rubredoxin Oxidoreductase from the Hyperthermophilic Archaeon *Pyrococcus furiosus*, *J. Bacteriol. 181*, 5530-5533.

27. Yeh, A.P., Hu, Y., Jenney, F.E. Jr., Adams, M.W.W. & Rees, D.C. (2000) Structures of the Superoxide Reductase from *Pyrococcus furiosus* in the Oxidized and Reduced States, *Biochemistry. 39*, 2499-2508.

28. Clay, M.D., Jenney, F.E., Hagedoorn, P.L., George, G.N., Adams, M.W.W. & Johnson, M.K. (2002) Spectroscopic Studies of *Pyrococcus furiosus* Superoxide Reductase: Implications for Active Site Structures and the Catalytic Mechanism, *J. Am. Chem. Soc. 124*, 788-805.

29. Adams, M.W.W. (1992) Novel Iron-Sulfur Centers in Metalloenzymes and Redox Proteins from Extremely Thermophilic Bacteria, *Adv. Inorg. Chem. 38*, 341-396.

30. Imai, T., Taguchi, K., Ogawara, Y, Ohmori, D., Yamakura, F., Ikezawa, H. & Urushiyama, A. (2001) Characterization and Cloning of an Extremely Thermostable, *Pyrococcus furiosus*-type 4Fe Ferredoxin from *Thermococcus profundus*, *J. Biochem. (Tokyo). 130*, 649-655.

31. Staples, C.R., Dhawan, I.K., Finnegan, M.G., Dwinell, D.A., Zhou, Z.H., Huang, H., Verhagen, M.F.J.M., Adams, M.W.W. & Johnson, M.K. (1997) Electronic, Magnetic and Redox Properties of [MFe_3S_4] Clusters (M = Cd, Cu, Cr) in *Pyrococcus furiosus* Ferredoxin, *Inorg. Chem. 36*, 5740-5749.
32. Hagedoorn, P.L. (2002) *Unpublished*.
33. Finnegan, M.G., Conover, R.C., Park, J.B., Zhou, Z.H., Adams, M.W.W. & Johnson, M.K. (1995) Electronic, Magnetic and Ligand-Binding Properties of M[Fe_3S_4] Clusters (M = Zn, Co, Mn) in *Pyrococcus furiosus* Ferredoxin, *Inorg. Chem. 34*, 5358-5369.
34. Fu, W., Telser, J., Hoffman, B.M., Smith, E.T., Adams, M.W.W., Finnegan, M.G., Conover, R.C. & Johnson, M.K. (1994) Interaction of Tl^+ and Cs^+ with the [Fe_3S_4] cluster of *Pyrococcus furiosus* Ferredoxin: Investigation by Resonance Raman, MCD, EPR, and ENDOR Spectroscopy, *J. Am. Chem. Soc. 116*, 5722-5729.
35. Fawcett, S.E.J., Davis, D., Breton, J.L., Thomson, A.J. & Armstrong, F.A. (1998) Voltammetric Studies of the Reactions of Iron-Sulphur Clusters ([3Fe-4S] or [M3Fe-4S]) Formed in *Pyrococcus furiosus* Ferredoxin, *Biochem. J. 335*, 357-368.
36. Aono, S., Bryant, F.O. & Adams, M.W.W. (1989) A Novel and Remarkably Thermostable Ferredoxin form the Hyperthermophilic Archaebacterium *Pyrococcus furiosus*, *J. Bacteriol. 171*, 3433-3439.
37. Mai, X. & Adams, M.W.W. (1994) Indolepyruvate Ferredoxin Oxidoreductase from the Hyperthermophilic Archaeon *Pyrococcus furiosus*, *J. Biol. Chem. 269*, 16726-16732.
38. Mai, X. & Adams, M.W.W. (1996) Characterization of a Fourth Type of 2-Keto Acid-Oxidizing Enzyme from a Hyperthermophilic Archaeon: 2-Ketoglutarate Ferredoxin Oxidoreductase from *Thermococcus litoralis*, *J. Bacteriol. 178*, 5890-5896.
39. Heider, J., Mai, X. & Adams, M.W.W. (1996) Characterization of 2-Ketoisovalerate Ferredoxin Oxidoreductase, a New and Reversible Coenzyme A-Dependent Enzyme Involved in Peptide Fermentation by Hyperthermophilic Archaea, *J. Bacteriol. 178*, 780-787.
40. Collins, M.D., Lawson, P.A., Willems, A., Cordoba, J.J., Fernandez-Garayzabal, J., Garcia, P., Cai, J., Hippe, H. & Farrow, J.A. (1994) The

Phylogeny of the Genus Clostridium: Proposal of Five New Genera and Eleven New Species Combinations, *Int. J. Syst. Bacteriol. 44*, 812-826.

41. Andreesen, J.R. & Ljungdahl, L.G. (1973) Formate Dehydrogenase of *Clostridium thermoaceticum*: Incorporation of Selenium-75 and the Effects of Selenite, Molybdate, and Tungstate on the Enzyme, *J. Bacteriol. 116*, 867-873.
42. Hille, R. (1996) The Mononuclear Molybdenum Enzymes, *Chem. Rev. 96*, 2757-2816.
43. Johnson, M.K., Rees, D.C. & Adams, M.W.W. (1996) Tungstoenzymes, *Chem. Rev. 96*, 2817-2839.
44. Mukund, S. & Adams, M.W.W. (1991) The Novel Tungsten-Iron-Sulfur Protein of the Hyperthermophilic Archaebacterium, *Pyrococcus furiosus*, is an Aldehyde Ferredoxin Oxidoreductase, *J. Biol. Chem. 266*, 14208-14216.
45. Chan, M.K., Mukund, S., Kletzin, A., Adams, M.W.W. & Rees, D.C. (1995) Structure of a Hyperthermophilic Tungstopterin Enzyme, Aldehyde Ferredoxin Oxidoreductase, *Science. 267*, 1463-1469.
46. Koehler, B.P., Mukund, S., Conover, R.C., Dhawan, I.K., Roy, R., Adams, M.W.W. & Johnson, M.K. (1996) Spectroscopic Characterization of the Tungsten and Iron Centers in Aldehyde Ferredoxin Oxidoreductases from Two Hyperthermophilic Archaea, *J. Am. Chem. Soc. 118*, 12391-12405.
47. Arendsen, A.F., Vocht, M. de, Bulsink, Y.B.M. & Hagen, W.R. (1996) Redox Chemistry of Biological Tungsten: An EPR Study of the Aldehyde Oxidoreductase from *Pyrococcus furiosus*, *J. Biol. Inorg. Chem. 1*, 292-296.
48. Heider, J., Kesen, M. & Adams, M.W.W. (1995) Purification, Characterization, and Metabolic Function of Tungsten-Containing Aldehyde Ferredoxin Oxidoreductase from the Hyperthermophilic and Proteolytic Archaeon *Thermococcus* Strain ES-1, *J. Bacteriol. 177*, 4757-4764.
49. Johnson, J.L., Rajagopalan, K.V., Mukund, S. & Adams, M.W.W. (1993) Identification of Molybdopterin as the Organic Component of the Tungsten Cofactor in Four Enzymes from Hyperthermophilic Archaea, *J. Biol. Chem. 268*, 4848-4852.
50. Mukund, S. (1995) *Biochemical and Biophysical Characterization of Novel Tungsten-Containing Enzymes from Hyperthermophilic Archaea*, Ph.D. Dissertation, University of Georgia, Athens.

51. White, H., Strobl, G., Feicht, R. & Simon, H. (1989) Carboxylic Acid Reductase: a New Tungsten Enzyme Catalyses the Reduction of Non-Activated Carboxylic Acids to Aldehydes, *Eur. J. Biochem. 184*, 89-96.

52. Strobl, G., Feicht, R., White, H., Lottspeich, F. & Simon, H. (1992) The Tungsten-Containing Aldehyde Oxidoreductase from *Clostridium thermoaceticum* and its Complex with a Viologen-Accepting NADPH Oxidoreductase, *Biol. Chem. 373*, 123-132.

53. White, H., Feicht, R., Huber, C., Lottspeich, F. & Simon, H. (1991) Purification and Some Properties of the Tungsten-Containing Carboxylic Acid Reductase from *Clostridium formicoaceticum*, *Biol. Chem. 372*, 999-1005.

54. Huber, C., Caldeira, J., Jongejan, J.A. & Simon, H. (1994) Further Characterization of Two Different, Reversible Aldehyde Oxidoreductases from *Clostridium formicoacteticum*, one Containing Tungsten and the Other Molybdenum, *Arch. Microbiol. 162*, 303-309.

55. Hu, Y., Faham, S., Roy, R., Adams, M.W.W. & Rees, D.C. (1999) Formaldehyde Ferredoxin Oxidoreductase from *Pyrococcus furiosus*: The 1.85 Å Resolution Crystal Structure and its Mechanistic Implications, *J. Mol. Biol. 286*, 899-914.

56. Roy, R., Mukund, S., Shut, G.J., Dunn, D.M., Weiss, R. & Adams, M.W.W. (1999) Purification and Molecular Characterization of the Tungsten-Containing Formaldehyde Ferredoxin Oxidoreductase from the Hyperthermophilic Archaeon *Pyrococcus furiosus*: the Third of a Putative Five-Member Tungstoenzyme Family, *J. Bacteriol. 181*, 1171-1180.

57. Mukund, S. & Adams, M.W.W. (1993) Characterization of a Novel Tungsten-containing Formaldehyde Ferredoxin Oxidoreductase from the Hyperthermophilic Archaeon, *Thermococcus litoralis*, *J. Biol. Chem. 268*, 13592-13600.

58. Dhawan, I.K., Roy, R., Koehler, B.P., Mukund, S., Adams, M.W.W. & Johnson, M.K. (2000) Spectroscopic Studies of the Tungsten-containing Formaldehyde Ferredoxin Oxidoreductase from the Hyperthermophilic Archaeon *Thermococcus litoralis*, *J. Biol. Inorg. Chem. 5*, 313-327.

59. Mukund, S. & Adams, M.W.W. (1995) Glyceraldehyde-3-phosphate Ferredoxin Oxidoreductase, a Novel Tungsten-containing Enzyme with a

Potential Glycolytic Role in the Hyperthermophilic Archaeon *Pyrococcus furiosus*, *J. Biol. Chem. 270*, 8389-8392.

60. Oost, J. van der, Schut, G., Kengen, S.W.M., Hagen, W.R., Thomm, M. & Vos, W.M. de. (1998) The Ferredoxin-dependent Conversion of Glyceraldehyde-3-phosphate in the Hyperthermophilic Archaeon *Pyrococcus furiosus* Represents a Novel Site of Glycolytic Regulation, *J. Biol. Chem. 273*, 28149-28154.
61. Hagedoorn, P.-L., Freije, J.R. & Hagen, W.R. (1999) *Pyrococcus furiosus* Glyceraldehyde 3-phosphate Oxidoreductase has Comparable W(6+/5+) and W(5+/4+) Reduction Potentials and Unusual [4Fe-4S] EPR Properties, *FEBS Lett. 462*, 66-70.
62. Adams, M.W.W. (2002) *Unpublished*.
63. Hensgens, C.M.H., Hagen, W. R. & Hansen, T.A. (1995) Purification and Characterization of a Benzylviologen-Linked, Tungsten-Containing Aldehyde Oxidoreductase from *Desulfovibrio gigas*, *J. Bacteriol. 177*, 6195-6200.
64. Trautwein, T., Krauss, F., Lottspeich, F. & Simon, H. (1994) The (2R)-Hydroxycarboxylate-Viologen-Oxidoreductase from *Proteus vulgaris* is a Molybdenum-Containing Iron-Sulphur Protein, *Eur. J. Biochem. 222*, 1025-1032.
65. Yamamoto, I., Saiki, T., Liu, S.M. & Ljungdahl, L.G. (1983) Purification and Properties of NADP-dependent Formate Dehydrogenase from *Clostridium thermoaceticum*, a Tungsten-Selenium-Iron Protein, *J. Biol. Chem. 258*, 1826-1832.
66. Durfor, C.N., Wetherbee, P.J., Deaton, J.C. & Solomon, E.I. (1983) Characterization and Spectroscopic Properties of Reduced Mo and W Formate Dehydrogenase from *Clostridium thermoaceticum*, *Biochem. Biophys. Res. Commun. 115*, 61-67.
67. Deaton, J. C., Solomon, E. I., Watt, G. D., Wetherbee, P.J. & Dufor, C. N. (1987) Electron Paramagnetic Resonance Studies of the Tungsten-Containing Formate Dehydrogenase from *Clostridium thermoaceticum*, *Biochem. Biophys. Res. Commun. 149*, 424-430.
68. Wagner, R. & Andreesen, J.R. (1987) Accumulation and Incorporation of ^{185}W-Tungsten into Proteins of *Clostridium acidiurici* and *Clostridium cylindrosporum*, *Arch. Microbiol. 147*, 295-299.

69. Leonhardt, U. & Andreesen, J.R. (1977) Some Properties of Formate Dehydrogenase, Accumulation and Incorporation of ^{185}W-Tungsten into Proteins of *Clostridium formicoaceticum*, *Arch. Microbiol. 115*, 277-284.

70. Gräntzdörffer, A. (2000) *Formiat-Stoffwechsel in Eubacterium acidaminophilum: Molekulare und Biochemische Charakterisierung der Wolfram- und Selen-haltigen Formiat-Dehydrogenasen sowie einer Eisen-Hydrogenase*, Ph.D. Dissertation, Martin-Luther-University Halle-Wittenberg, Halle.

71. Bok, F.A.M. de, Hagedoorn, P.L., Silva, P.J., Hagen, W.R., Schiltz, E. & Stams, A.J.M. (2002) Two W-containing formate dehydrogenases (CO_2-reductases) involved in syntrophic propionate oxidation by *Syntrophobacter fumaroxidans*, *submitted J. Bacteriol.*

72. Almendra, M.J., Brondino, C.D., Gavel, O., Pereira, A.S., Tavares, P., Bursakov, S., Duarte, R., Caldeira, J., Moura, J.J.G. & Moura, I. (1999) Purification and Characterization of a Tungsten-Containing Formate Dehydrogenase form *Desulfovibrio gigas*, *Biochemistry. 38*, 16366-16372.

73. Raaijmakers, H., Teixeira, S., Dias, J.M., Almendra, M.J., Brondino, C.D., Moura, I., Moura, J.J.G. & Romão, M.J. (2001) Tungsten-Containing Formate Dehydrogenase From *Desulfovibrio gigas*: Metal Identification and Preliminary Structural Data by Multi-Wavelength Crystallography, *J. Biol. Inorg. Chem. 6*, 398-404.

74. Schmitz, R.A., Richter, M., Linder, D. & Thauer, R.K. (1992) A Tungsten-Containing Active Formylmethanofuran Dehydrogenase in the Thermophilic Archaeon *Methanobacterium wolfei*, *Eur. J. Biochem. 207*, 559-565.

75. Bertram, P.A., M., Karrasch, Schmitz, R.A., Böcher, R., Albracht, S.P.J. & Thauer, R.K. (1994) Formylmethanofuran Dehydrogenases from Methanogenic Archaea. Substrate Specificity, EPR Properties and Reversible Inactivation by Cyanide of the Molybdenum or Tungsten Iron-Sulfur Proteins, *Eur. J. Biochem. 220*, 477-484.

76. Bertram, P.A., Schmitz, R.A., Linder, D. & Thauer, R.K. (1994) Tungstate can Substitute for Molybdate in Sustaining Growth of *Methanobacterium thermoautotrophicum*. Identification and Characterization of a Tungsten Isoenzyme of Formylmethanofuran Dehydrogenase, *Arch. Microbiol. 161*, 220-228.

77. Vorholt, J.A., Vaupel, M. & Thauer, R.K. (1997) A Selenium-Dependent and a Selenium-Independent Formylmethanofuran Dehydrogenase and Their Transcriptional Regulation in the Hyperthermophilic *Methanopyrus kandleri*, *Mol. Microbiol. 23*, 1033-1042.

78. Rosner, B.M. & Schink, B. (1995) Purification and Characterization of Acetylene Hydratase of *Pelobacter acetylenicus*, a Tungsten Iron-Sulfur Protein, *J. Bacteriol. 177*, 5767-5772.

79. Meckenstock, R.U., Krieger, R., Ensign, S., Kroneck, P.M.H. & Schink, B. (1999) Acetylene Hydratase of *Pelobacter acetylenicus*, *Eur. J. Biochem. 264*, 176-182.

80. Stewart, L.J., Bailey, S., Bennet, B., Charnock, J.M., Garner, C.D. & McAlpine, A.S. (2000) Dimethylsulfoxide Reductase: An Enzyme Capable of Catalysis with Either Molybdenum or Tungsten at the Active Site, *J. Mol. Biol. 299*, 593-600.

81. Stewart, L.J., Bailey, S., Collison, D., Morris, G.A., Preece, I. & Garner, C.D. (2001) In Vivo Oxo Transfer: Reactions of Native and W-Substituted Dimethyl Sulfoxide Reductase Monitored by ^{1}H NMR Spectroscopy, *ChemBioChem. 2*, 703-706.

82. Buc, J., Santini, C.-L., Giordani, R., Czjzek, M., Wu, L.-F. & Giordano, G. (1999) Enzymatic and Physiological Properties of the Tungsten-substituted Molybdenum TMAO Reductase form *Escherichia coli*, *Mol. Microbiol. 32*, 159-168.

83. Park, J.B., Fan, C., Hoffman, B.M. & Adams, M.W.W. (1991) Potentiometric and Electron Nuclear Double Resonance Properties of the Two Spin Forms of the [4Fe-4S]$^{+}$ Cluster in the Novel Ferredoxin from the Hyperthermophilic Archaebacterium *Pyrococcus furiosus*, *J. Biol. Chem. 266*, 19351-19356.

84. Brereton, P.S., Verhagen, M.F.J.M., Zhou, Z.H. & Adams, M.W.W. (1998) Effect of Iron-Sulfur Cluster Environment in Modulating the Thermodynamic Properties and Biological Function of Ferredoxin from *Pyrococcus furiosus*, *Biochemistry. 37*, 7351-7362.

85. Smith, E.T., Blamey, J.M., Zhou, Z.H. & Adams, M.W.W. (1995) A Variable-Temperature Direct Electrochemical Study of Metalloproteins from Hyperthermophilic Microorganisms Involved in Hydrogen Production from Pyruvate, *Biochemistry. 34*, 7161-7169.

86. Christen, R.P., Nomikos, S.I. & Smith, E.T. (1996) Probing Protein Electrostatic Interactions Through Temperature/Reduction Potential Profiles, *J. Biol. Inorg. Chem. 1*, 515-522.

87. Swartz, P.D. & Ichiye, T. (1996) Temperature Dependence of the Redox Potential of Rubredoxin from *Pyrococcus furiosus*: a Molecular Dynamics Study, *Biochemistry. 35*, 13772-13779.

88. Arendsen, A.F., Veenhuizen, P.Th.M. & Hagen, W.R. (1995) Redox Properties of the Sulfhydrogenase from *Pyrococcus furiosus*, *FEBS Lett. 368*, 117-121.

89. Hagen, W.R. (1989) Direct Electron Transfer of Redox Proteins at the Bare Glassy Carbon Electrode, *Eur. J. Biochem. 182*, 523-530.

90. Pierik, A.J., Hagen, W.R., Redeker, J.S., Wolbert, R.B.G., Boersma, M., Verhagen, M.F.J.M., Grande, H.J., Veeger, C., Mutsaerts, P.H.A., Sands, R.H. & Dunham, W.R. (1992) Redox Properties of the Iron-sulfur Clusters in Activated Fe-hydrogenase from *Desulfovibrio vulgaris* (Hildenborough), *Eur.J. Biochem. 209*, 63-72.

91. Duyvis, M.G., Mensink, R.E., Wassink, H. & Haaker, H. (1997) Evidence for Multiple Steps in the Pre-Steady-State Electron Transfer Reaction of Nitrogenase from *Azotobacter vinelandii*, *Biochim. Biophys. Acta. 1320*, 34-44.

92. Dawson, R.M.C., Elliott, D.C., Elliott, W.H. & Jones, K.M. (1984) in *Data for Biochemical Research 3rd ed.* pp. 424, Clarendon Press, Oxford.

93. Koller, K.B. & Hawkridge, F.M. (1988) The Effects of Temperature and Electrolyte at Acidic and Alkaline pH on the Electron Transfer Reactions of Cytochrome c at Indium Sesquioxide Electrodes, *J. Electroanal. Chem. Interfacial Electrochem. 239*, 291-306.

94. Eidsness, M.K., Richie, K.A., Burden, A.E., Kurtz, D.M. & Scott, R.A. (1997) Dissecting Contributions to the Thermostability of *Pyrococcus furiosus* Rubredoxin: Beta-Sheet Chimeras, *Biochemistry. 36*, 10406-10413.

95. Ma, K., Zhou, Z.H. & Adams, M.W.W. (1994) Hydrogen Production from Pyruvate by Enzymes Purified from the Hyperthermophilic Archaeon, *Pyrococcus furiosus*: A Key Role for NADPH, *FEMS Microbiol. Lett. 122*, 245-250.

96. Verhagen, M.F.J.M. (1995) *Characterization of Redox Proteins using Electrochemical Methods*, Ph.D. Dissertation, Wageningen University, Wageningen.

97. Christen, R.P., Janic, T., Zhou, Z.H., Adams, M.W.W., Tomich, J.M. & Smith, E.T. (1997) Physical Characterization of a Totally Synthetic Rubredoxin, *J. Inorg. Biochem. 65*, 53-56.

98. Heering, H.A., Bulsink, Y.B.M., Hagen, W.R. & Meyer, T.E. (1995) Reversible Super-Reduction of the Cubane [4Fe-4S](3+,2+,1+) in the High-Potential Iron-Sulfur Protein under Non-Denaturing Conditions. EPR Spectroscopic and Electrochemical Studies, *Eur. J. Biochem. 232*, 811-817.

99. Calzolai, L., Gorst, C.M., Zhao, Z.H., Teng, Q., Adams, M.W.W. & Mar, G.N. La. (1995) ^{1}H NMR Investigation of the Electronic and Molecular Structure of the Four-Iron Cluster Ferredoxin from the Hyperthermophile *Pyrococcus furiosus*. Identification of Asp 14 as a Cluster Ligand in Each of the Four Redox States, *Biochemistry. 34*, 11373-11384.

100. Zhou, Z.H. & Adams, M.W.W. (1997) Site-Directed Mutations of the 4Fe-Ferredoxin from the Hyperthermophilic Archaeon *Pyroccus furiosus*: Role of the Cluster-Coordinating Aspartate in Physiological Electron Transfer Reactions, *Biochemistry. 36*, 10892-10900.

101. Dhawan, I.K., Roy, R., Koehler, B.P., Adams, M.W.W. & Johnson, M.K. (1999) Spectroscopic Studies of Tungsten-Containing Formaldehyde Ferredoxin Oxidoreductase and Glyceraldehyde-3-Phosphate Ferredoxin Oxidoreductase from Two Hyperthermophilic Archaea, *J. Inorg. Biochem. 74*, 112.

102. Segel, I.H. (1975) in *Biochemical Calculations: How to Solve Mathematical Problems in General Biochemistry* pp. 414-415, Wiley and Sons, New York.

103. Pierik, A.J. & Hagen, W.R. (1991) S=9/2 EPR Signals are Evidence Against Coupling between the Siroheme and the Fe/S Cluster Prosthetic Groups in *Desulfovibrio vulgaris* (Hildenborough) Dissimilatory Sulfite Reductase, *Eur. J. Biochem. 195*, 505-516.

104. Hagedoorn, P.-L., Driessen, M.C., Bosch, M. van den, Landa, I. & Hagen, W.R. (1998) Hyperthermophilic Redox Chemistry: a Re-evaluation, *FEBS Lett. 440*, 311-314.

105. Nicholson, R.S. & Shain, I. (1964) Theory of Stationary Electrode Polarography. Single Scan and Cyclic Methods Applied to Reversible, Irreversible, and Kinetic Systems, *Anal. Chem. 36*, 706-723.

106. Bastian, N. R., Kay, C. J., Barber, M. J. & Rajagopalan, K.V. (1991) Spectroscopic Studies of the Molybdenum-containing Dimethyl Sulfoxide Reductase from *Rhodobacter sphaeroides* f.sp. *denitrificans*, *J. Biol. Chem. 266*, 45-51.

107. Vincent, S.P. & Bray, R.C. (1978) Electron-Paramagnetic-Resonance Studies on Nitrate Reductase from *Escherichia Coli* K12, *Biochem. J. 171*, 639-647.

108. Barber, M.J. & Siegel, L.W. (1982) Oxidation-Reduction Potentials of Molybdenum, Flavin, and Iron-Sulfur Centers in Milk Xanthine Oxidase: Variation with pH, *Biochemistry. 21*, 1638-1647.

109. Duderstadt, R.E., Brereton, P.S., Adams, M.W.W. & Johnson, M.K. (1999) A Pure S = 3/2 $[Fe4S4]^{+}$ Cluster in the A33Y Variant of *Pyrococcus furiosus* Ferredoxin, *FEBS Lett. 454*, 21-26.

110. Vanoni, M.A., Edmondson, D.E., Zanetti, G. & Curti, B. (1992) Characterization of the Flavins and the Iron-Sulfur Centers of Glutamate Synthase from *Azospirillum brasilense* by Absorption, Circular Dichroism, and Electron Paramagnetic Resonance Spectroscopies, *Biochemistry. 31*, 4613-4623.

111. Ma, K. & Adams, M.W.W. (1994) Sulfide Dehydrogenase from the Hyperthermophilic Archaeon *Pyrococcus furiosus*: A New Multifunctional Enzyme Involved in the Reduction of Elemental Sulfur, *J. Bacteriol. 176*, 6509-6517.

112. Rupp, H., Rao, K.K., Hall, D.O. & Cammack, R. (1978) Electron Spin Relaxation of Iron-Sulfur Proteins Studied by Microwave Power Saturation, *Biochim. Biophys. Acta. 537*, 255-260.

113. Luykx, D.M.A.M., Duine, J.A. & Vries, S. de. (1998) Molybdopterin Radical in Bacterial Aldehyde Dehydrogenases, *Biochemistry. 37*, 11366-11375.

114. Dickinson, R.G. & Jacobsen, N.W. (1970) A New Sensitive and Specific Test for the Detection of Aldehydes: Formation of 6-Mercapto-3-Substituted-s-Triazolo[4,3-b]-s-Tetrazines, *J. Chem. Soc. D*, 1719-1720.

115. Wang, J., Araki, T., Ogawa, T., Matsouka, M. & Fukuda, H. (1999) A Method of Graphically Analyzing Substrate-Inhibition Kinetics, *Biotechnol. Bioeng. 62*, 402-411.

116. Furfine, C.S. & Velick, S.F. (1965) The Acyl-Enzyme Intermediate and the Kinetic Mechanism of the Glyceraldehyde 3-Phosphate Dehydrogenase Reaction, *J. Biol. Chem. 240*, 844-855.

117. Binsted, N. (1998) *CCLRC Daresbury Laboratory EXCURV98 program*.

118. Lee, P.A. & Pendry, J.B. (1975) Theory of the Extended X-Ray Absorption Fine Structure, *Phys. Rev. B. 11*, 2795-2811.

119. Gurman, S.J., Binsted, N. & Ross, I. (1984) A Rapid, Exact Curved-Wave Theory for EXAFS Calculations, *J. Phys. C. 17*, 143-151.

120. Hedin, L. & Lundqvist, S. (1969) Effects of Electron-Electron and Electron-Phonon Interactions on the One-Electron States of Solids, *Solid State Phys. 23*, 1-181.

121. Binsted, N., Strange, R.W. & Hasnain, S.S. (1992) Constrained and Restrained Refinement in EXAFS Data Analysis with Curved Wave Theory, *Biochemistry. 31*, 12117-12125.

122. Humeres, E. & Quijano, J. (1996) The Mechanisms of Hydrolysis of Glyceraldehyde-3-phosphate, *Gazz. Chim. Ital. 126*, 449-456.

123. McLellan, A.C., Phillips, S.A. & Thornally, P.J. (1992) The Assay of Methylglyoxal in Biological Systems by Derivatization with 1,2-Diamino-4,5-dimethoxybenzene, *Anal. Biochem. 206*, 17-23.

124. Melander, L. & Saunders, W.H. (1980) *Reaction Rates of Isotopic Molecules*, John Wiley & Sons, New York.

125. Musgrave, K.B., Lim, B.S., Sung, K.-M., Holm, R.H., Hedman, B. & Hodgson, K.O. (2000) X-ray Spectroscopy of Enzyme Active Site Analogues and Related Molecules: Bis(dithiolene)molybdenum(IV) and -tungsten (IV,VI) Complexes with Variant Terminal Ligands, *Inorg. Chem. 39*, 5238-5247.

126. Dobbek, H. & Huber, R. (2002) The Molybdenum and Tungsten Cofactors: A Crystallographic View, *Met. Ions Biol. Syst. 39*, 227-263.

127. Kalapos, M.P. (1999) Methylglyoxal in Living Organisms. Chemistry, Biochemistry, Toxicology and Biological Implications, *Toxicol. Lett. 110*, 145-175.

128. Stetter, K.O. (1999) Extremophiles and their Adaptation to Hot Environments, *FEBS Lett. 452*, 22-25.

129. Dunford-Shore, B.H., Sulaman, W., Feng, B., Fabrizio, F., Holcomb, J., Wise, W. & Kazic, T. (2002) Klotho: Biochemical Compounds Declarative Database in

130. Kisker, C., Schindelin, H. & Rees, D.C. (1997) Molybdenum-Cofactor-Containing Enzymes: Structure and Mechanism, *Annu. Rev. Biochem. 66*, 233-267.

131. George, G.N., Prince, R.C., Mukund, S. & Adams, M.W.W. (1992) Aldehyde Ferredoxin Oxidoreductase from the Hyperthermophilic Archaebacterium *Pyrococcus furiosus* Contains a Tungsten Oxo-Thiolate Center, *J. Am. Chem. Soc. 114*, 3521-3523.

132. Cramer, S.P., Liu, C.-L., Mortenson, L.E., Spence, J.T., Liu, S.-M., Yamamoto, I. & Ljungdahl, L.G. (1985) Formate Dehydrogenase Molybdenum and Tungsten Sites - Observation by EXAFS of Structural Differences, *J. Inorg. Biochem. 23*, 119-124.

133. Garner, C.D., Banham, R., Cooper, S.J., Davies, E.S. & Stewart, L.J. (2001) in *Handbook of Metalloproteins* pp. 1023-1090, Marcel Dekker, Inc., New York, USA.

134. Kletzin, A. & Adams, M.W.W. (1996) Tungsten in Biological Systems, *FEMS Microbiol. Rev. 18*, 5-63.

135. Hagen, W.R. & Arendsen, A.F. (1998) The Bio-Inorganic Chemistry of Tungsten, *Struct. Bond. 90*, 161-191.

136. Greenwood, N.N. & Earnshaw, A. (1984) in *The Chemistry of the Elements* pp. 1170, Pergamon Press, Oxford, UK.

137. Johnson, J.L. & Rajagopalan, K.V. (1976) Electron Paramagnetic Resonance of the Tungsten Derivative of Rat Liver Sulfite Oxidase, *J. Biol. Chem. 251*, 5505-5511.

138. Stiefel, E.I. (1973) Proposed Molecular Mechanism for the Action of Molybdenum in Enzymes: Couples Proton and Electron Transfer, *Proc. Natl. Acad. Sci. USA. 70*, 988-992.

139. Garner, C.D. & Stewart, L.J. (2002) Tungsten-Substituted Molybdenum Enzymes, *Met. Ions Biol. Syst. 39*, 699-726.

140. McAlpine, A.S., McEwan, A.G., Shaw, A.L. & Bailey, S. (1997) Molybdenum Active Center of DMSO Reductase from *Rhodobacter capsulatus*: Crystal Structure of the Oxidized Enzyme at 1.82 Å Resolution and the Dithionite-Reduced Enzyme at 2.8 Å Resolution, *J. Biol. Inorg. Chem. 2*, 690-701.

141. Li, H-K., Temple, C., Rajagopalan, K.V. & Schindelin, H. (2000) The 1.3 Å Crystal Structure of *Rhodobacter sphaeroides* Dimethyl Sulfoxide Reductase Reveals Two Distinct Molybdenum Coordination Environments, *J. Am. Chem. Soc. 122*, 7673-7680.

142. George, G.N., Hilton, J., Temple, C., Prince, R.C. & Rajagopalan, K.V. (1999) Structure of the Molybdenum Site of Dimethyl Sulfoxide Reductase, *J. Am. Chem. Soc. 121*, 1256-1266.

143. Hagedoorn, P.-L., Slot, P. van 't, Leeuwen, H.P. van & Hagen, W.R. (2001) Electroanalytical Determination of Tungsten and Molybdenum in Proteins, *Anal. Biochem. 297*, 71-78.

144. Bray, R.C., Adams, B., Smith, A.T., Bennett, B. & Bailey, S. (2000) Reversible Dissociation of Thiolate Ligands from Molybdenum in an Enzyme of the Dimethyl Sulfoxide Reductase Family, *Biochemistry. 39*, 11258-11269.

145. Bennet, B., Benson, N., McEwan, A.G. & Bray, R.C. (1994) Multiple States of the Molybdenum Centre of Dimethylsulphoxide Reductase from *Rhodobacter capsulatus* revealed by EPR spectroscopy, *Eur. J. Biochem. 225*, 321-331.

146. Bray, R.C., Adams, B., Smith, A.T., Richards, R.L., Lowe, D.J. & Bailey, S. (2001) Reactions of Dimethylsulfoxide Reductase in the Presence of Dimethyl Sulfide and the Structure of the Dimethyl Sulfide-Modified Enzyme, *Biochemistry. 40*, 9810-9820.

147. Ziegler, T. (1991) Approximate Density Functional Theory as a Practical Tool in Molecular Energetics and Dynamics, *Chem. Rev. 91*, 651-667.

148. Figgis, B.N. (1966) *Introduction to Ligand Fields*, Wiley-Interscience, New York.

149. McClure, D.S. (1949) Triplet-Singlet Transitions in Organic Molecules. Lifetime Measurements of the Triplet State, *J. Chem. Phys. 17*, 905-913.

150. Davies, E.S., Aston, G.M., Beddoes, R.L., Collison, D., Dinsmore, A., Docrat, A., Joule, J.A., Wilson, C.R. & Garner, C.D. (1998) Oxo-tungsten Bis-

dithiolene Complexes Relevant to Tungsten Centres in Enzymes, *J. Chem. Soc. Dalton*, 3647-3656.

151. Hanson, G.R., Brunette, A.A., McDonell, A.C., Murray, K.S. & Wedd, A.G. (1981) Electronic Properties of Thiolate Compounds of Oxomolybdenum (V) and their Tungsten and Selenium Analogues. Effects of ^{17}O, ^{98}Mo, and ^{95}Mo Isotope Substitution upon ESR Spectra, *J. Am. Chem. Soc. 103*, 1953-1959.
152. Romão, M.J., Archer, M., Moura, I., Moura, J.J.G., LeGall, J., Engh, R., Schneider, M., Hof, P. & Huber, R. (1995) Crystal Structure of the Xanthine Oxidase-Related Aldehyde Oxido-Reductase from *D. gigas*, *Science. 270*, 1170-1176.
153. Sung, K.-M. & Holm, R.H. (2000) Synthesis and Structures of Bis(dithioline)-Tungsten(IV) Complexes Related to the Active Sites of Tungstoenzymes, *Inorg. Chem. 39*, 1275-1281.
154. Barnard, K.R., Gable, R.W. & Wedd, A.G. (1997) Dioxo-, Oxothio- and Dithio-Tungsten(VI) and Tungsten(V) Complexes of the Ligand N,N'-Dimethyl-N,N'-bis(2-mercaptophenyl)ethylenediamine, *J. Biol. Inorg. Chem. 2*, 623-633.
155. Wood, P.M. (1981) The Redox Potential for Dimethyl Sulphoxide Reduction to Dimethyl Sulphide: Evaluation and Biochemical Implications, *FEBS Lett. 124*, 11-14.
156. Mukund, S. & Adams, M.W.W. (1996) Molybdenum and Vanadium Do Not Replace Tungsten in the Catalytically Active Forms of the Three Tungstoenzymes in the Hyperthermophilic Archaeon *Pyrococcus furiosus*, *J. Bacteriol. 178*, 163-167.
157. Cardenas, Jacobo & Mortenson, Leonard E. (1974) Determination of Molybdenum and Tungsten in Biological Materials, *Anal. Biochem. 60*, 372-381.
158. El-Sayed, A.A.Y., Saad, E.A., Ibrahime, B.M.M. & Zaki, M.T.M. (2000) Flavonol Derivatives for Determination of Cr(III) and W(VI), *Mikrochim. Acta. 135*, 19-27.
159. Poucheret, P., Lamer, S. Le, Cros, G., Richter, R. K. de, Bonnet, P.-A. & Bressole, F. (2000) Tungsten Determination in Rat and Dog Plasma by Inductively Coupled Plasma Emission Spectrometry. Application to Preclinical Pharmacokinetic Studies, *Anal. Chim. Acta. 405*, 221-226.

160. Wang, T., Ge, Z., Wu, J., Li, B. & Liang, A. (1999) Determination of Tungsten in Bulk Drug Substance and Intermediates by ICP-AES and ICP-MS, *J. Pharm. Biomed. Anal. 19*, 937-943.

161. Marquet, P., Francois, B., Lotfi, H., Turcant, A., Debord, J., Nedelec, G. & Lachatre, G. (1997) Tungsten Determination in Biological Fluids, Hair and Nails by Plasma Emission Spectrometry in a Case of Severe Acute Intoxication in Man, *J. Forensic Sci. 42*, 527-530.

162. Pournaghi-Azar, M.H. & Nahalparvar, H. (2000) Extraction Differential Pulse Polarographic Determination of Mo(VI) in Cereals, *Electroanalysis. 12*, 527-530.

163. Gao, Z. & Siow, K.S. (1996) Catalytic-adsorptive Stripping Voltammetric Determination of Molybdenum in Plant Foodstuffs, *Talanta. 43*, 719-726.

164. Wang, J. & Lu, J. (1992) Catalytic-adsorptive Stripping Voltammetric Measurements of Ultratrace Levels of Tungsten, *Talanta. 39*, 801-804.

165. Massey, V. & Hemmerich, P. (1978) Photoreduction of Flavoproteins and Other Biological Compounds Catalyzed by Deazaflavins, *Biochemistry. 17*, 9-16.

166. Langmuir, I. (1916) Constitution and Fundamental Properties of Solids and Liquids. I. Solids, *J. Am. Chem. Soc. 38*, 2221-2295.

167. Jones, G.B. & Belling, G.B. (1970) Comparison of Protein Precipitants Used prior to Determination of Citrate in Biological Materials, *Anal. Biochem. 37*, 105-111.

168. Hart, L.I., McGartoll, M.A., Chapman, H.R. & Bray, R.C. (1970) The Composition of Milk Xanthine Oxidase, *Biochem. J. 116*, 851-864.

169. Lim, B.S., Sung, K.-M. & Holm, R.H. (2000) Structural and Functional Bis(dithiolene)-Molybdenum/Tungsten Active Site Analogues of the Dimethylsulfoxide Reductase Enzyme Family, *J. Am. Chem. Soc. 122*, 7410-7411.

170. Tucci, G.C., Donahue, J.P. & Holm, R.H. (1998) Comparative Kinetics of Oxo Transfer to Substrate Mediated by Bis(dithiolene)dioxomolybdenum and -tungsten Complexes, *Inorg. Chem. 37*, 1602-1608.

171. Sun, Y.-C., Mierzwa, J. & Lan, C.-R. (2000) Direct Determination of Molybdenum in Seawater by Adsorption Cathodic Stripping Square-wave Voltammetry, *Talanta. 52*, 417-421.

172. Ali, A.M.M., Ghandour, M.A., El-Shatoury, S.A. & Ahmed, S.M. (2000) Adsorptive Cathodic Stripping Voltammetric Determination of Molybdenum in Synthetic Solutions and Environmental Samples, *Electroanalysis. 12*, 155-158.

173. Yokoi, K. & Berg, C.M.G. van den. (1992) Simultaneous Determination of Titanium and Molybdenum in Natural Waters by Catalytic Cathodic Stripping Voltammetry, *Anal. Chim. Acta. 257*, 293-299.

174. Hinton, S.M. & Mortenson, L.E. (1985) Identification of Molybdoproteins in *Clostridium pasteurianum*, *J. Bacteriol. 162*, 477-484.

175. Hinton, S.M. & Mortenson, L.E. (1985) Regulation and Order of Involvement of Molybdoproteins During Synthesis of Molybdoenzymes in *Clostridium pasteurianum*, *J. Bacteriol. 162*, 485-493.

176. Pienkos, P.T. & Brill, W.J. (1981) Molybdenum Accumulation and Storage in *Klebsiella pneumoniae* and *Azotobacter vinelandii*, *J. Bacteriol. 145*, 743-751.

177. Müller, A., Suer, W., Pohlmann, C., Schneider, K., Thies, W.-G. & Appel, H. (1997) Comparative *In-vivo* and *In-vitro* ^{99}Mo-time-differential-perturbed-angular-correlation Studies on the Nitrogenase MoFe Protein and on Other Mo Species of Different N_2-fixing Bacteria, *Eur. J. Biochem. 246*, 311-319.

178. Corcuera, G.L., Bastidas, M. & Dubourdieu, M. (1993) Molybdenum Uptake in *Escherichia coli* K12, *J. Gen. Microbiol. 139*, 1869-1875.

179. Erlandsen, H., Fusetti, F., Martinez, A., Flatmark, T. & Stevens, R.C. (1997) Crystal Structure of the Catalytic Domain of Human Phenylalanine Hydroxylase Reveals the Structural Basis for Phenylketonuria, *Nat. Struct. Biol. 4*, 995-1000.

180. Fusetti, F., Erlandsen, H., Flatmark, T. & Stevens, R.C. (1998) Structure of Tetrameric Human Phenylalanine Hydroxylase and its Implications for Phenylketonuria, *J. Biol. Chem. 273*, 16962-16967.

181. Kobe, B., Jennings, I.G., House, C.M., Michell, B.J., Goodwill, K.E., Santarsiero, B.D., Stevens, R.C., Cotton, R.G. & Kemp, B.E. (1999) Structural Basis of Autoregulation of Phenylalanine Hydroxylase, *Nature Struct. Biol. 6*, 442-448.

182. Goodwill, K.E., Sabatier, C., Marks, C., Raag, R., Fitzpatrick, P.F. & Stevens, R.C. (1997) Crystal Structure of Tyrosine Hydroxylase at 2.3 Å and its

Implications for Inherited Neurodegenerative Diseases, *Nature Struct. Biol. 4*, 578-585.

183. Lange, S. & Que, L. Jr. (1998) Oxygen Activating Nonheme Iron Enzymes, *Curr. Opin. Chem. Biol. 2*, 159-172.
184. Que, L. Jr. (2000) One Motif - Many Different Reactions, *Nature Struct. Biol. 7*, 182-184.
185. Goodwill, K.E., Sabatier, C. & Stevens, R.C. (1998) Crystal Structure of Tyrosine Hydroxylase with Bound Cofactor Analogue and Iron at 2.3 Å Resolution: Self-Hydroxylation of Phe300 and the Pterin-Binding Site, *Biochemistry. 37*, 13437-13445.
186. Erlandsen, H., Bjørgo, E., Flatmark, T. & Stevens, R.C. (2000) Crystal Structure and Site-Specific Mutagenesis of Pterin-Bound Human Phenylalanine Hydroxylase, *Biochemistry. 39*, 2208-2217.
187. Teigen, K., Froystein, N.A. & Martínez, A. (1999) The Structural Basis of the Recognition of Phenylalanine and Pterin Cofactors by Phenylalanine Hydroxylase: Implications for the Catalytic Mechanism, *J. Mol. Biol. 294*, 807-823.
188. Dix, T.A. & Benkovic, S.J. (1988) Mechanism of Oxygen Activation by Pteridine-Dependent Monooxygenases, *Acc. Chem. Res. 21*, 101-107.
189. Davis, M.D. & Kaufman, S. (1989) Evidence for the Formation of the 4a-Carbinolamine during the Tyrosine-Dependent Oxidation of Tetrahydrobiopterin by Rat Liver Phenylalanine Hydroxylase, *J. Biol. Chem. 264*, 8585-8596.
190. Fitzpatrick, P.F. (1999) Tetrahydropterin-Dependent Amino Acid Hydroxylases, *Annu. Rev. Biochem. 68*, 355-381.
191. Erlandsen, H., Flatmark, T., Stevens, R.C. & Hough, E. (1998) Crystallographic Analysis of the Human Phenylalanine Hydroxylase Catalytic Domain with Bound Catechol Inhibitors at 2.0 Å Resolution, *Biochemistry. 37*, 15638-15646.
192. Cox, D.D., Benkovic, S.J., Bloom, L.M., Bradley, F.C., Nelson, M.J., Que, L. Jr. & Wallick, D.E. (1988) Catecholate LMCT Bands as Probes for the Active Sites of Nonheme Iron Oxygenases, *J. Am. Chem. Soc. 110*, 2026-2032.
193. Andersson, K.K., Cox, D.D., Que, L. Jr., Flatmark, T. & Haavik, J. (1988) Resonance Raman Studies on the Blue-Green-Colored Bovine Adrenal

Tyrosine 3-Monooxygenase (Tyrosine Hydroxylase). Evidence that the Feedback Inhibitors Adrenaline and Noradrenaline are Coordinated to Iron, *J. Biol. Chem. 263*, 18621-18626.

194. Flatmark, T. & Stevens, R.C. (1999) Structural Insight into the Aromatic Amino Acid Hydroxylases and Their Disease-Related Mutant Forms, *Chem. Rev. 99*, 2137-2160.
195. Wallick, D.E., Bloom, L.M., Gaffney, B.J. & Benkovic, S.J. (1984) Reductive Activation of Phenylalanine Hydroxylase and its Effect on the Redox State of the Non-Heme Iron, *Biochemistry. 23*, 1295-1302.
196. Bloom, L.M., Benkovic, S.J. & Gaffney, B.J. (1986) Characterization of Phenylalanine Hydroxylase, *Biochemistry. 25*, 4204-4210.
197. Martínez, A., Andersson, K.K., Haavik, J. & Flatmark, T. (1991) EPR and ^{1}H-NMR Spectroscopic Studies on the Paramagnetic Iron at the Active Site of Phenylalanine Hydroxylase and its Interaction with Substrates and Inhibitors, *Eur. J. Biochem. 198*, 675-682.
198. Kappock, T.J., Harkins, P.C., Friedenberg, S. & Caradonna, J.P. (1995) Spectroscopic and Kinetic Properties of Unphosphorylated Rat Hepatic Phenylalanine Hydroxylase Expressed in *Escherichia coli*. Comparison of Resting and Activated States, *J. Biol. Chem. 270*, 30532-30544.
199. Marota, J.J. & Shiman, R. (1984) Stoichiometric Reduction of Phenylalanine Hydroxylase by its Cofactor: a Requirement for Enzymatic Activity, *Biochemistry. 23*, 1303-1311.
200. Francisco, W.A., Tian, G., Fitzpatrick, P.F. & Klinman, J.P. (1998) Oxygen-18 Kinetic Isotope Effect Studies of the Tyrosine Hydroxylase Reaction: Evidence of Rate Limiting Oxygen Activation, *J. Am. Chem. Soc. 120*, 4057-4062.
201. Shiman, R., Gray, D.W. & Hill, M.A. (1994) Regulation of Rat Liver Phenylalanine Hydroxylase. I. Kinetic Properties of the Enzyme's Iron and Enzyme Reduction Site, *J. Biol. Chem. 269*, 24637-24646.
202. Kaufman, S. (1993) The Phenylalanine Hydroxylating System, *Adv. Enzymol. Relat. Areas Mol. Biol. 67*, 77-264.
203. Andersson, K.K., Haavik, J., Martínez, A., Flatmark, T. & Petersson, L. (1989) Evidence from EPR Spectroscopy that Phosphorylation of Ser-40 in

Bovine Adrenal Tyrosine-Hydroxylase Facilitates the Reduction of High-Spin Fe(III) Under Turnover Conditions, *FEBS Lett. 258*, 9-12.

204. Haavik, J., Martínez, A. & Flatmark, T. (1990) pH-Dependent Release of Catecholamines from Tyrosine Hydroxylase and the Effect of Phosphorylation of Ser-40, *FEBS Lett. 262*, 363-365.
205. Kumer, S.C. & Vrana, K.E. (1996) Intricate Regulation of Tyrosine Hydroxylase Activity and Gene Expression, *J. Neurochem. 67*, 443-462.
206. Martínez, A., Haavik, J., Flatmark, T., Arrondo, J.L.R. & Muga, A. (1996) Conformational Properties and Stability of Tyrosine Hydroxylase Studied by Infrared Spectroscopy. Effect of Iron/Catecholamine Binding and Phosphorylation, *J. Biol. Chem. 271*, 19737-19742.
207. Flatmark, T., Almås, B., Knappskog, P.M., Berge, S.V., Svebak, R.M., Chehin, R., Muga, A. & Martínez, A. (1999) Tyrosine Hydroxylases Binds Tetrahydrobiopterin Cofactor with Negative Cooperativity, as Shown by Kinetic Analyses and Surface Plasmon Resonance Detection, *Eur. J. Biochem. 262*, 840-849.
208. Martínez, A., Knappskog, P.M., Olafsdottir, S., Døskeland, A.P., Eiken, H.G., Svebak, R.M., Bozzini, M., Apold, J. & Flatmark, T. (1995) Expression of Recombinant Human Phenylalanine Hydroxylase as Fusion Protein in *Escherichia coli* Circumvents Proteolytic Degradation by Host Cell Proteases. Isolation and Characterization of the Wild-Type Enzyme, *Biochem. J. 306*, 589-597.
209. Knappskog, P.M., Flatmark, T., Aarden, J.M., Haavik, J. & Martínez, A. (1996) Structure/Function Relationships in Human Phenylalanine Hydroxylase. Effect of Terminal Deletions on the Oligomerization, Activation and Cooperativity of Substrate Binding to the Enzyme, *Eur. J. Biochem. 242*, 813-821.
210. Aasa, R. & Vänngård, T. (1975) EPR Signal Intensity and Powder Shapes. A Reexamination., *J. Magn. Reson. 19*, 308-315.
211. Gottschall, D.W., Dietrich, R.F., Benkovic, S.J. & Shiman, R. (1982) Phenylalanine Hydroxylase. Correlation of the Iron Content with Activity and the Preparation and Reconstitution of the Apoenzyme, *J. Biol. Chem. 257*, 845-849.

212. Citron, B.A., Davis, M.D. & Kaufman, S. (1992) Purification and Biochemical Characterization of Recombinant Rat Liver Phenylalanine Hydroxylase Produced in *Escherichia coli*, *Protein Expression Purif. 3*, 93-100.

213. Michaud-Soret, I., Andersson, K.K., Que, L. Jr. & Haavik, J. (1995) Resonance Raman Studies of Catecholate and Phenolate Complexes of Recombinant Human Tyrosine Hydroxylase, *Biochemistry. 34*, 5504-5510.

214. Presta, A., Weber-Main, A.M., Stankovich, M.T. & Stuehr, D.J. (1998) Comparative Effects of Substrates and Pterin Cofactor on the Heme Midpoint Potential in Inducible and Neuronal Nitric Oxide Synthases, *J. Am. Chem. Soc. 120*, 9460-9465.

215. Parniak, M.A. & Kaufman, S. (1981) Rat Liver Phenylalanine Hydroxylase. Activation by Sulfhydryl Modification, *J. Biol. Chem. 256*, 6876-6882.

216. Phillips, R.S., Parniak, M.A. & Kaufman, S. (1984) The Interaction of Aromatic Amino Acids with Rat Liver Phenylalanine Hydroxylase, *J. Biol. Chem. 259*, 271-277.

217. Martínez, A., Haavik, J. & Flatmark, T. (1990) Cooperative Homotropic Interaction of L-Noradrenaline with the Catalytic Site of Phenylalanine 4-Monooxygenase, *Eur. J. Biochem. 193*, 211-219.

218. Archer, M.C. & Scrimgeour, K.G. (1970) Reduction Potentials of Tetrahydropterins, *Can. J. Biochem. 48*, 526-527.

219. Archer, M.C., Vonderschmitt, D.J. & Scrimgeour, K.G. (1972) Mechanism of Oxidation of Tetrahydropterins, *Can. J. Biochem. 50*, 1174-1182.

220. Martínez, A., Olafsdottir, S. & Flatmark, T. (1993) The Cooperative Binding of Phenylalanine to Phenylalanine 4-Monooxygenase Studied by ^{1}H-NMR Paramagnetic Relaxation. Changes in Water Accessibility to the Iron at the Active Site Upon Substrate Binding, *Eur. J. Biochem. 211*, 259-266.

221. Olafsdottir, S. & Martínez, A. (1999) The Accessibility of Iron at the Active Site of Recombinant Human Phenylalanine Hydroxylase to Water as Studied by ^{1}H NMR Paramagnetic Relaxation. Effect of L-Phe and Comparison with the Rat Enzyme, *J. Biol. Chem. 274*, 6280-6284.

222. Bublitz, C. (1971) Two Mechanisms for the Inhibition In Vitro of Phenylalanine Hydroxylase by Catecholamines, *Biochem. Pharmacol. 20*, 2543-2553.

223. Haavik, J., Martínez, A., Olafsdottir, S., Mallet, J. & Flatmark, T. (1992) The Incorporation of Divalent Metal Ions into Recombinant Human Tyrosine Hydroxylase Apoenzymes Studied by Intrinsic Fluorescence and ^{1}H-NMR Spectroscopy, *Eur. J. Biochem. 210*, 23-31.

224. Ramsey, A.J. & Fitzpatrick, P.F. (1998) Effects of Phosphorylation of Serine 40 of Tyrosine Hydroxylase on Binding of Catecholamines: Evidence for a Novel Regulatory Mechanism, *Biochemistry. 37*, 8980-8986.

225. Ellis, H.R., Daubner, S.C. & Fitzpatrick, P.F. (2000) Mutation of Serine 395 of Tyrosine Hydroxylase Decouples Oxygen-Oxygen Bond Cleavage and Tyrosine Hydroxylation, *Biochemistry. 39*, 4174-4181.

226. Bailey, S.W. & Ayling, J.E. (1983) 6,6-Dimethylpterins: Stable Quinoid Dihydropterin Substrate for Dihydropteridine Reductase and Tetrahydropterin Cofactor for Phenylalanine Hydroxylase, *Biochemistry. 22*, 1790-1798.

227. Shiman, R., Xia, T., Hill, M.A. & Gray, D.W. (1994) Regulation of Rat Liver Phenylalanine Hydroxylase. II. Substrate Binding and the Role of Activation in the Control of Enzymatic Activity, *J. Biol. Chem. 269*, 24647-24656.

228. Døskeland, A.P., Døskeland, S.O., Øgreid, D. & Flatmark, T. (1984) The Effect of Ligands of Phenylaline 4-monooxygenase on the cAMP-Dependent Phosphorylation of the Enzyme, *J. Biol. Chem. 259*, 11242-11248.

229. Kemsley, J.N., Mitic, N., Zaleski, K.L., Caradonna, J.P. & Solomon, E.I. (1999) Circular Dichroism and Magnetic Circular Dichroism Spectroscopy of the Catalytically Competent Ferrous Active Site of Phenylalanine Hydroxylase and Its Interaction with Pterin Cofactor, *J. Am. Chem. Soc. 121*, 1528-1536.

230. Noble, M.A., Munro, A.W., Rivers, S.L., Robledo, L., Daff, S.N., Yellowlees, L.J., Shimizu, T., Sagami, I., Guillemette, J.G. & Chapman, S.K. (1999) Potentiometric Analysis of the Flavin Cofactors of Neuronal Nitric Oxide Synthase, *Biochemistry. 38*, 16413-16418.

231. Ehrenberg, A., Hemmerich, P., Muller, F. & Pfleiderer, W. (1970) Electron Spin Resonance of Pteridine Radicals and the Structure of Hydropteridines, *Eur. J. Biochem. 16*, 584-591.

232. Hurshman, A.R., Krebs, C., Edmondson, D.E., Huynh, B.H. & Marletta, M.A. (1999) Formation of a Pterin Radical in the Reaction of the Heme Domain of Inducible Nitric Oxide Synthase with Oxygen, *Biochemistry. 38*, 15689-15696.

233. Schmidt, P.P., Lange, R., Gorren, A.C.F., Werner, E.R., Mayer, B. & Andersson, K.K. (2001) Formation of a Protonated Trihydrobiopterin Radical Cation in the First Reaction Cycle of Neuronal and Endothelial Nitric Oxide Synthase Detected by Electron Paramagnetic Resonance Spectroscopy, *J. Biol. Inorg. Chem. 6*, 151-158.

234. Rikken, G.B., Kroon, A.G.M. & Ginkel, C.G. van. (1996) Transformation of (Per)Chlorate into Chloride by a Newly Isolated Bacterium: Reduction and Dismutation, *Appl. Microbiol. Biotechnol. 45*, 420-426.

235. Kengen, S.W.M., Rikken, G.B., Hagen, W.R., Ginkel, C.G. van & Stams, A.J.M. (1999) Purification and Characterization of (Per)Chlorate Reductase from the Chlorate-Respiring Strain GR-1, *J. Bacteriol. 181*, 6706-6711.

236. Schempp, H., Reim, M. & Dornisch, K. (2001) Chlorite-hemoprotein Interaction as Key Role for the Pharmacological Activity of the Chlorite-based Drug WF10, *Arzneimittelforschung. 51*, 554-562.

237. Hagen, W. R. (1992) EPR Spectroscopy of Iron-sulfur Proteins, *Adv. Inorg. Chem. 38*, 165-222.

238. Giulivi, C. & Cadenas, E. (1998) Heme Protein Radicals: Formation, Fate, and Biological Consequences, *Free Radic. Biol. Med. 24*, 269-279.

239. Craven, P.A., DeRubertis, F.R. & Pratt, D.W. (1979) Electron Spin Resonance Study of the Role of Nitric Oxide. Catalase in the Activation of Guanylate Cyclase by Sodium Azide and Hydroxylamine. Modulation of Enzyme Responses by Heme Proteins and Their Nitrosyl Derivatives., *J. Biol. Chem. 254*, 8213-8222.

240. Zhao, Y., Hoganson, C., Babcock, G.T. & Marletta, M.A. (1998) Structural Changes in the Heme Proximal Pocket Induced by Nitric Oxide Binding to Soluble Guanylate Cyclase, *Biochemistry. 37*, 12458-12464.

241. Ascenzi, P., Coletta, M., Desideri, A. & Brunori, M. (1985) pH-induced Cleavage of the Proximal Histidine to Iron Bond in the Nitric Oxide Derivative of Ferrous Monomeric Hemoproteins and of the "Chelated" Protoheme Model Compound, *Biochim. Biophys. Acta. 829*, 299-302.

242. Taylor, C.P.S. (1977) The EPR of Low Spin Heme Complexes. Relation of the t_{2g} Hole Model to the Directional Properties of the g Tensor, and a New Method for Calculating the Ligand Field Parameters, *Biochim. Biophys. Acta. 491*, 137-149.

243. Blumberg, W.E., Peisach, J., Wittenberg, B.A. & Wittenberg, J.B. (1968) The Electron Structure of Protoheme Proteins. I. An Electron Paramagnetic Resonance and Optical Study of Horseradish Peroxidase and Its Derivatives, *J. Biol. Chem. 243*, 1854-1862.

244. Wittenberg, B.A., Kampa, L., Wittenberg, J.B., Blumberg, W.E. & Peisach, J. (1968) The Electron Structure of Protoheme Proteins. II. An Electron Paramagnetic Resonance and Optical Study of Cytochrome c Peroxidase and Its Derivatives, *J. Biol. Chem. 243*, 1863-1870.

245. Blumberg, W.E. & Peisach, J. (1971) A Unified Theory for Low Spin Forms of All Ferric Heme Proteins as Studied by EPR in *Probes of Structure and Function of Macromolecules and Membranes* (Chance, B., Yanetani, T. & Mildvan, A. S., eds) pp. 215-229, Academic Press, New York.

246. Berzofsky, J.A., Peisach, J. & Blumberg, W.E. (1971) Sulfheme Proteins. I. Optical and Magnetic Properties of Sulfmyoglobin and its Derivatives, *J. Biol. Chem. 246*, 3367-3377.

247. Antonini, E. & Brunori, M. (1971) Hemoglobin and Myoglobin in their Reactions with Ligands in *Frontiers of Biology* (Neuberger, A. & Tatum, E. L., eds) pp. 445, North-Holland Publishing Co., Amsterdam.

248. Stone, J.R. & Marletta, M.A. (1994) Soluble Guanylate Cyclase from Bovine Lung: Activation with Nitric Oxide and Carbonmonoxide and Spectral Characterization of the Ferrous and Ferric States, *Biochemistry. 33*, 5636-5640.

249. Decatur, S.M., Franzen, S., DePillis, G.D., Dyer, R.B., Woodruff, W.H. & Boxer, S.G. (1996) *Trans* Effects in Nitric Oxide Binding to Myoglobin Cavity Mutant H93G, *Biochemistry. 35*, 4939-4944.

250. Koesling, D. (1999) Studying the Structure and Regulation of Soluble Guanylyl Cyclase, *Methods. 19*, 485-493.

251. Banci, L., Bertini, I., Turano, P., Tien, M. & Kirk, T.K. (1991) Proton NMR Investigation into the Basis for the Relatively High Redox Potential of Lignin Peroxidase, *Proc. Natl. Acad. Sci. USA. 88*, 6956-6960.

252. Behere, D.V. & Shedbalkar, V.P. (1987) Oxidation of Metmyoglobin by Chlorite ion: a Spectrophotometric Study, *Indian. J. Biochem. Biophys. 24*, 244-247.

Summary

Important chemical reactions in the metabolic pathways of living organisms involve redox reactions. Frequently transitions metals are used in enzymes to perform redox catalysis. This thesis reports studies on a set of proteins and enzymes containing iron and/or tungsten as redox catalysts or electron carriers: the [4Fe-4S] containing ferredoxin, $Fe(Cys)_4$ containing rubredoxin , the [4Fe-4S] and tungsten containing glyceraldehyde-3-phosphate oxidoreductase, the tungsten containing DMSO reductase, the non-heme iron containing human phenylalanine hydroxylase, and the heme iron containing chlorite dismutase.

The redox properties of the hyperthermophilic electron-transfer proteins ferredoxin and rubredoxin have been studied with EPR monitored redox titrations and direct voltammetry (chapter 2). The midpoint potentials (E_m) of the proteins, determined with direct voltammetry, are independent of the pH and show a regular (linear) temperature dependent decrease of approximately 1 mV/ºC. Previous reports of unusual dependencies on temperature and pH of these proteins have been falsified. EPR monitoring is not a reliable method to determine the temperature dependence of the E_m: upon rapid freezing the proteins take their conformation corresponding to the freezing point of the solution.

The tungsten and [4Fe-4S] cluster containing enzyme glyceraldehyde-3-phosphate oxidoreductase (GAPOR) from *Pyrococcus furiosus* has been studied in EPR monitored redox titrations (chapter 3), steady-state kinetics, and EXAFS spectroscopy (chapter 4). Two different W^V signals have been found with EPR spectroscopy. $W^V{}_1$ is an intermediate species in the catalytic cycle, with $E_m(W^{VI/V})$ = -507 mV and $E_m(W^{V/IV})$ = -491 mV. $W^V{}_2$ represents an inactivated species with E_m $(W^{VI/V})$= -326 mV. The $[4Fe\text{-}4S]^+$ cluster exhibits a mixture of S=3/2 and an unusual S=1/2 signal with the same midpoint potential: E_m = -335 mV. The electron-transfer chain from glyceraldehyde-3-phosphate (GAP) to ferredoxin via GAPOR has been reconstituted in vitro as shown by cyclic voltammetry. GAPOR catalyzes the oxidation of D-GAP to D-3-phosphoglycerate. L-GAP is neither a substrate nor an inhibitor for the enzyme. The activity of the enzyme is partially inhibited by the substrate GAP. This inhibition is affected by the concentration of benzyl viologen and the ionic strength of the solution. At 1 M NaCl GAPOR shows uninhibited Michaelis-Menten kinetics. The activity is furthermore strongly dependent on pH, with optimal

activity at pH 9. A primary deuterium isotope effect of the substrate formaldehyde on the activity of the tungsten containing formaldehyde oxidoreductase is the first experimental evidence for a hydride abstraction as part of the reaction mechanism of the tungsten containing aldehyde oxidoreductases. Tungsten L(III)-edge EXAFS of GAPOR poised at potentials expected to give W^{VI} and W^{IV} showed structural changes upon reduction of the tungsten center. The tungsten center is coordinated by all four pterin-dithiolene sulfurs.

The tungsten substituted molybdenum enzyme DMSO reductase retains activity and structure and offers the opportunity to compare tungsten and molybdenum redox properties in the same enzyme. The midpoint potentials of the tungsten center have been determined with EPR monitored redox titrations. At pH 7.0 $E_m(W^{VI/V})$ = -194 mV and $E_m(W^{V/IV})$ = -134 mV, which are ca. 335 mV lower than the corresponding couples of the molybdenum enzyme. This E_m difference is in accordance with the incapability of the tungsten enzyme to perform the back-reaction, i.e. oxidation of DMS (chapter 5). Maximal W^V EPR signals were observed at pH 5 and decreased at higher pH. The W^V EPR spectrum shows a pH dependent mixture of two species: one with and one without superhyperfine coupling to a nearby proton.

For the study of tungsten and molybdenum in proteins, a sensitive and accurate determination of these metals is important. An electroanalytical technique can be used to determine the tungsten and molybdenum content of 1-10 μg of pure proteins simultaneously with little or no sample handling (chapter 6). More crude protein samples require precipitation of interfering surface active materials with 10% perchloric acid. A tungsten screening of the soluble proteins from *Pyrococcus furiosus* resulted in the recovery of the three known tungsten containing enzymes.

The EPR and redox properties of the non-heme iron containing recombinant human phenylalanine hydroxylase have been studied for effects of the substrate (L-Phe), a cofactor analog (BH_2) and an inhibitor (dopamine) (chapter 7). An E_m = +207 mV is found for the native iron center, wich is close to the redox potential of the cofactor. Addition of ligands results in a decrease of the E_m by approximately 100 mV for L-Phe and BH_2 and 200 mV for dopamine. Redox dependent changes of binding affinities of these ligands have been calculated using these E_m changes. The E_m value of the enzyme with both L-Phe and BH_2, which is an inactive model of the iron environment under turnover conditions, resulted in a value close to that of the native enzyme.

The heme containing enzyme chlorite dismutase from the (per)chlorate respiring bacterial strian GR-1 has been spectroscopically characterized (chapter 8). Spectroscopic properties of the ferrous enzyme and ferric OH^- and imidazole adducts are indicative of an axial histidine ligand to the iron center. Binding of NO to ferrous chlorite dismutase results in loss of the axial His-Fe bond resulting in the formation of a five-coordinate heme iron nitrosyl species. The E_m of chlorite dismutase is -23 mV, which is high for a heme enzyme. The redox and spectroscopic properties of chlorite dismutase show more similarities with gas-sensing hemoproteins, such as guanylate cyclase and globins, than with the heme enzymes.

The study of a set of metalloproteins containing iron and tungsten has provided biocatalytic links between "organic" (i.e. electron pair) and "inorganic" (i.e. single electron) redox chemistry. Tungsten and molybdenum are metals that can perform one and two electron redox reactions. In our working model for the catalysis of the tungsten containing aldehyde oxidoreductases, the tungsten center catalyzes the oxo-transfer (two electron step) to the aldehyde and is regenerated in two one-electron steps. Tungsten and molybdenum can use organic substrates (two electron reactions) and iron containing redox partners (one electron reactions), such as ferredoxin . Iron can serve, apart from one-electron transfer reactions (ferredoxin and rubredoxin), to perform redox reactions with more electrons as well. This can be done, e.g., by stabilizing high valence states of iron with a heme cofactor (chlorite dismutase), or by using a separate organic cofactor like tetrahydrobiopterin (phenylalanine hydroxylase).

Samenvatting

Belangrijke chemische reacties in de metabole routes van levende organismen zijn dikwijls redoxreacties. Overgangsmetalen worden vaak gebruikt in enzymen als redoxkatalysatoren. Dit proefschrift handelt over een reeks eiwitten en enzymen die ijzer en/of wolfraam bevatten als redoxkatalysator of voor electronentransport namelijk het [4Fe-4S] bevattende ferredoxine, het $Fe(Cys)_4$ bevattende rubredoxine, het [4Fe-4S] en wolfraam bevattende glyceraldehyde-3-fosfaat oxidoreductase, het wolfraam bevattende DMSO reductase, het niet-heem ijzer bevattende humane fenylalanine hydroxylase, en het heem ijzer bevattende chloriet dismutase uit het bacteriele isolaat GR-1.

De redoxeigenschappen van de hyperthermofiele electronentransport eiwitten ferredoxine en rubredoxine zijn bestudeerd met behulp van EPR gevolgde redoxtitraties en directe voltammetrie (hoofdstuk 2). De midpuntspotentialen (E_m) van de eiwitten, bepaald met directe voltammetrie, zijn pH onafhankelijk en vertonen een normale (lineaire) temperatuurafhankelijke afname van ongeveer 1 mV/°C. EPR monitoring is geen betrouwbare methode om de temperatuurafhankelijkheid van de E_m te bepalen: bij snel invriezen neemt het eiwit een conformatie aan welke overeenkomt met het vriespunt van de oplossing.

Het wolfraam en [4Fe-4S] cluster bevattende enzym glyceraldehyde-3-fosfaat oxidoreductase (GAPOR) uit *Pyrococcus furiosus* is bestudeerd met EPR gevolgde redoxtitraties (hoofdstuk 3), evenwichtstoestand-kinetiek en EXAFS spectroscopie (hoofdstuk 4). Twee verschillende W^V signalen zijn gevonden. W^V_1 is een tussenproduct in de katalysche cyclus, met $E_m(W^{VI/V}) = -507$ mV en $E_m(W^{V/IV}) = -491$ mV. W^V_2 vertegenwoordigt een inactieve vorm met E_m $(W^{VI/V}) = -326$ mV. Het $[4Fe\text{-}4S]^+$ cluster vertoont een S=3/2 en een ongebruikelijk S=1/2 signal met de gemeenschappelijke midpuntspotentiaal: $E_m = -335$ mV. De electronentransportketen van glyceraldehyde-3-fosfaat (GAP) naar ferredoxine via GAPOR is gereconstitueerd in vitro zoals aangetoond met cyclische voltammetry. GAPOR katalyseerd de oxidatie van D-GAP naar D-3-fosfoglyceraat. L-GAP is geen substraat of inhibitor voor the enzym. GAPOR activiteit is gedeeltelijk geinhibeerd door het substraat glyceraldehyde-3-fosfaat. Deze inhibitie wordt beinvloed door de concentratie van het tweede substraat (benzyl viologeen) en de ionsterkte van de oplossing. Bij 1 M NaCl vertoont GAPOR ongeinhibeerde Michaelis-Menten kinetiek. De activiteit van

GAPOR is sterk pH afhankelijk met optimale activiteit bij pH 9. Een primair deuterium isotoopeffect van het substraat formaldehyde op de activiteit van het wolfraam bevattende formaldehyde oxidoreductase is het eerste experimentele bewijs voor een hydride abstractie als onderdeel van het reactiemechanisme van wolfraam bevattende aldehyde oxidoreductases. Wolfraam L(III)-edge EXAFS van GAPOR, op potentialen gesteld waarbij het wolfraam W^{VI} en W^{IV} is, toont structurele veranderingen aan als gevolg van de reductie van het wolfraamcentrum. Het wolfraamcentrum wordt door alle vier de pterine-dithioleen zwavels gecoördineerd.

Het wolfraam gesubstitueerde molybdeenenzym DMSO reductase behoudt zijn activiteit en structuur en biedt de mogelijkheid om de redoxeigenschappen van wolfraam en molybdeen in hetzelfde enzym te vergelijken. De midpuntspotentialen van het wolfraamcentrum zijn bepaald met behulp van EPR gevolgde redoxtitraties (chapter 5). Bij pH 7.0 $E_m(W^{VI/V})$ = -194 mV en $E_m(W^{V/IV})$ = -134 mV, en deze waarden zijn ca. 335 mV lager dan de overeenkomstige koppels van het molybdeenenzym. Dit E_m verschil klopt met het feit dat het wolfraamenzym niet in staat is de teruggaande reactie, de oxidatie van DMS, te katalyseren. Maximale W^V EPR signalen worden gevonden bij pH 5 en nemen af met toenemende pH. Het W^V EPR spectrum vertoont een pH afhankelijk mengsel van twee vormen: één met en één zonder superhyperfijnkoppeling met een nabijgelegen proton.

Voor het bestuderen van wolfraam en molybdeen in eiwitten is een gevoelige en nauwkeurige bepaling van deze metalen belangrijk. Een elektroanalytische techniek kan gebruikt worden om de wolfraam- en molybdeengehaltes van 1-10 μg van zuivere eiwitten tegelijkertijd te bepalen met geen of weinig monstervoorbewerking (hoofdstuk 6). Minder zuivere eiwitmonsters hebben precipitatie van interfererende oppervlakteactieve stoffen met 10% perchloorzuur nodig. Een screening van de oplosbare eiwitten uit *Pyrococcus furiosus* resulteert in het terugvinden van de drie al bekende wolfraam bevattende enzymen.

De EPR- en redoxeigenschappen van het non-heem ijzer bevattende recombinante humane fenylalanine hydroxylase zijn bestudeerd voor effecten van het substraat (L-Phe), een cofactor analoog (BH2) en een remmer (dopamine) (hoofdstuk7). Een E_m = +207 mV is gevonden voor het natieve ijzercentrum, wat dicht bij de redoxpotentiaal van de cofactor ligt. Toevoeging van liganden resulteert in een daling van de E_m met ongeveer 100 mV voor L-Phe en BH_2 en 200 mV voor dopamine. Redoxafhankelijke veranderingen in bindingsaffiniteiten van deze liganden

zijn berekend uitgaande van deze E_m-veranderingen. De E_m-waarde van het enzym met zowel L-Phe als BH_2, dat een inactief model voor de ijzer omgeving bij turnover condities is, ligt dichtbij de waarde van het natieve enzym.

Het heem bevattende chloriet dismutase uit de (per)chloraat respirerende bacteriële stam GR-1 is spectroscopisch gekarakteriseerd (chapter 8). De spectroscopische eigenschappen van het ferro-enzym en de ferri OH- en imidazool adducten zijn indicatief voor een axiaal histidine ligand van het ijzer centrum. Binding van NO aan ferro chloriet dismutase verbreekt de His-Fe binding met een vijf-gecoördineerde heem ijzer nitrosyl als product. De E_m van chloriet dismutase is -23 mV, hetgeen hoog is voor een heem enzym. De redox- en spectroscopische eigenschappen van chloriet dismutase vertonen meer overeenkomst met gas-voelende heemeiwitten, zoals guanylaat cyclase en de globines, dan met de heemenzymen.

De studie van een set van metalloeiwitten die ijzer en wolfraam bevatten heeft biokatalytische links tussen “organische” (d.w.z. electron paar) en “anorganische” (d.w.z. één electron) redoxchemie opgeleverd. Wolfraam en molybdeen zijn metalen die zowel één als twee-electron redoxreacties kunnen uitvoeren. In ons werkmodel voor de katalyse van de wolfraam bevattende aldehyde oxidoreductases, katalyseert het wolfraam centrum de oxo-overdracht naar het aldehyde en wordt het geregenereerd in twee één-electron stappen. Wolfraam en molybdeen kunnen dus organische substraten (twee-electron stap) en ijzer bevattende redoxpartners (één-electron stap), zoals ferredoxine, gebruiken. IJzer kan, naast één-electron overdracht (ferredoxine en rubredoxine), ook dienen voor redoxreacties met meer electronen. Dit kan door, bijvoorbeeld, de hoge valentietoestanden van ijzer te stabiliseren met de heem-cofactor (chlorite dismutase), of door additionele organische cofactoren te gebruiken, zoals tetrahydrobiopterin (phenylalanine hydroxylase).

Curriculum Vitae

Peter-Leon Hagedoorn werd geboren op 10 januari 1975 te Amersfoort. Hij behaalde in juni 1993 zijn VWO diploma aan de Scholengemeenschap Buys Ballot (tegenwoordig Cambium) te Zaltbommel. In september 1993 begon hij met de studie Moleculaire Wetenschappen aan de Landbouwuniversiteit Wageningen (tegenwoordig Wageningen Universiteit). Voor het behalen van het doctoraalexamen werden afstudeerprojecten uitgevoerd bij de leerstoelgroepen Bio-Anorganische Chemie (Prof. W.R. Hagen) en Moleculaire Fysica (Dr. M. Hemminga en Dr.Ir. I. van den Dries). Een buitenlandse stage werd gelopen op het Chemistry Department van The University of Georgia Athens in de Verenigde Staten (Prof. M.K. Johnson). In 1998 studeerde hij cum laude af. In hetzelfde jaar begon hij als onderzoeker in opleiding aan een promotieonderzoek bij de leerstoelgroep Bio-Anorganische Chemie (Prof. W.R. Hagen) te Wageningen. In 2000 verhuisde hij met zijn promoter naar het Kluyver Laboratorium voor Biotechnologie van de Technische Universiteit Delft, alwaar hij het project voortzette. Na zijn promotie zal hij in 2002 als post-doc blijven werken in het Kluyver Laboratorium

.

List of abbreviations

3PG	3-phosphoglycerate
6-MPH_4	6-methyl-5,6,7,8-tetrahydropterin
AdSV	adsorptive stripping voltammetry
AH	acetylene hydratase
AOR	aldehyde oxidoreductase
BH_2	L-erythro-7,8-dihydrobiopterin
BH_4	(6R)-L-erythro-5,6,7,8-tetrahydrobiopterin
BSA	bovine serum albumine
DMS	dimethylsulfide
DMSO	dimethylsulfoxide
DMSOR	dimethylsulfoxide reductase
DTT	dithiothreitol
E_m	midpoint potential
EPR	electron paramagnetic resonance
EXAFS	enhanced X-ray absorption fine structure
Fd	ferredoxin
FDH	formate dehydrogenase
FMDH	formylmethanofuran dehydrogenase
FNOR	ferredoxin:$NAD(P)^+$ oxidoreductase
FOR	formaldehyde oxidoreductase
GAP	glyceraldehyde-3-phosphate
GAPDH	glyceraldehyde-3-phosphate dehydrogenase
GAPOR	glyceraldehyde-3-phosphate oxidoreductase
H_2ase	hydrogenase
HMDE	hanging mercury drop electrode
hPAH(Gly^{103}-Gln^{428})	N- and C-terminal truncated form of human phenylalanine hydroxylase, i.e. ΔN102/ΔC24-hPAH
HVOR	(2R)-hydroxycarboxylate:viologen oxidoreductase
ICP-AES	inductively coupled plasma atomic emission spectroscopy
ICP-MS	inductively coupled plasma mass spectrometry
IOR	indolepyruvate oxidoreductase

KGOR	2-ketoglutarate oxidoreductase
MGD-PTE	guanine dinucleotide bis-pterin cofactor
MPT	molybdopterin cofactor
NHE	normal hydrogen electrode
OD	optical density
P½	microwave power at 50% saturation of the EPR signal
PAH	phenylalanine hydroxylase
PGK	phosphoglycerate kinase
PKU	phenylketonuria
POR	pyruvate oxidoreductase
PTE	bis-pterin cofactor
TH	tyrosine hydroxylase
TMAO	trimethylamine-N-oxide
VOR	2-ketoisovalerate oxidoreductase
WOR	tungsten containing oxidoreductase
wt-hPAH	recombinant human wild-type phenylalanine hydroxylase
XAS	X-ray absorption spectroscopy

List of publications

1 Hasan, M.N., **Hagedoorn, P.L.**, Hagen, W.R., *Pyrococcus furiosus* ferredoxin is a functional dimer, *submitted.*

2 De Bok, F.A.M., **Hagedoorn, P.L**., Silva, P.J., Hagen, W.R., Schiltz, E., Stams, A.J.M., Two W-containing formate dehydrogenases (CO_2-reductases) involved in syntrophic propionate oxidation by *Synthophobacter fumaroxidans*, *submitted*.

3 De Bok, F.A.M., Silva, P.J., **Hagedoorn, P.L.**, Hagen, W.R., Schiltz, W., Stams, A.J.M., Isolation and characterization of a NiFe Hydrogenase from the syntrophic propionate oxidizing bacterium *Syntrophobacter fumaroxidans*, *submitted*.

4 **Hagedoorn, P.L.**, De Geus, D.C., Hagen, W.R., Spectroscopic characterization and ligand binding properties of chlorite dismutase from the chlorate respiring bacterial strain GR-1 (2002) *Eur. J. Biochem. in press*.

5 Clay, M.D., Jenney, F.E. Jr., Noh, H., **Hagedoorn, P.L.**, Adams, M.W.W., Johnson, M.K., Resonance Raman characterization of the mononuclear iron active-site vibrations and putative electron transport pathways in *Pyrococcus furiosus* superoxide reductase (2002) *Biochemistry 41*, 9833-9841.

6 Clay, M.D., Jenney, F.E. Jr., **Hagedoorn, P.L**., George, G.N., Adams, M.W.W., Johnson, M.K., Spectroscopic studies of *Pyrococcus furiosus* superoxide reductase: implications for active site structures and the catalytic mechanism (2002) *J. Am. Chem. Soc. 124*, 788-805.

7 J.L. Primus, S. Grunenwald, **P.L. Hagedoorn**, A.M. Albrecht-Gary, D. Mandon, C. Veeger, The nature of the intermediates in the reactions of Fe(III)- and Mn(III)-microperoxidase-8 with H_2O_2; a rapid kinetics study (2002) *J. Am. Chem. Soc. 124*,1214-1221.

8 **Hagedoorn, P.L.**, Van 't Slot, P., Van Leeuwen, H.P., Hagen, W.R., Electroanalytical determination of tungsten and molybdenum in proteins (2001) *Analytical Biochemistry 297*, 71-78.

9 **Hagedoorn, P.L.**, Schmidt, P.P., Andersson, K.K., Hagen, W.R., Flatmark, T., Martínez, A., The effect of substrate, dihydrobiopterin and dopamine in the EPR spectroscopic properties and the redox potential of the non-heme iron in recombinant human phenylalanine hydroxylase (2001) *J. Biol. Chem. 276*, 22850-22856.

10 Hagen WR, Silva PJ, Amorim MA, **Hagedoorn P.L.**, Wassink H, Haaker H, Robb FT, Novel structure and redox chemistry of the prostethic groups of the iron-sulfur flavoprotein sulfide dehydrogenase from *Pyrococcus furiosus*; evidence for a [2Fe-2S] cluster with $Asp(Cys)_3$ ligands (2000) *J. Biol. Inorg. Chem. 5*, 527-534.

11 **Hagedoorn, P.L.**, Freije, J.R.,Hagen, W.R., *Pyrococcus furiosus* glyceraldehyde-3-phosphate oxidoreductase has comparable $W^{6+/5+}$ and $W^{5+/4+}$ reduction potentials and unusual [4Fe-4S] EPR properties (1999) *FEBS Lett. 462*, 66-70.

12 **Hagedoorn, P.L.**, Driessen, M.C.P.F., Van den Bosch, M., Landa, I., Hagen, W.R., Hyperthermophilic redox chemistry: a re-evaluation (1998) *FEBS Lett. 440*, 311-314.

Nawoord

Gedurende de vier jaar van mijn promotieonderzoek hebben talloze mensen op uiteenlopende wijze een bijdrage geleverd aan dit proefschrift. Het is haast te veel om op te noemen, maar ik ga toch een poging wagen. Op de eerste plaats wil ik mijn promotor Fred Hagen bedanken voor zijn uitstekende begeleiding. Je hebt de intresse in de bio-anorganische chemie bij mij gewekt, en ik blik met genoegen terug op het oio-schap bij jou. Maar je bent nog niet van me af, want ik blijf nog even in het Delftse. Van onschatbare waarde zijn de bijdragen van de vier afstudeervakkers die ik in Wageningen heb mogen begeleiden: Robert Freije, Petra van 't Slot, Daniel de Geus en Juul Slits. Jullie hebben niet alleen een wetenschappelijke bijdrage geleverd, maar ook mij gedwongen goed uitleg te geven en daardoor beter na te denken over mijn eigen werk. Marieke van den Bosch, Martijn Driessen en Ilse Landa wil ik bedanken voor hun bijdrage aan hoofdstuk 2 van dit proefschift.
Daarnaast ben ik al mijn collega's in Wageningen en Delft dank verschuldigt voor de gezelligheid en praktische hulp. Een speciaal bedankje is er voor Pedro, Maria, Eyke, Roelco, Huub en Hans voor het sociale gebeuren, de hulp en discussies tijdens mijn Wageningse periode. Mijn (ex)mede-labbewoners in Delft wil ik ook bedanken voor de goede sfeer en samenwerking: Branko, Yana, Harti, Simon, Jaap, Marc, Daan, Nahid, Marcia, Miguel, Dirk, Alidin, Emile, Tony, Alexei, Esengül, Patty.
Special thanks for my international collaborators. Aurora Martinez showed me that human enzymes can be very interesting as well. Who would have known? And I would like to thank, John Charnock, Arefa Docrat and Lisa Stewart for a very pleasant collaboration. I owe many thanks to Dave Garner for his contributions to the chapters 4 and 5 and for patiently correcting my manuscripts, and for allowing me to visit the Daresbury Laboratory. I hope we can continue our collaboration on these interesting molybdenum and tungsten enzymes in the future. Furthermore, I would like to thank Jean-Louis Primus and Cees Veeger for a brief, but very fruitfull collaboration.
Ook heb ik het genoegen gehad om met een aantal Wageningse microbiologen samen te werken. Met Frank de Bok heb ik een verdienstelijke samenwerking achter de rug. En meer recentelijk met Arthur Wolterink, die ik het beste toewens bij de voltooing van zijn eigen proefschrift.

En natuurlijk wil ik ook mijn ouders en andere dierbaren bedanken. En Eugenie voor alle liefde, steun, geduld en begrip tijdens de afgelopen vier jaar.